

AD-A137 404

HEAT TRANSFER AND THERMAL STABILITY OF ALTERNATIVE
AIRCRAFT FUELS VOLUME 1. (U) PRATT AND WHITNEY AIRCRAFT
GROUP WEST PALM BEACH FL GOVERNMENT.

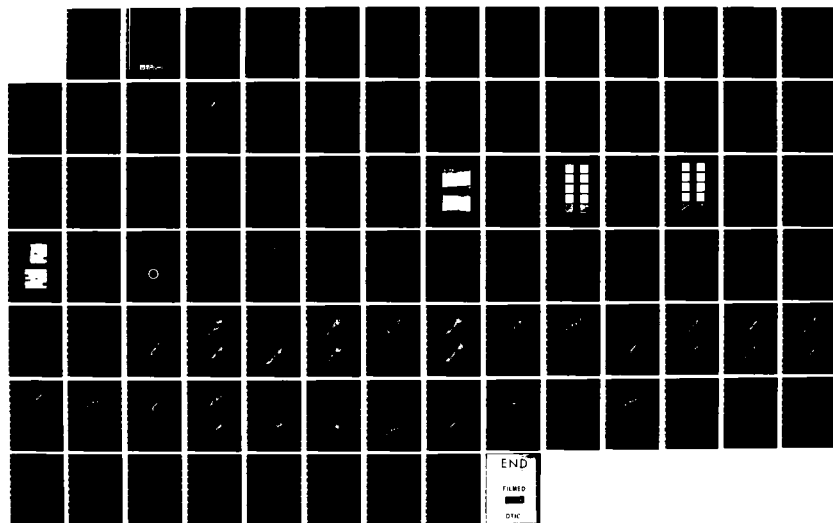
1/1

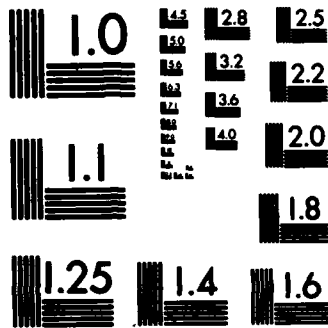
UNCLASSIFIED

J A TEVELDE ET AL. NOV 83

F/G 21/4

NL





MICROCOPY RESOLUTION TEST CHART
 NATIONAL BUREAU OF STANDARDS-1963-A

120

AD A 137404

HEAT TRANSFER AND THERMAL STABILITY OF ALTERNATIVE AIRCRAFT FUELS

VOLUME I

FINAL REPORT NOVEMBER 1983

By
J. A. TeVelde
M. R. Glickstein

Prepared for:
Naval Air Propulsion Center
Under Contract N00140-80-C-0097, Lot III

Naval Air Propulsion Center
Trenton, New Jersey 08628

DTIC
JAN 31 1984
A

APPROVED FOR PUBLIC RELEASE; DISTRIBUTION UNLIMITED

DTIC FILE COPY



84 01 30 097

30

UNCLASSIFIED

SECURITY CLASSIFICATION OF THIS PAGE (When Data Entered)

REPORT DOCUMENTATION PAGE		READ INSTRUCTIONS BEFORE COMPLETING FORM
1. REPORT NUMBER NAPC-PE-87C	2. GOVT ACCESSION NO. AD-A137 489	3. RECIPIENT'S CATALOG NUMBER
4. TITLE (and Subtitle) Heat Transfer and Thermal Stability of Alternative Aircraft Fuels		5. TYPE OF REPORT & PERIOD COVERED Final Report — 1 January 1982 to 1 February 1983
		6. PERFORMING ORG. REPORT NUMBER P&WA/GPD/FR-17404
7. AUTHOR(s) J. A. TeVelde M. R. Glickstein		8. CONTRACT OR GRANT NUMBER(s) N00140-80-C-0097, Lot III
		10. PROGRAM ELEMENT, PROJECT, TASK AREA & WORK UNIT NUMBERS PE63724N Project No. Z0838 Work Unit NAPC-617
9. PERFORMING ORGANIZATION NAME AND ADDRESS United Technologies Corporation Pratt & Whitney Aircraft Government Products Division P. O. Box 2691, West Palm Beach, FL 33402		11. CONTROLLING OFFICE NAME AND ADDRESS Naval Air Propulsion Center P. O. Box 7176 Trenton, New Jersey 08628
12. REPORT DATE November 1983		13. NUMBER OF PAGES
14. MONITORING AGENCY NAME & ADDRESS (if different from Controlling Office)		15. SECURITY CLASS. (of this report) Unclassified
		15a. DECLASSIFICATION/DOWNGRADING SCHEDULE
16. DISTRIBUTION STATEMENT (of this Report) Approved for Public Release; Distribution Unlimited.		
17. DISTRIBUTION STATEMENT (of the abstract entered in Block 20, if different from Report)		
18. SUPPLEMENTARY NOTES		
19. KEY WORDS (Continue on reverse side if necessary and identify by block number) Alternative fuels, fuels, jet and gas turbine fuels, thermal stability, coking, heat transfer.		
20. ABSTRACT (Continue on reverse side if necessary and identify by block number) A test and evaluation program was conducted to determine the heat transfer and thermal stability characteristics of several selected alternative fuels. Accelerated fuel coking tests were conducted with three alternative fuels and a specification grade JP-5 fuel, in a heated tube apparatus. Test conditions included both simulated engine conditions and higher-temperature accelerated coking conditions. Resulting deposit rates were evaluated and correlated as a function of the test conditions. Deposit effects on heat transfer were also evaluated and correlated as a function of test condition.		

TABLE OF CONTENTS

Section		Page
VOLUME I		
I	SUMMARY	1
	A. Program Objective and Methodology	1
	B. Phase I — Methods and Correlative Model	2
	C. Phase II — Verification of the Methodology	5
II	INTRODUCTION	7
III	TECHNICAL APPROACH	10
	A. Fuel Selection and Characterization	10
	B. Test Facility and Hardware	11
	C. Data Acquisition and Control System	12
	D. Test Matrix and Operating Procedures	12
IV	EXPERIMENTAL RESULTS AND DISCUSSION	15
	A. Baseline Fuel Tests	15
	B. NAPC-7 Fuel Tests	28
	C. NAPC-11 Fuel Tests	34
	D. NAPC-14 Fuel Tests	37
V	COMPLEMENTARY ANALYSIS	39
	A. Data Pre-Processing	39
	B. Heat Transfer Analysis	40
	C. Fuel Physical Properties	40
	D. Analysis of Deposit Properties	41
	E. Analysis of Fuel Specific Heat	42
	F. Pressure Loss Analysis	43
	G. Data Correlations	43
	H. Baseline Fuel (NAPC-5)	43
	I. NAPC-7 Fuel	44
	J. NAPC-11 Fuel	60
	K. NAPC-14 Fuel	60
VI	COMPARISON OF RESULTS	69
VII	SUMMARY PLAN	73
	A. Thermal Evaluation of Fuel	73
	B. Test Conditions	74
	C. Deposit Evaluation	75
	D. Deposit Data Correlation	76
VIII	CONCLUDING REMARKS	77

TABLE OF CONTENTS (Continued)

<i>Section</i>		<i>Page</i>
IX	REFERENCES	78
VOLUME II		
	APPENDIX A	A-1
	APPENDIX B	B-1

LIST OF ILLUSTRATIONS

<i>Figure</i>		<i>Page</i>
1	Heat Transfer and Thermal Stability Program	1
2	Environmental Envelope for a Typical Current Military Engine	2
3	Comparison of Deposit Formation Rates of Test Fuels	4
4	Carbon Deposition vs JFTOT Breakpoint Temperature	4
5	Deposit Thermal Conductivity vs Deposit Function for NAPC-5, Test No. 1	5
6	Aircraft Fuel Deposit Test Apparatus	9
7	Test Assembly Instrumentation	12
8	Deposit Burnoff Apparatus	14
9	Effect of Flow Rate on Carbon Deposition from NAPC-5 Fuel	16
10	Tube Wall Temperature Distribution for NAPC-5 With SS316 Tube ..	18
11	Tube Wall Temperature Distribution for NAPC-5 With Inconel 600 Tube	19
12	Rate of Carbon Deposition for NAPC-5 Fuel	20
13	Effect of Time on Deposit Formation Rate	21
14	Pressure Drop History for NAPC-5 Test	22
15	Wall Temperature History for NAPC-5 Test	22
16	Deposit Surface Morphology for NAPC-5 Test	23
17	Composition of NAPC-5 Deposits	25
18	Effect of Fuel Prestressing on Carbon Deposition	26
19	Effect of Fuel Prestressing on NAPC-5 Deposit Composition	27
20	Photomicrograph of NAPC-5 Deposit for Test 5	30
21	Rate of Carbon Deposition for NAPC-7 Fuel	31
22	Verification of Data Repeatability	32
23	Fuel Deposit Heat Transfer Model	32
24	Deposit Thermal Resistance for NAPC-7 Fuel	33

LIST OF ILLUSTRATIONS (Continued)

<i>Figure</i>		<i>Page</i>
25	Deposit Loading vs Calculated Deposit Resistance for NAPC-7 Fuel ...	33
26	Comparison of Measured and Calculated Deposit Formation Rates for NAPC-7	34
27	Rate of Carbon Deposition for NAPC-11 Fuel	35
28	Deposit Thermal Resistance for NAPC-11 Fuel	36
29	Deposit Loading vs Calculated Deposit Resistance for NAPC-11 Fuel .	36
30	Comparison of Measured vs Calculated Deposit Formation Rate for NAPC-11 Fuel	37
31	Rate of Carbon Deposition for NAPC-14 Fuel	38
32	Heat Transfer Characteristics of NAPC-5, Test No. 1	46
33	Heat Transfer Characteristics of NAPC-5, Tests No. 1 Through 10	46
34	Deposit Thermal Conductivity vs Deposit Thickness for NAPC-5, Test No. 1	47
35	Deposit Thermal Conductivity vs Deposit Function for NAPC-5, Test No. 1	47
36	Deposit Thermal Conductivity vs Deposit Function for NAPC-5, Test No. 2	48
37	Deposit Thermal Conductivity vs Deposit Function for NAPC-5, Test No. 4	49
38	Deposit Thermal Conductivity vs Deposit Function for NAPC-5, Test No. 5	49
39	Deposit Thermal Conductivity vs Deposit Function for NAPC-5, Test No. 6	50
40	Deposit Thermal Conductivity vs Deposit Function for NAPC-5, Test No. 7	50
41	Deposit Thermal Conductivity vs Deposit Function for NAPC-5, Test No. 8	51
42	Deposit Thermal Conductivity vs Deposit Function for NAPC-5, Test No. 9	51
43	Deposit Thermal Conductivity vs Deposit Function for NAPC-5, Test No. 10	52

LIST OF ILLUSTRATIONS (Continued)

<i>Figure</i>		<i>Page</i>
44	Deposit Thermal Conductivity vs Deposit Function for NAPC-5, Tests No. 1 Through 10	52
45	Specific Heat vs Bulk Temperature for NAPC-5 at 400 psia, Tests No. 1, 2, and 4	53
46	Specific Heat vs Bulk Temperature for NAPC-5 at 800 psia, Test No. 10	53
47	Friction Factor vs Reynolds Number for NAPC-5	54
48	Heat Transfer Characteristics of NAPC-7 Fuel, Tests No. 11 Through 19	54
49	Deposit Thermal Conductivity vs Deposit Function for NAPC-7, Test No. 11	55
50	Deposit Thermal Conductivity vs Deposit Function for NAPC-7 Fuel, Test No. 12	55
51	Deposit Thermal Conductivity vs Deposit Function for NAPC-7 Fuel, Test No. 15	56
52	Deposit Thermal Conductivity vs Deposit Function for NAPC-7 Fuel, Test No. 16	56
53	Deposit Thermal Conductivity vs Deposit Function for NAPC-7 Fuel, Test No. 17	57
54	Deposit Thermal Conductivity vs Deposit Function for NAPC-7 Fuel, Test No. 18	57
55	Deposit Thermal Conductivity vs Deposit Function for NAPC-7 Fuel, Test No. 19	58
56	Deposit Thermal Conductivity vs Deposit Function for NAPC-7 Fuel, Tests No. 11 Through 19	58
57	Specific Heat vs Bulk Temperature for NAPC-7 Fuel Tests No. 11 Through 19	59
58	Friction Factor vs Reynolds Number for NAPC-7 Fuel, Tests No. 11 Through 19	59
59	Heat Transfer Characteristics of NAPC-11 Fuel, Tests No. 20 Through 25	60
60	Deposit Thermal Conductivity vs Deposit Function for NAPC-11 Fuel, Test No. 20	61

LIST OF ILLUSTRATIONS (Continued)

<i>Figure</i>		<i>Page</i>
61	Deposit Thermal Conductivity vs Deposit Function for NAPC-11 Fuel, Test No. 21	61
62	Deposit Thermal Conductivity vs Deposit Function for NAPC-11 Fuel, Test No. 22	62
63	Deposit Thermal Conductivity vs Deposit Function for NAPC-11 Fuel, Test No. 23	62
64	Deposit Thermal Conductivity vs Deposit Function for NAPC-11 Fuel, Test No. 24	63
65	Deposit Thermal Conductivity vs Deposit Function for NAPC-11 Fuel, Test No. 25	63
66	Deposit Thermal Conductivity vs Deposit Function for NAPC-11 Fuel, Tests No. 20 Through 25	64
67	Specific Heat vs Bulk Temperature for NAPC-11 Fuel Tests No. 20 Through 25	64
68	Friction Factor vs Reynolds Number for NAPC-11 Fuel, Tests No. 20 Through 25	65
69	Heat Transfer Characteristics of NAPC-14 Fuel, Tests No. 26 through 30	65
70	Deposit Thermal Conductivity vs Deposit Function for NAPC-14 Fuel, Test No. 26	66
71	Deposit Thermal Conductivity vs Deposit Function for NAPC-14 Fuel, Test No. 28	66
72	Deposit Thermal Conductivity vs Deposit Function for NAPC-14 Fuel, Test No. 29	67
73	Deposit Thermal Conductivity vs Deposit Function for NAPC-14 Fuel, Tests No. 26 through 30	67
74	Specific Heat vs Bulk Temperature for NAPC-14 Fuel, Tests No. 26 through 30	68
75	Friction Factor vs Reynolds Number for NAPC-14 Fuel, Tests No. 26 through 30	68
76	Comparison of Deposit Formation Rates of Test Fuels	69
77	Carbon Deposition vs JFTOT Breakpoint Temperature	71

LIST OF ILLUSTRATIONS (Continued)

<i>Figure</i>		<i>Page</i>
78	Comparison of Tube Wall Temperature Histories for Three Test Fuels	71
79	Composite of Deposit Loading vs Calculated Deposit Resistance	72

LIST OF TABLES

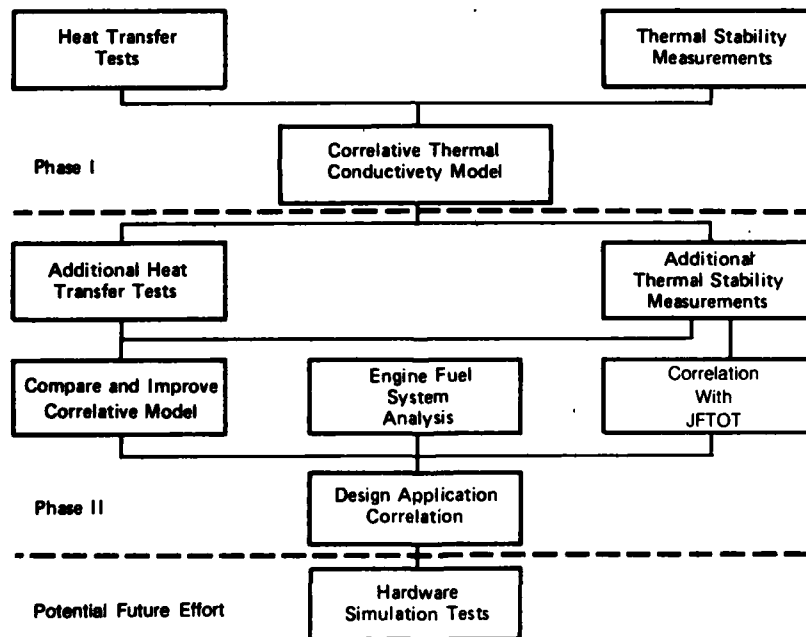
<i>Table</i>		<i>Page</i>
1	Selected Properties of Test Fuels	10
2	Summary of NAPC-5 Test Conditions	15
3	Tube Deposit Distribution for NAPC-5 Fuel	17
4	Summary of NAPC-7 Test Conditions	31
5	Summary of NAPC-11 Test Conditions	35
6	Summary of NAPC-14 Test Conditions	37
7	Thermophysical Properties of JP-5	45
8	Summary of Test Conditions	48
9	Activation Energies for Deposit Formation	69
10	Thermal Stability Rankings of Fuels Tested	70

SECTION I

SUMMARY

A. PROGRAM OBJECTIVE AND METHODOLOGY

The objective of the Heat Transfer and Thermal Stability Program is to provide design application data for the thermal stability of Navy aircraft fuels with a minimum of test effort. The program logic is shown in Figure 1. In the selected approach, the thermal stability of a fuel is evaluated by measuring the accumulations of fuel deposits in heated tubes and correlating the accumulation of deposits with the degradation of heat transfer. The overall methodology consists of (a) direct measurement of the heat transfer at simulated engine conditions, (b) determination of the deposit accumulation and development of a correlative heat transfer model, and (c) prediction of the resulting deposit rates and correlation with the engine environmental conditions for subsequent use in engine design. Successful application of the methodology requires the measurement of small changes in heat transfer caused by surface deposits, and the ability to quantify the amount of deposits causing the observed changes. Although the required heat transfer methods currently exist, quantification of deposit formation from measured heat transfer data requires the accumulation of thermal stability data simultaneously with heat transfer data in order to develop correlations between the two processes.



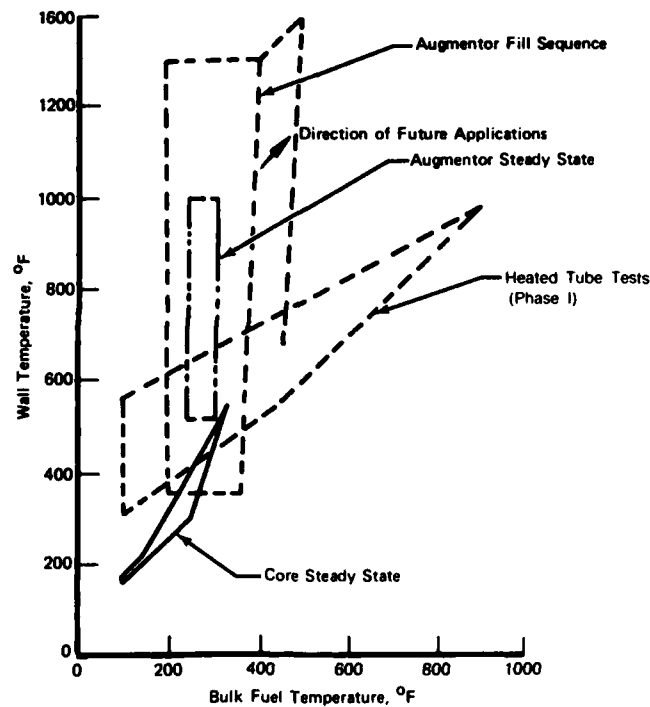
FD 267801

Figure 1. Heat Transfer and Thermal Stability Program

As illustrated in Figure 1, the objective of the program is being addressed in two phases. The primary objectives of Phase I are the development of a thermal stability data base for four selected fuels, and the development of a correlative model relating deposit accumulation to resulting heat transfer effects. The objectives of Phase II are the expansion of the thermal stability data base, verification and improvement of the correlative model with additional fuels, and evaluation of the effect of the JFTOT breakpoint temperature on fuel deposition rates. Results of these efforts will be incorporated into an overall design-application data correlation,

and the effects of changes in thermal stability levels on various components of an engine fuel system will be predicted for a selected engine application. A logical future extension of the Program, also shown in Figure 1, would be a hardware simulation test, applying the design-application correlations developed in Phase II to analyze a fuel application in an engine.

Because the specific nature of fuel stability effects on engine operation depend both on the characteristics of the fuel and on the engine operation, the experimental program has been defined to explore fuel characteristics over the range of current and future engine applications. A typical environmental envelope for a current military engine is shown in Figure 2, which illustrates the local fuel and wall temperatures. The most severe operating condition occurs in the augmentor during fuel system fill, with fuel temperatures reaching 400°F and wall temperatures exceeding 1200°F. The steady state temperature conditions, although less severe, are also sufficiently hot to cause thermal decomposition. Considering the direction in which engine development appears to be heading, the problem will become more severe in the future as engines operate at increasingly higher temperatures.



FD 267802

Figure 2. Environmental Envelope for a Typical Current Military Engine

B. PHASE I — METHODS AND CORRELATIVE MODEL

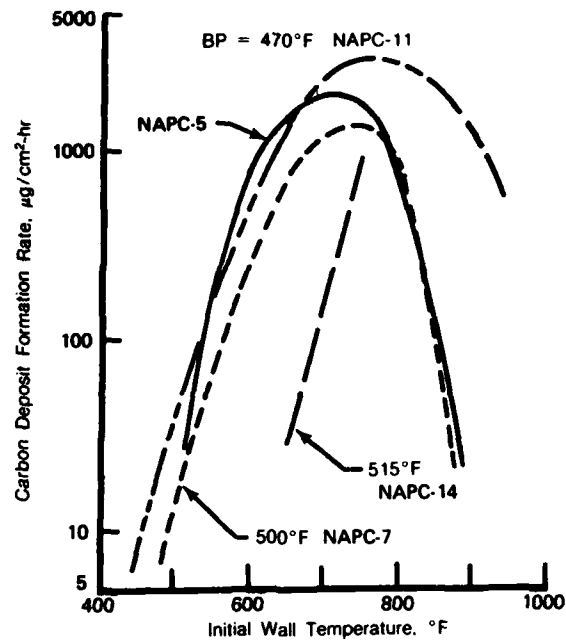
The method selected for obtaining fuel thermal stability and heat transfer data consists of exposing fuel to a thermal environment which simulates engine operating conditions. In this method fuel flows through a length of thin walled metal tubing that is heated by an electric current passing through it. Because the tube is an electrically resistive material, such as a stainless steel or a nickel alloy, it acts as a resistance heater, converting the electrical energy to heat. Insulating the outside of the tube eliminates external heat loss and results in essentially all of the heat being absorbed by the fuel. Thermocouples attached to the tube provide a measurement of the temperature of the fuel-surface interface. From measurements of the inlet

and outlet fuel temperatures, the electric power dissipated in the tube (the heat generation), and the fuel flow rate and pressure, sufficient information is known to determine the heat transfer characteristics at any environmental condition being simulated. If the simulated conditions are severe enough to cause thermal decomposition of the fuel and they are maintained for a sufficient period of time, deposits accumulate on the tube surface. After completion of the heated tube test, the test tube is cut into short sections and the deposits are burned away by heating each tube in a retort while flowing air through the tube. The air is then passed through an analyzer to measure the total carbon dioxide and carbon monoxide evolved, from which the total carbon accumulated in the tube and the rate of deposition are calculated.

Since deposit accumulations will result in measurable changes in surface temperature, the potential exists for developing an indirect non-destructive technique for measuring deposit formation by means of a change in heat transfer. The difference in observed surface temperature from the "clean", no-deposit, condition at the beginning of a fuel test is used to evaluate the thermal resistance caused by the deposited material on the tube surface. The thermal resistance to the flow of heat, caused by a deposit layer, is a function of the deposit thickness and the effective thermal conductivity of the deposited material. Since the structure and density of a carbonaceous deposit can vary widely, the effective thermal conductivity also varies, ranging from a low value approximating that for the fuel to an upper value approaching that for graphitic material. Because the thermal conductivity is required if the deposit thickness is to be determined from thermal measurements alone, a correlative model is formulated to describe the conductivity as a function of the environmental conditions during the deposit formation.

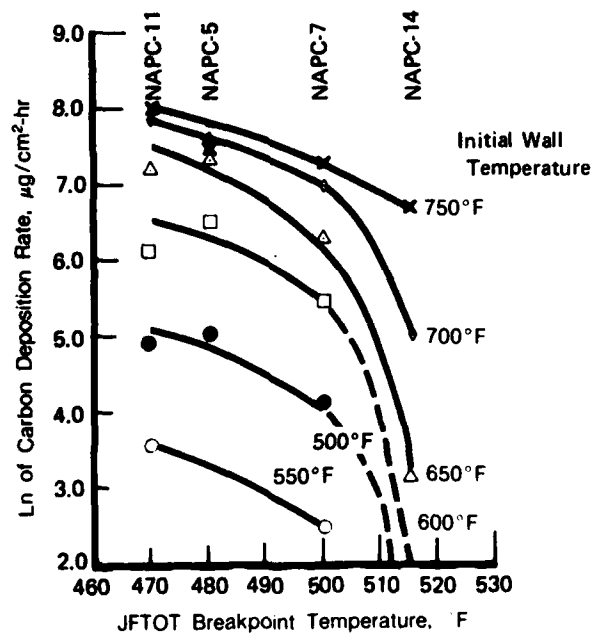
Four fuels, namely NAPC-5, NAPC-7 (80% JP-5/20% hydrocracked gas oil), NAPC-11 (50% JP-5/50% No. 2 heating oil), and NAPC-14 (shale derived JP-5 with stripped nitrogen compounds partially replaced), were evaluated in Phase I for the purpose of developing methods and data for engineering design. Tests were conducted in Stainless 316 and in Inconel 600 tubes at pressures of 400 and 800 psig, fuel exit temperatures up to 900°F, fuel flow rates from 60 to 120 lbm/hr, and test durations from 1 to 20 hours. Deposit quantities were measured, and average rates of deposition were calculated for each test and correlated with respect to wall temperature. Resulting deposition rates ranged from 10 to 3000 micrograms/sq.cm-hr when initial wall temperatures ranged from 400 to 980°F. Peak deposit formation rates occurred at surface temperatures of 700 to 750°F. The tests were performed at relatively high temperatures, providing large deposit yields with short test durations, thereby permitting verification of the procedure while minimizing the amount of fuel and testing time required. Figure 3 shows a comparison of the deposit rates measured for the four fuels tested in Phase I. The thermal stabilities of the four fuels, based on the measured carbon deposition rates, show relatively good agreement with their corresponding JFTOT breakpoint temperatures, ie., fuels with higher JFTOT breakpoint temperatures result in lower carbon deposition rates. The NAPC-14 fuel exhibits significantly better stability than the other fuels tested. A preliminary correlation of carbon deposition rate as a function of JFTOT breakpoint temperature was developed for the four fuels tested, and is illustrated in Figure 4. Development of a general correlation would allow obtaining engineering design data (e.g., deposition rate) from the current ASTM test method.

Measurements were made of the effect of fuel deposition on heat transfer, and the test results were analyzed to determine the thermal characteristics of the deposits. Thermal conductivity of the deposits, calculated from the measured heat transfer data, showed a strong correlation with deposit thickness and wall temperature. This correlation, shown in Figure 5, was observed in varying degrees for all four fuels, and lends support to the potential method for a nondestructive measurement of wall deposits. If a general correlation of the deposit thermal conductivity can be developed for a class of fuels, the amount of deposits formed during a heated tube test can be determined by measurement of the heat transfer degradation caused by deposit accumulation.



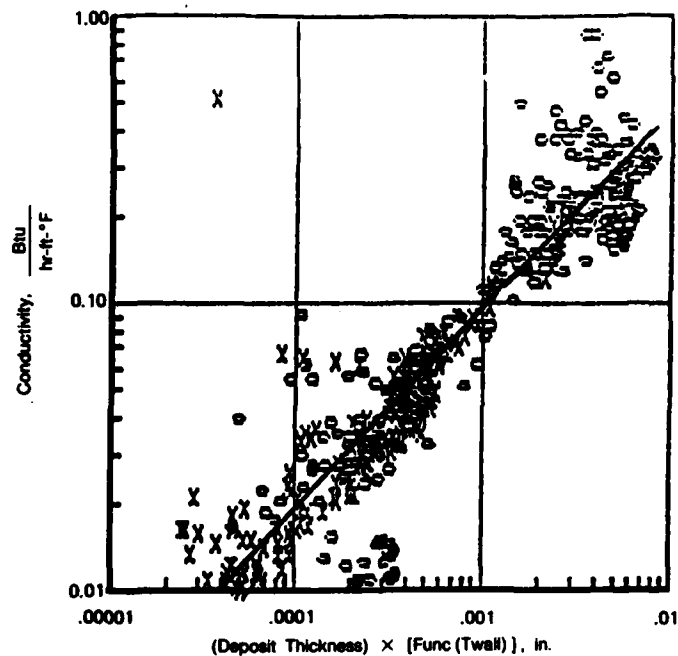
FD 267803

Figure 3. Comparison of Deposit Formation Rates of Test Fuels



FD 267804

Figure 4. Carbon Deposition vs JFTOT Breakpoint Temperature



FD 267805

Figure 5. Deposit Thermal Conductivity vs Deposit Function for NAPC-5, Test No. 1

C. PHASE II — VERIFICATION OF THE METHODOLOGY

In Phase II, the correlative thermal conductivity model will be validated and the data base will be expanded through additional tests at lower temperatures. In addition, a series of tests will be performed with fuels selectively doped with compounds which are known to reduce fuel breakpoint temperature. These tests will provide data for a wider range of JFTOT breakpoint temperature, allowing an extension of the preliminary JFTOT — deposit rate correlation developed in Phase I. The deposit data resulting from both phases of the program will be commingled and used to develop a final design correlation, relating the environmental conditions to the rate of deposit accumulation for each fuel.

An engine fuel system analysis will be performed to evaluate the environmental history of a fuel in a current high-performance military engine. The conditions of the fuel thermal stability tests from Phase I, and planned for Phase II, will be reviewed with regard to the engine environmental conditions identified in this analysis to establish the adequacy of the thermal stability data base.

The extended test program will be performed using NAPC-5 and three additional alternative fuels. Tests will be performed with the fuels in the as-received condition, and with the addition of a selected additive(s) for systematically reducing the JFTOT breakpoint temperatures. Possible additives include compounds of sulfur, nitrogen, copper, or selected hydrocarbons.

It is anticipated that, pending the results of the environmental analysis, test conditions will cover the range of fuel exit pressures from 250 to 400 psig, fuel exit temperatures from 400 to 600°F, and flow rates from 60 to 480 lb/hr. Tube wall temperatures at the exit will range from 450 to 650°F. These conditions will generally produce lower levels of accumulated deposits than

experienced in the Phase I tests, and will be used to define the lower limits of the deposit regime.

Independent deposit measurements will be performed on the specimen tubes using the same techniques used in Phase I, but with increased accuracy. Effective thermal conductivity of the deposits will be determined from the heat transfer and deposit data, and used to improve the correlative model.

The fuel deposition-rate data will be related to the engine fuel system environmental-history analysis in order to identify problem areas which might be encountered in a typical engine. In addition to relating fuel deposition rates to engine conditions, an attempt will be made to extend the correlations relating JFTOT breakpoint temperature to fuel deposition rates over the entire range of operating temperatures. A detailed map of the variation in the deposition rate of the fuel over a wide range of JFTOT breakpoint temperatures will be developed for each fuel tested.

SECTION II

INTRODUCTION

In recent years, increased attention has been directed toward the effective utilization of alternative fuels in aircraft gas turbines. New fuel blends derived from crude oil, coal liquids, or shale oil require careful study prior to effective implementation, since significant deviations from conventional fuel specifications may occur. An important area of concern that is directly impacted by deviations in fuel specification is that of fuel thermal stability. Changes in fuel composition which may be detrimental to thermal stability include higher fractions of aromatics and olefins as well as increased concentrations of minor species such as sulfur, nitrogen, and trace metal contaminants. Furthermore, environmental conditions in current and advanced technology military gas turbine engines are such that fuels and lubricating oils are exposed to a wide range of temperatures and pressures. At more severe heat fluxes, fuel may undergo thermal decomposition, resulting in the formation and accumulation of deposit (coke). Determinations of whether or not deposits will form and where they are likely to accumulate in a particular engine require that the thermal stability characteristics of the fuel be known at the conditions of intended application. As an example, an envelope of fuel-and wall-temperature conditions that are typical of a current military engine fuel system is shown in Figure 6. As can be seen, the highest temperatures occur in the augmentor spray bars during fuel system fill, and steady-state temperatures that are conducive to fuel decomposition can be found within the augmentor and core fuel systems. Higher performance engines will result in increased heat fluxes and higher thermal loadings on the fuel systems.

Hydrocarbon fuel thermal stability has been investigated for many years by numerous authors (References 1 to 10). The rate of deposit formation on heated surfaces has been found to vary with temperature in a unique manner (References 2, 3, 7 and 9) characterized by a rapid increase with increasing surface temperature, up to approximately 750°F, followed by a rapid decrease and yet another more gradual increase as the reaction mechanism shifts from oxidation controlled to pyrolysis controlled. In addition to surface temperature, previous studies have shown that fuel deposition is a function of fuel composition, fuel temperature, fuel pressure, and velocity. While there is presently only a superficial understanding of the mechanisms involved in deposit formation, it is generally believed that deposits are produced by free radical autooxidation of hydrocarbon molecules. Although questions regarding the mechanisms involved during deposit formation still remain, it is generally believed that deposit precursors produced by oxidation of the fuel are condensed out of the fuel in a stepwise manner (Reference 1).

Except for recent investigations (References 7 and 9), little effort has been directed toward evaluating the effects of fuel deposits on the fuel system heat transfer characteristics. Because of the number of factors influencing hydrocarbon decomposition, determination of the useful heat sink capacity (or temperature limits) for a specific fuel should be made at the conditions of planned application. While a standardized coker test yields a direct comparison with a fuel specification, it does not provide data for design of a new fuel application. Such data can only be obtained by evaluating decomposition-deposition characteristics at conditions simulating the desired application. Of the various possible experimental arrangements for conducting such simulation tests, the use of electrically-heated tubes provides the simplest and the most direct approach and was the method adopted in this study. The method consists of using the tube itself as the resistance element by passing current axially through the tube, thereby causing uniform internal heat generation with the tube wall. Control and measurement of the thermal parameters (e.g., heat flux, wall temperature, and fuel temperature) during the test, and subsequent measurement of the resulting deposits, allowed the determination of the rate of

deposition and development of correlations relating the effect fuel deposits have on heat transfer.

The overall objective of this study is the development of an appropriate methodology to be used to evaluate the behavior of alternative fuels in a thermal environment typical of present and future aircraft fuel systems, and to provide information useful to fuel system designers regarding the impact of fuel deposition on heat transfer. The study is being conducted in two phases. The first phase, described herein, demonstrates the usefulness of the selected methodology and the ability to quantify the effect that deposit formation has on heat transfer. The second phase will provide additional data regarding the effect of fuel deposits on heat transfer and also will provide correlations which relate the standard ASTM JFTOT (Jet Fuel Thermal Oxidation Tester) breakpoint temperature to fuel deposit formation rate. The information obtained from these tests is vital to developing a thermal stability/heat transfer subroutine that could be incorporated into the U. S. Navy's Alternate Test Procedure (Reference 11) for qualifying new fuels for Navy aircraft use.

The key elements of the Phase I study included: (a) thermal stressing of fuels in electrically-heated tubes, (b) evaluation of deposit heat transfer characteristics, (c) determination of the mass of carbonaceous deposits, (d) characterization of the deposit morphology, and (e) correlation of fuel thermal stability and deposit heat transfer measurements. Included in the investigation were the following tasks:

Task I — *Development of a Test Procedure*, including a thorough checkout of all facilities and development of a detailed set of procedures to be followed for the heated tube testing and subsequent deposit characterization.

Task II — *Fuel Deposit Testing*, which included tests performed with a baseline fuel to validate the Test Procedure, and additional heated tube tests with three additional fuels.

Task III — *Post Test Deposit Analysis*, including quantitative measurement of deposits in selected tube specimens and a characterization of deposit structure and composition.

Task IV — *Data Analysis and Correlation*, including determination of heat transfer coefficients and friction factors, correlation of deposit characteristics and the effects of deposits on heat transfer.

Task V — *Development of a Summary Plan* outlining a recommended procedure for thermal stability evaluation of alternative and broad-specification fuels.

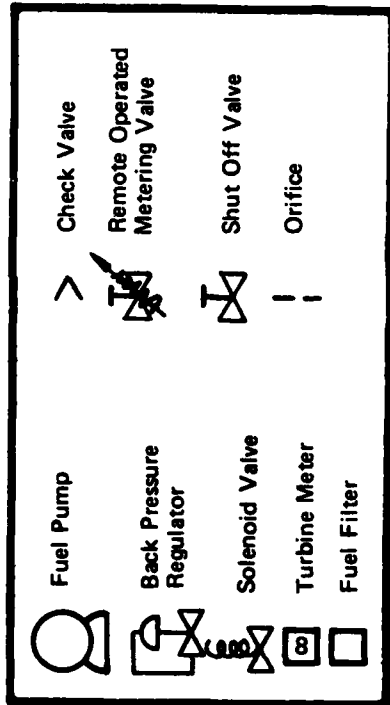
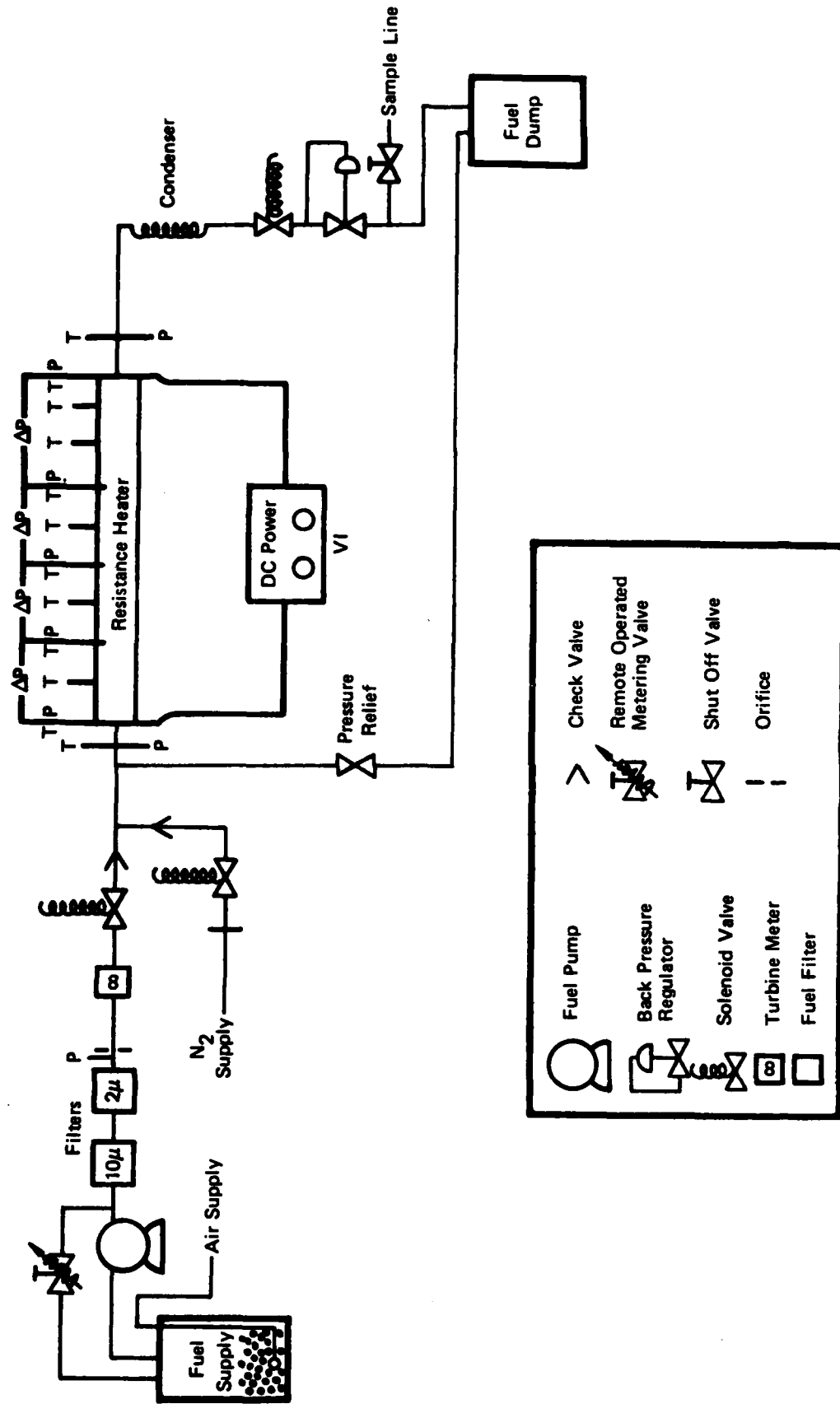


Figure 6. Aircraft Fuel Deposit Test Apparatus

SECTION III

TECHNICAL APPROACH

A. FUEL SELECTION AND CHARACTERIZATION

The main objectives of this study were to develop an appropriate methodology to be used to investigate the thermal stability characteristics of several hydrocarbon fuels whose properties may be typical of future fuels and to evaluate the impact of fuel deposition on heat transfer and pressure loss. To develop the methodology for evaluation of thermal stability of alternative fuels, the effects of the most important physical parameters, such as pressure, temperature and flow rate, were evaluated using a standard, well characterized baseline fuel. The selected baseline fuel was NAPC-5 (JP-5), which is currently used in all Navy aircraft gas turbine engines. Since the chemistry of the deposit formation mechanisms were considered beyond the scope of this study, no attempt was made to systematically vary fuel composition. However, three additional fuels thought to span a relatively wide range of thermal stability were selected for evaluation. The fuels chosen by the Navy were: an acid treated shale-derived JP-5 with stripped nitrogen compounds partially replaced (NAPC-14), a mixture of 80 percent JP-5 and 20 percent hydrocracked gas oil (NAPC-7), and a mixture of 50 percent JP-5 and 50 percent No. 2 heating oil (NAPC-11). It is believed that these fuels represented a stability range sufficiently broad to allow a meaningful evaluation of the utility of the test apparatus and the effect of deposit formation on heat transfer and pressure loss. A tabulation of selected properties of the test fuels was provided by the Navy and is presented in Table 1.

TABLE 1. SELECTED PROPERTIES OF TEST FUELS

	NAPC-5	NAPC-7	NAPC-11	NAPC-14
Aromatics (vol %)	14.99	32.57	21.6	24
Olefins (vol %)	0.79	0.86	1.1	1.6
Sulfur (wt %)	0.005	0.047	0.07	0.002
Nitrogen, ppm	neg	57	33	2.6
Acidity, total (mg, KOH/g)	0.004	0.006	0.049	negligible
Hydrogen (wt %)	13.79	12.83	13.5	13.7
Viscosity (cs at 100°F)	1.58	1.77	1.98	1.38
API Gravity (at 59°F)	41.8	35.6	39.6	43.7
Flash Pt. (°F)	144	160	156	145
Volatility				
Distillation (°F)				
IBP	358	379	369	363
10%	390	399	401	379
20%	397	408	415	385
50%	423	439	451	401
90%	469	522	561	448
EP	502	550	579	495
Residue (ml)	1.2	3.6	6.0	1.2
Loss (ml)	0.2	0.4	—	0.4
Copper Strip (2 hr at 212°F)	1-a	1-a	1-a	1-a
JFTOT Thermal Stability				
Breakpoint Temperature (°F)	520	500	470	515
ΔP (25 mm Hg) Failure Temp (°F)	480	>500	>470	>515
Existent Gum (mg/100 ml)	2.6	0.1	12.4	0.0
Particulates (mg/liter)	1.0	1.817	3.9	0.3
Water Separation Index	85	22	—	98
— values not reported				

B. TEST FACILITY AND HARDWARE

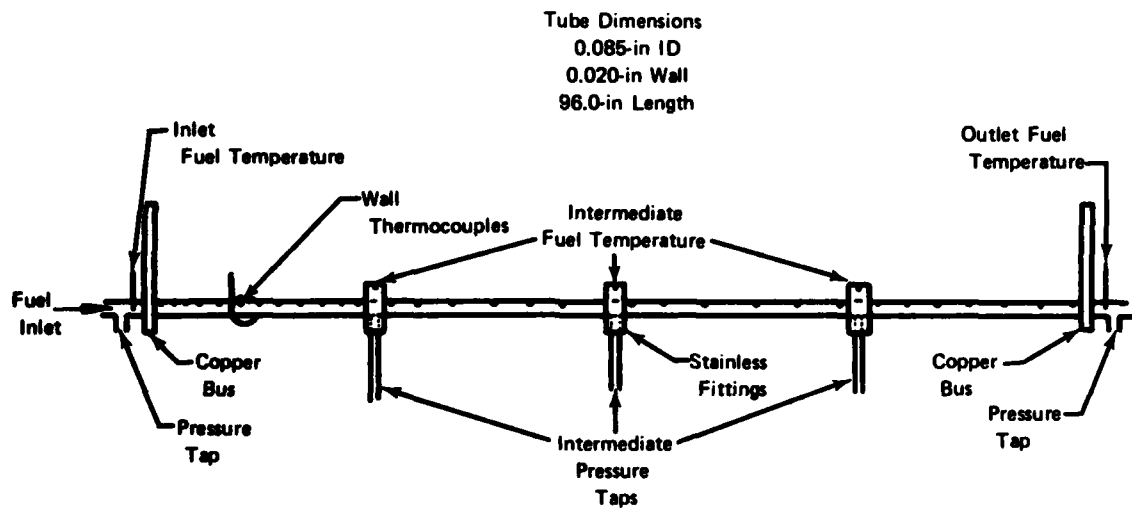
The deposit formation experiments were conducted in a resistance-heated tube apparatus which was insulated from the surroundings and capable of continuous operation. The apparatus, shown schematically in Figure 6, consisted of the following major components: (1) a 275-gal. fuel reservoir equipped with an air sparging system to ensure that the fuel is air saturated, (2) a fuel delivery system consisting of a 1000 psig fuel pump and associated filters to remove solid particulate contaminants above 2 microns, (3) a turbine-type flow meter, (4) a high-pressure-drop orifice to render the fuel supply insensitive to pressure changes in the test apparatus, (5) a resistance-heated tube connected electrically to a 64 kW d-c power supply, (6) a proportional temperature controller used to maintain a constant fuel exit temperature by regulating the input power, (7) a fuel condenser, (8) a back-pressure regulator, (9) another 275-gal. reservoir for fuel collection, and (10) a nitrogen purge system. The apparatus was located in a concrete test cell and operated remotely from a separate control room. It was capable of continuous operation at fuel flow rates up to 200 lb/hr and pressures up to 1000 psig.

The test tubes were fabricated from AISI 316 stainless steel except in one test, in which an Inconel 600 tube was used to study surface material effects. The standard length of the test tubes was 8-ft. However, a few tests were conducted using 4-ft tubes in order to investigate the effect of fuel residence time. All tests were conducted with 0.125-in. OD \times 0.020-in. wall tubes.

Each 8-ft test tube was instrumented with thirty-three thermocouples (spaced every 2 to 3.5 in.) to measure the outside wall temperature distribution. Twenty-six thermocouples (spaced every 1.5 to 2 in.) were used along the 4-ft tube. Fuel pressures and temperatures were measured at the tube inlet, tube exit, and at three equally spaced intermediate locations along the 8-ft tube and two equally spaced locations along the 4-ft tube. A schematic drawing of an instrumented 8-ft tube is shown in Figure 7. Absolute fuel pressures were measured at the tube inlet and exit, and differential pressure transducers were used to measure pressure drops across each 2-ft section of the tube. In order to measure fuel temperatures within the heated tube, without introducing preferential sites for deposition (as would result from use of immersion thermocouples), an alternative procedure, used successfully in an earlier program (Reference 7), was adopted. It involves installation of short (0.75-in. long) sections of heavy-wall 316 stainless steel tubing (0.375-in. OD \times 0.085-in. ID) at the desired measurement locations, which, because of their low electrical resistances relative to the thin-wall test tube, result in negligible local heat generation. Thus, these short sections of tubing are not heated electrically, but by convective heat transfer from the fuel. It was experimentally verified that, over the range of test conditions, the outer wall temperatures of the heavier cylinders very closely approximated (within 8°F) the fuel temperature as measured by fine-wire immersion thermocouples.

In order to obtain an accurate measurement of wall temperature, each thermocouple was electrically isolated from the tube by a thin layer of ceramic paint. The thermocouple junction, whose size was no greater than 0.010-in., was tightly pressed against the tube and then secured with additional layers of ceramic cement. In order to minimize heat losses to the surroundings, the tube was inverted into a rectangular box which was completely filled with bulk Fiberfrax insulation.

A standard procedure was used for tube fabrication. Prior to assembly, all tubing and fittings were soaked in acetone, rinsed and blown dry with clean filtered nitrogen. The tube sections, fittings and bus-bar connections were then silver soldered together and pressure checked to ensure no blockage in the tube. Prior to testing, the tube assembly was again soaked in acetone, rinsed, and blown dry with clean filtered nitrogen.



FD 267807

Figure 7. Test Assembly Instrumentation

C. DATA ACQUISITION AND CONTROL SYSTEM

All test data were recorded using a microprocessor-controlled datalogger. The data system is capable of scanning up to 70 input channels continuously or at pre-programmed scan intervals at a scan rate of 35 channels per second. It records the output signals from thermocouples, pressure transducers, etc., in precisely scaled d-c voltages, converting and displaying the data in appropriate engineering units. The data were output simultaneously on paper tape and on magnetic tape at programmed intervals. The paper tape was used for on-line data examination, and the magnetic tape was used for post-test data manipulation on a UNIVAC 1100 computer system. A built-in cathode ray tube displayed key operating variables, thereby providing a continuous visual display of up to 13 channels. In the event that any variable exceeded a specified set point, automatic shutdown procedures were initiated.

The data reduction program was used to calculate heat transfer coefficients at each wall temperature measurement location, and friction factors across each 2-ft section of tubing. A linear interpolation procedure was performed to obtain the local bulk fuel temperature distribution. The local bulk fuel temperatures used in the calculations were derived from the fuel temperature distributions measured at the start of a test.

D. TEST MATRIX AND OPERATING PROCEDURES

The experimental program consisted of two parts: (1) a series of parametric screening tests using the baseline (NAPC-5) fuel, and (2) a series of tests designed to evaluate the thermal stability and deposition characteristics of three alternative fuels. The baseline test matrix was structured to permit evaluation of fuel thermal stability and deposit heat transfer over a range of conditions encompassing the intended application limits, and to identify an appropriate set of test conditions for alternative fuel evaluations. The baseline test matrix comprised fuel inlet pressures of 400 and 800 psig, fuel flow rates of 45, 60 and 75 lb/hr (tube entrance Reynolds number of 2250, 3000 and 3750), a fuel exit temperature of 900°F, tube material of Inconel 600 and 316 stainless steel, and test durations ranging from 1 to 20 hours.

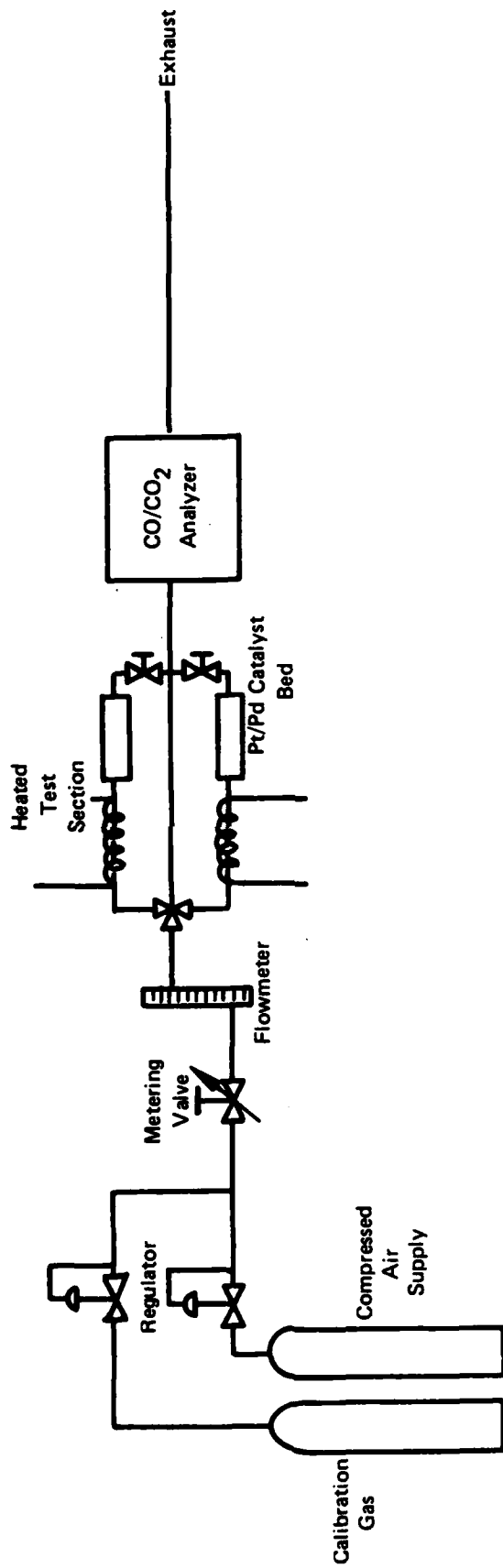
Based upon the results of the baseline fuel testing, tube surface temperature was identified as the key physical variable affecting deposit formation. The ranges of other specific test

variables were adjusted as required to elucidate their effect on deposit formation. Therefore, the alternative fuel test matrix comprised fuel flow rates of 60 and 120 lb/hr (tube entrance Reynolds numbers of 3000 and 6000), fuel exit temperatures of 500, 700 and 900°F, and test times of 1, 5, and 10 hours. The baseline pressure was maintained at 400 psig, except in one test which was run at 800 psig.

As described earlier, each tube was thoroughly cleaned prior to testing and the fuel in the supply tanks was saturated by sparging with air for a minimum of twenty-four hours. Fuel filters were changed prior to each test. The test was initiated by adjusting the back pressure regulator and fuel bypass metering valve until the desired pressure and flow rate was obtained. The power supply was then activated and the power level was adjusted until the desired fuel exit temperature was achieved. The time necessary for achievement of a steady fuel exit temperature was typically less than one minute. The interlocks were then activated allowing unattended operation, and data acquisition was initiated and continued at regular programmed intervals. Any improper thermocouple attachments were readily identified from the initial wall temperature profiles and those were ignored in data analysis. At the conclusion of the test, the fuel flow and power were simultaneously terminated and a three minute nitrogen bleed initiated. The test tube was then removed and sectioned for deposit analysis.

The quantity of deposit accumulated was determined by oxidizing several 2-in. tube sections in heated air with continuous analysis of the evolved gases. The 2-in. sections were obtained by carefully sectioning the 8-ft test tube. Tube sectioning was done in steps, first dividing the 8-ft tube into four 2-ft lengths for ease of handling. Four 2-in. sections to be used in the burnoff (oxidation) tests were then cut from each 2-ft length of tube using a special jig that was designed to minimize tube vibration and heating and thereby preserve the morphology of the deposit. A jeweler's saw with a 0.012-in. thick blade was used to cut the tubes. To permit optical inspection of the tube inner surface, short (0.25-in. long) axial sections were made adjacent to each burnoff sample. All remaining test tube pieces were identified by run number and location.

The quantity of carbon deposited in each tube specimen was measured using a deposit burnoff apparatus shown schematically in Figure 8. Prior to analysis, each 2-in. specimen was vacuum dried at 250°F for a minimum of sixteen hours to remove any residual liquid fuel. The tubes were then installed in the burnoff apparatus, placed inside a high temperature laboratory furnace and the deposit was reacted with heated air, which was flowing through the tube. The effluent gas stream was passed through a catalytic converter to ensure complete oxidation of all carbonaceous species of CO₂ and was continuously analyzed for both the CO and CO₂ concentrations. The output of a dual gas nondispersive infrared analyzer (Infrared Industries, Model 702) was continuously recorded on a two-pen strip chart recorder. The deposit (i.e., carbon) mass was determined from a knowledge of the air flow rate and the concentrations of CO and CO₂ in the reaction products. This procedure was checked by running several calibration runs in which pre-weighed samples of spectrographic grade carbon (ranging from 5 to 25 mg) were oxidized. Agreement between the amount of carbon input and the amount calculated in the exhaust products was consistently within five percent.



FD 267808

Figure 8. Deposit Burnoff Apparatus

SECTION IV

EXPERIMENTAL RESULTS AND DISCUSSION

The experimental program comprised (a) a series of nine tests designed to establish baseline thermal stability and heat transfer data for NAPC-5 fuel (JP-5) and to verify the adequacy of the technical approach, and (b) a series of eighteen tests to evaluate the thermal stability of three alternative fuels over appropriate ranges of temperature, pressure, flowrate and test time. A discussion of the results of these experiments is contained in the following sections. A tabulation of all the heat transfer data, including calculated parameters (e.g., fuel side heat transfer coefficients, tube friction factors, and deposit thicknesses) is contained in a separately bound Comprehensive Data Report. Deposit formation results are presented in tabular form in Volume II.

A. BASELINE FUEL TESTS

As stated earlier, the purpose of the initial tests was to establish a data base using a well characterized fuel and to identify the important physical parameters that affect deposit formation. The experiments were designed to evaluate the effects of key operating variables, such as test duration, fuel pressure and temperature, and fuel flow rate, and to determine the impact of deposits on the fuel system heat transfer characteristics. Several items were considered to be of importance when formulating the baseline fuel test matrix. It was considered necessary that measurable amounts of deposits and significant increases in tube wall temperatures be obtained over a relatively wide range of wall temperatures so that the meaningful trends could be developed. It was also important that the data be obtained over relatively short test times so that unacceptably large quantities of fuel would not be required for each test. A constant exit fuel temperature of 900°F was chosen as the baseline and resulted in a relatively wide range of surface temperatures (i.e., approximately 500 to 980°F). This condition was considered to satisfactorily meet the above-mentioned requirements. A summary of the test conditions is given in Table 2.

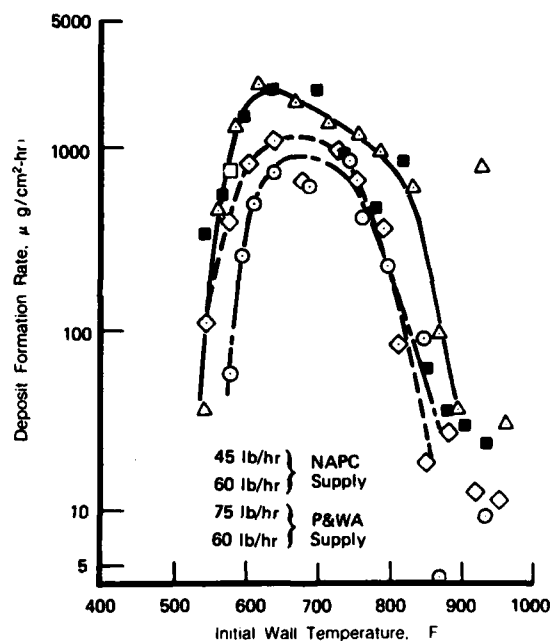
TABLE 2. SUMMARY OF NAPC-5 TEST CONDITIONS

<i>Fuel Source</i>	<i>Test No.</i>	<i>Test Duration (hr)</i>	<i>Flow Rate (lb/hr)</i>	<i>Pressure (psig)</i>	<i>Tube Length (feet)</i>	<i>Tube Material</i>	<i>Exit Fuel Temp (°F)</i>	<i>Comments</i>
NAPC	1	19.5	45	400	8	316 SS	900	Continuous
NAPC	2	19.0	60	400	8	316 SS	900	Continuous
P&WA	4	14.0	75	400	8	316 SS	900	Continuous
P&WA	5	14.0	60	400	8	316 SS	900	Continuous
P&WA	6	10.5	60	400	8	316 SS	900	Continuous
P&WA	7	1.2	60	400	8	316 SS	900	Continuous
P&WA	8	18.0	60	400	8	Inconel 600	900	Continuous
P&WA	9	10.0	60	400	8	316 SS	900	Intermittent (2 hr hot fuel, 1 min cold fuel)
P&WA	10	8.0	60	800	8	316 SS	900	Continuous
NAPC	3	19.0	60	400	8	316 SS	900	Heat stressed fuel recycled from Test No. 2

Although all the baseline fuel originated from the same lot, two different batches were received. Approximately 400 gal were shipped directly from NAPC, and approximately 750 gal were transferred from P&WA as residual Government Property. Because minor variations in fuel composition can have a very significant effect on thermal stability, the batches were kept

separate and subjected to independent analyses to identify any possible differences. Several independent laboratories analyzed the two NAPC-5 fuel supplies for copper, iron, sulfur, and nitrogen and the results indicated that, within each laboratory analysis, there were no dissimilarities. However, JFTOT tests performed on a sample from the P&WA supply subsequent to baseline testing indicated a failure to satisfy the pressure drop criterion at a temperature of 480°F, as compared with a breakpoint temperature value of 520°F reported for the NAPC fuel supply.

Tests were conducted to investigate whether fuel flow rate (velocity) had an effect on deposit formation. Tests were conducted at fuel flow rates of 45, 60, and 75 lb/hr for constant fuel exit temperature (900°F), pressure (400 psig), and wall material (316 SS). The results of these tests are presented in Figure 9. The deposit mass fractions relative to the total fuel throughput, as determined from the curves in Figure 9, are presented in Table 3 for various values of initial wall temperature. In addition, the integrated weight fraction of deposit determined for the entire 8-ft length of tubing is presented for each of the three tests, as well as for an additional test performed with the P&WA fuel batch at a flow rate of 60 lb/hr.



FD 267809

Figure 9. Effect of Flow Rate on Carbon Deposition from NAPC-5 Fuel

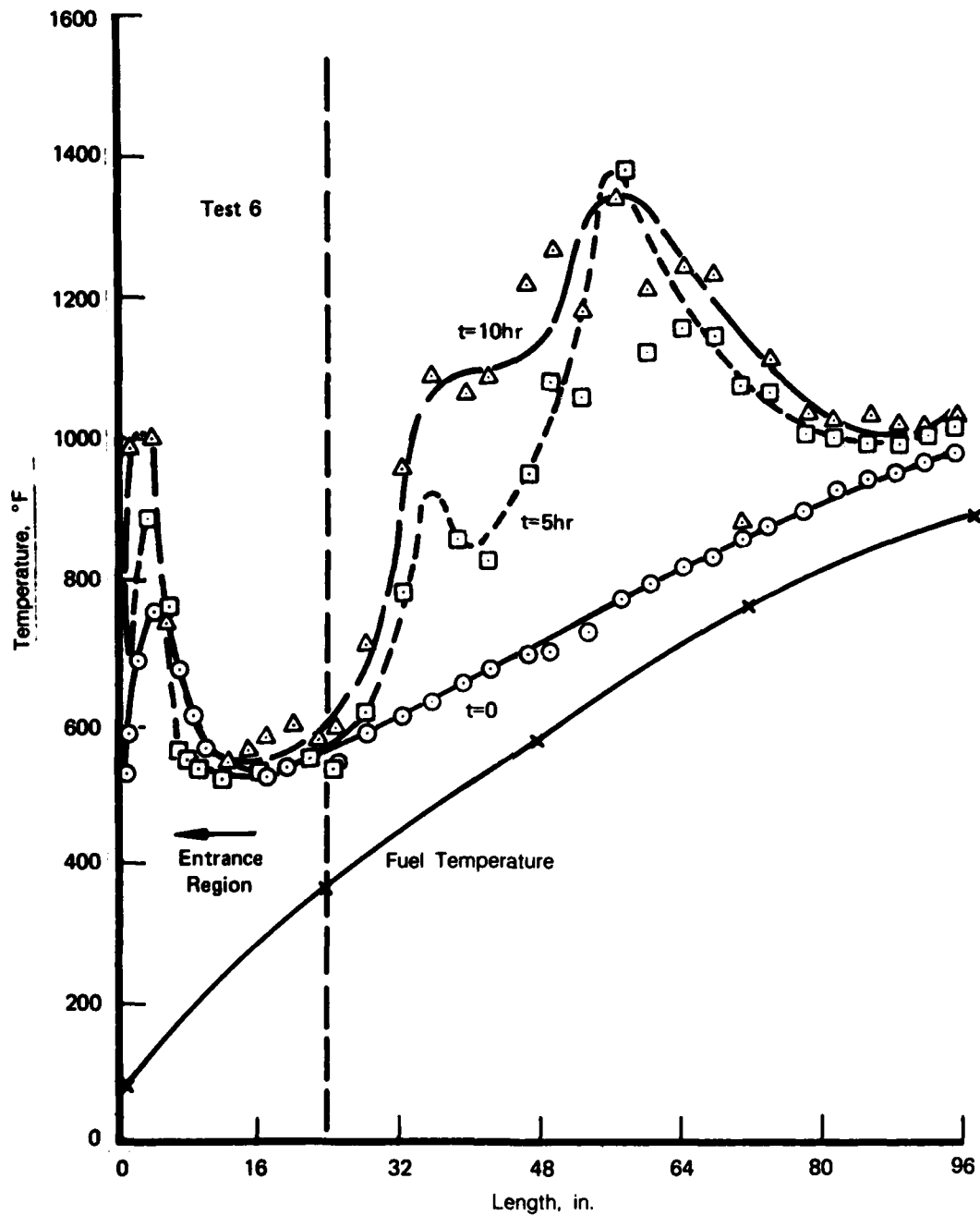
The curves presented in Figure 9, together with data shown in Table 3, suggest that there may have been a difference in the composition of the two batches of NAPC-5. Although the fuel analyses did not reveal any obvious dissimilarities in trace contaminants, the analyses were limited regarding the number of species analyzed. Stability temperatures measured with a JFTOT apparatus did confirm that there were some differences in fuel supplies which manifested themselves in different stability levels. The differences in total deposit weight fractions between the P&WA fuel and the NAPC fuel supply indicate that the amount of fuel which participated in deposit formation was approximately fifty percent higher with the P&WA fuel supply. The data in Figure 9 indicates that flow velocity appeared to have an effect on the rate of deposition from the NAPC fuel supply; however, no noticeable effect was observed with the P&WA fuel supply. Because questions concerning fuel contamination render the results inconclusive, flow velocity was retained as a variable to be investigated with the alternative fuel.

Table 3. TUBE DEPOSIT DISTRIBUTION FOR NAPC-5 FUEL

Wall Temperature (°F)	Deposit Mass/Unit Area/Total Mass of Fuel (ppm/cm ² × 10 ²)			
	45 lb/hr	60 lb/hr	75 lb/hr	60 lb/hr
	NAPC Supply	NAPC Supply	P&WA Supply	P&WA Supply
575	0.29	1.285	2.09	2.53
600	1.47	2.64	4.76	5.32
625	3.05	3.74	5.95	6.64
650	4.00	4.18	5.86	7.16
675	4.41	4.21	5.31	7.25
700	4.35	4.03	4.76	6.88
725	3.92	3.48	4.18	5.69
750	3.05	2.61	3.51	4.33
Integrated Total Deposit Weight Fraction	1.27	1.33	2.04	2.27

Typical tube wall temperature distributions are plotted in Figure 10 for three test times. The first 16 to 24-in. of the tube is dominated by entrance effects (i.e., a thermal boundary layer and transition from laminar to turbulent flow). All deposit formation data are obtained in the region of fully-developed turbulent flow downstream of the entrance region. The length of tube influenced by these entrance effects is strongly dependent on the fuel flow rate. Downstream of this region, the initial wall and fuel temperature gradients remain similar for the remainder of the tube. As fuel deposits form on the tube wall, the outer wall temperature begins to increase. The magnitude of the temperature increase is indicative of the amount of deposit formed. For example, for Test 6 shown in Figure 10, peak deposits occurred in the center of the tube. This response of wall temperature to deposit formation was typical of all tests performed.

Knowledge of the effect of surface material composition on deposit formation is necessary for the design of engine fuel system components. Based on a review of materials commonly used in aircraft engine fuel systems, it was concluded that, except for stainless steel, Inconel alloy was the most likely alternative material. Therefore, because of its ready availability, Inconel 600 alloy was chosen for additional testing. The Inconel tube sizes selected were identical to the 316 stainless steel tubes and, because of the similarities in electrical properties, input power levels were approximately equal. A test was performed at the same operating conditions as had been run previously, and the results shown in Figure 11 indicated that the temperature profile histories obtained on an Inconel 600 surface were nearly the same as those obtained on a 316 stainless steel surface over axial locations ranging from approximately 24 to 96-in. At axial locations less than 24-in., where entrance effects predominate, the Inconel 600 material had a markedly different effect on deposit formation, compared to the 316 stainless steel surface. Deposit formation rates measured at tube locations less than 24-in. for the Inconel 600 test were approximately a factor of three larger than those for 316 stainless steel (average of 520 μ g/cm²-hr for Inconel 600 and 180 μ g/cm²-hr for 316 stainless steel). It should be noted that deposit rates measured at tube locations less than 24-in. are not included in any of the subsequent deposit formation rate figures. In this area, the effect of the deposit thermal resistance on wall temperature is negligible when compared to the thermal entrance effects and the effect that transition to turbulent flow has on heat transfer. Therefore, correlations of deposit resistance with wall temperature are of no value to this area.

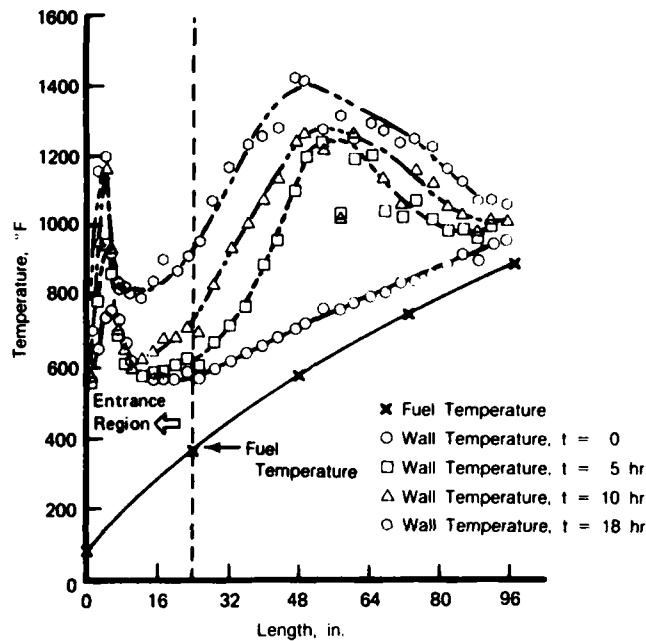


FD 267810

Figure 10. Tube Wall Temperature Distribution for NAPC-5 With SS316 Tube

A composite plot of all the deposit data obtained with NAPC-5 fuel is presented in Figure 12. The results indicate that the rate of carbon deposition increases with increasing temperature, reaches a maximum of approximately $2000\mu\text{g}/\text{cm}^2\text{-hr}$ at an initial wall temperature of approximately 700°F , and then falls off as temperature is increased further. Taylor (Reference 3) has reported a similar trend of wall temperature on deposit formation with air-saturated fuel. However, the magnitude of the deposit rates are higher in the present study. This

may be due to differences in the experiments, as well as the fact that Taylor had a very limited amount of data at conditions corresponding to peak formation. As is shown in the figure, deposit formation rate is strongly dependent on initial wall temperature and, therefore, the effects of other variables on deposit formation are not easily distinguished. The magnitudes of deposit formation rates compare favorably to those reported previously for Jet-A (Reference 7), but are approximately an order of magnitude higher than those reported by Taylor for air-saturated JP-5 (Reference 3).

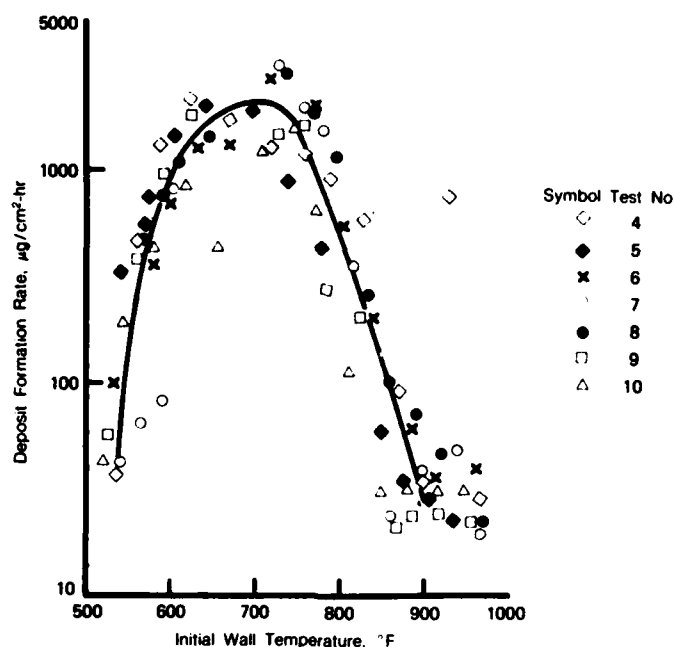


FD 267811

Figure 11. Tube Wall Temperature Distribution for NAPC-5 With Inconel 600 Tube

The effect of pressure on fuel thermal stability was investigated by performing Tests 5 and 6 at 400 psig, and Test 10 at 800 psig. Results (shown in Figure 12) indicate that, over the range of pressures investigated and within the experimental accuracy of the data, fuel thermal stability is not affected by operating pressure.

Test 9 was run to investigate whether intermittent fuel heating had any effect on deposit formation. A duty cycle, consisting of two hours of hot fuel flow followed by one minute of cold fuel flow, was repeated five times for a total test duration of ten hours. Results of the deposit burnoff measurements showed that intermittent operation had little effect on the amount of deposit formed. This was corroborated by the observation that, in almost all cases, upon the resumption of fuel testing the tube wall temperatures returned to their previous values prior to turning the electrical power off. There were a few minor exceptions to the typically observed behavior of wall temperature but, in general, intermittent operation had little or no effect on deposit formation of heat transfer.



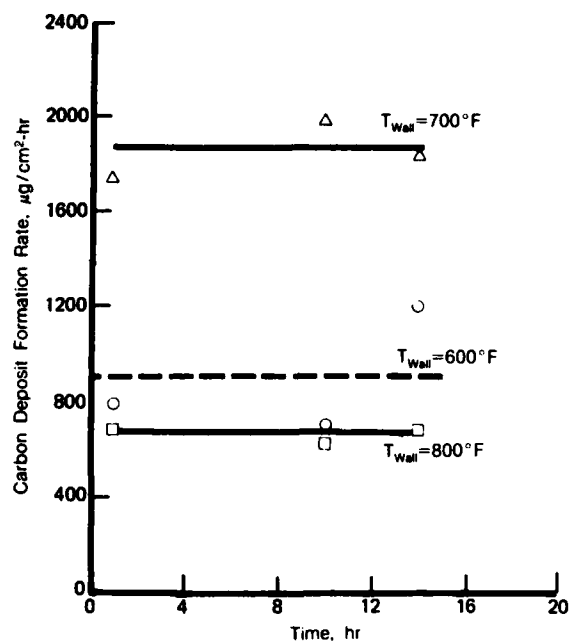
FD 267812

Figure 12. Rate of Carbon Deposition for NAPC-5 Fuel

Obviously, the time required for completing a test has a direct impact on the desirability of using this test procedure for determination of fuel thermal stability; therefore, test durations ranging from one to 18 hours were investigated. Because of the previously mentioned uncertainty regarding fuel contamination, only tests performed with the P&WA supplied NAPC-5 were used for this comparison. The data plotted in Figure 13 represent values extracted from a best approximation of the deposit formation rate versus temperature for the baseline operating condition (i.e., 60 lb/hr, 400 psig and 316 SS). Some of the data scatter is due to oscillations in tube wall temperatures caused by automatic cycling of the input power to maintain constant exit fuel temperatures. These oscillations could account for a wall temperature variation of approximately 7°F. Also, as deposits form, the porosity and roughness of the surface will change and this may affect the deposition rate. Furthermore, flaking is more likely to occur as the deposit thickness increases. It is clear that several explanations for the observed data scatter are possible. However, because there are no obvious trends with time evident in the data, it was concluded that deposit formation rate was not a strong function of test duration. Consequently, it was possible to significantly reduce the test duration, thereby resulting in a simplification of the test procedure for evaluating fuel thermal stability.

Histories of pressure drops across successive 2-ft increments of tube, and selected wall temperatures are presented in Figures 14 and 15, respectively. The magnitude of the pressure drop across the last section (72 to 96 in.) of the tube is substantially higher at the beginning of the test because it is in this region where the thermodynamic critical temperature of the fuel is reached, resulting in a large decrease in fuel density and therefore a large increase in velocity. Because pressure drop is inversely proportional to the fluid density (at constant mass flow per unit area), the pressure drop is increased significantly, as is shown. The temperatures plotted in Figure 15 correspond to temperature measurements at the entrance, exit, and midpoint of the third section of tubing (48 to 72 in.). The rate of temperature rise is relatively large during the first five hours of the test. However, the wall temperatures eventually begin to level off, suggesting a decrease in the rate of deposit formation, or a change in the deposit thermal

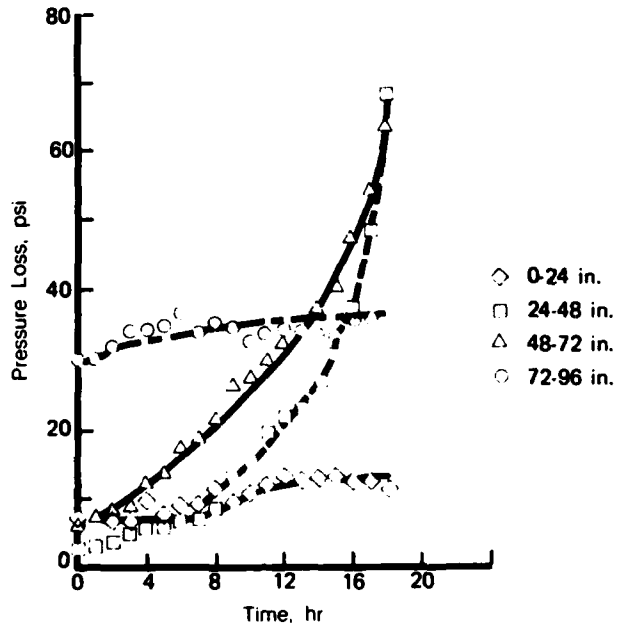
resistance or the forced convection heat transfer coefficient. At locations where a temperature plateau is evident, the pressure loss (shown in Figure 14) continued to increase, indicating that deposits were still being formed. The rate of increasing pressure drop in the two middle sections (24 to 48-in. and 48 to 72-in.) appears to correspond roughly to a linear increase in the rate of deposit buildup (i.e., the pressure profile is similar to what would exist for a linear decrease in tube diameter), suggesting approximately constant deposit formation rate. This observation, together with the levelling-off of the wall temperature, suggests that while deposits are still being formed on the tube walls, the structure of the deposit was changing (e.g., decreased porosity, increased roughness, etc.) in a way that increased the heat transfer characteristics (i.e., heat transfer coefficient and/or the deposit thermal conductivity).



FD 267813

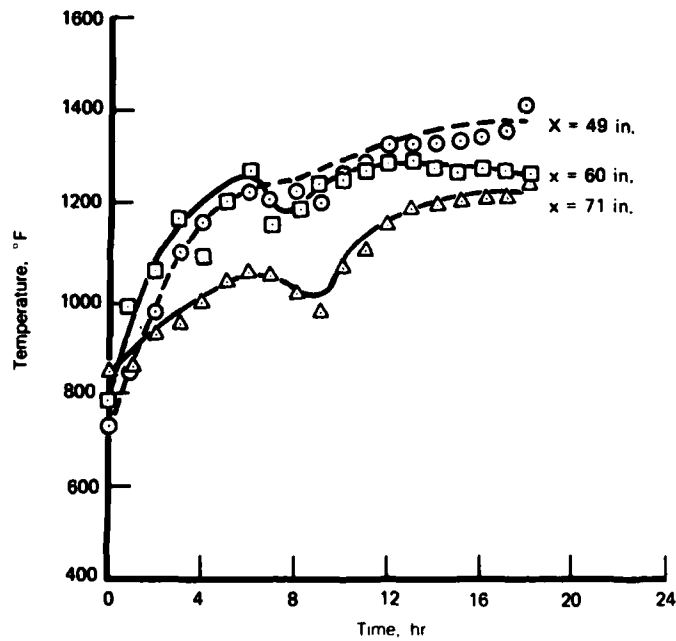
Figure 13. Effect of Time on Deposit Formation Rate

Evidence of such a change in surface morphology is presented in Figure 16, where deposit samples obtained from a long duration (18 hr) test and a short duration (5 hr) test are compared. The tube samples were obtained at the same axial locations near the midpoint of the tube. The deposit surface corresponding to the long duration test is clearly much rougher than that of the short test and enhanced heat transfer is therefore to be expected. To what level the heat transfer coefficient has been increased as a result of increased surface roughness cannot be accurately determined from the data available. In the sections having relatively light deposit accumulation (i.e., due to short test duration or low formation rates) the deposits were soft and powdery, whereas heavy deposit accumulations were hard, crystalline, and covered by a soft powdery surface coating. It is hypothesized that the thermal conductivity of the loosely bound powder is much lower than that of the harder more crystalline deposits. The poorer thermal conductivity attributed to the powdery deposits might result from low thermal conductivity fuel occupying the voids between the individual particle agglomerates, thereby resulting in a lower overall thermal conductivity of the deposit layer, as compared to values reported in the literature for carbon or graphite. Further discussion and some experimental verification of this hypothesis is contained in later sections.



FD 267814

Figure 14. Pressure Drop History for NAPC-5 Test



FD 267815

Figure 15. Wall Temperature History for NAPC-5 Test

5 hr
Test Duration



18 hr
Test Duration



FD 267816

Figure 16. Deposit Surface Morphology for NAPC-5 Test

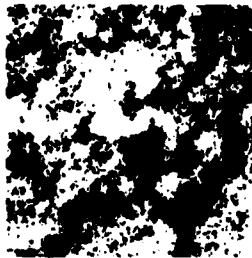
A limited number of NAPC-5 deposit samples were analyzed to determine their elemental composition, using a Scanning Electron Microprobe (SEMP). A qualitative scan of elements, with atomic numbers greater than twelve, is produced using an X-ray Energy Dispersive Spectrometer (EDS), which has a reported detectivity limit of approximately 200 ppm. A selective wavelength spectrometer was then used for qualitative X-ray mapping of selected elements. The mapped area matches exactly the Scanning Electron Micrograph (SEM) taken of the sample. White dots on a dark background serve to indicate the presence of an element. The elemental concentration is proportional to the density of the white dots. A SEMP analysis was made of three deposit samples taken from Test 6, one from the entrance region (5.5-in.) and two from the peak deposit area (54.0-in. and 59.0-in.). Single samples were taken from peak deposit areas (54.0-in.) of Tests 2 and 5. The samples from Test 6 and Test 2 were obtained by scraping some of the deposit from the tube surface prior to mounting. However, the Test 5 sample was mounted and polished intact, i.e., without removing the deposit from the tube surface. Selected elements scanned included C, O, N, S, Fe, Cu, K, Cl, Pb, Si, Zn and Cd. Except for the element shown in the ensuing figures, no differences in the concentrations of elements was noted in any samples analyzed. Results obtained from samples taken at the entrance region and at the 59.0-in. location of Test 6 are shown in Figure 17. It can be seen that the concentration levels of copper and sulfur are much higher in the entrance region than in the center region, where the deposit formation rates peak. However, concentrations of carbon, oxygen and nitrogen are similar throughout. It is well known that contaminants such as sulfur and copper significantly increase deposit formation rates. The high concentrations of Cu and S in the entrance region indicate that the contaminants act as catalysts resulting in accelerated reactions and higher than expected deposition rates at moderate fuel temperatures.

SEMP analyses were performed on samples taken from Tests 2 and 6 at the same axial locations and similar local run conditions. However, comparison of the SEMP data offers no explanation for the observed differences in deposition rates between the two different batches of NAPC-5 fuel tested. All the elements mentioned earlier were selectively analyzed and no differences in concentrations were observed.

The relatively high deposit rates observed in the entrance region are believed to be caused by the relatively high concentrations of impurities in the fuel. This observation, together with the observed decline in deposit formation rate at temperatures greater than approximately 750°F, suggests that fuel preheating might eliminate many of the deposit forming precursors and subsequent runs might result in higher thermal stability. Therefore, a test was conducted to investigate the effects of fuel prestressing on deposit formation. The fuel heated in Test 2 was collected, air-saturated and recycled through a new instrumented tube at the same operating conditions as in Test 2. The deposit burnoffs performed with tube samples taken from this test indicated that a significant reduction in deposit formation rates occurred over the entire range of wall temperatures, as indicated in Figure 18. The results of a SEMP analysis of a deposit sample taken at the peak formation location is shown in Figure 19 together with the analysis of Test 2. No significant differences in composition are evident, except that the sulfur content of the deposit formed from prestressed fuel was significantly lower than that of the unstressed fuel. Although further experimental work is required before any definitive conclusions regarding the benefits of fuel prestressing can be drawn, these initial results are encouraging.

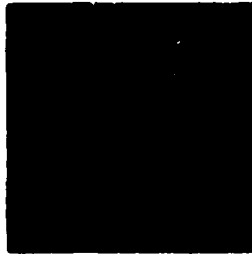
Test 6
Samp Analysis

Carbon

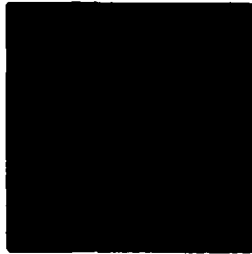


Entrance
Region
(x 5 in.)

Oxygen



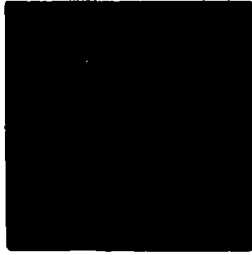
Nitrogen



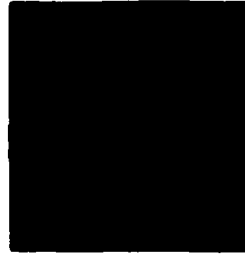
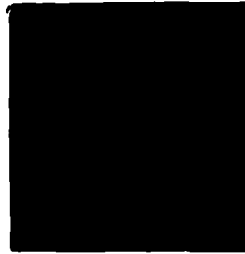
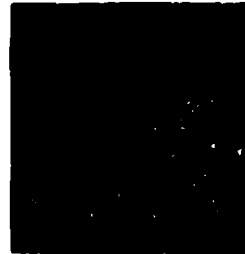
Copper



Sulfur

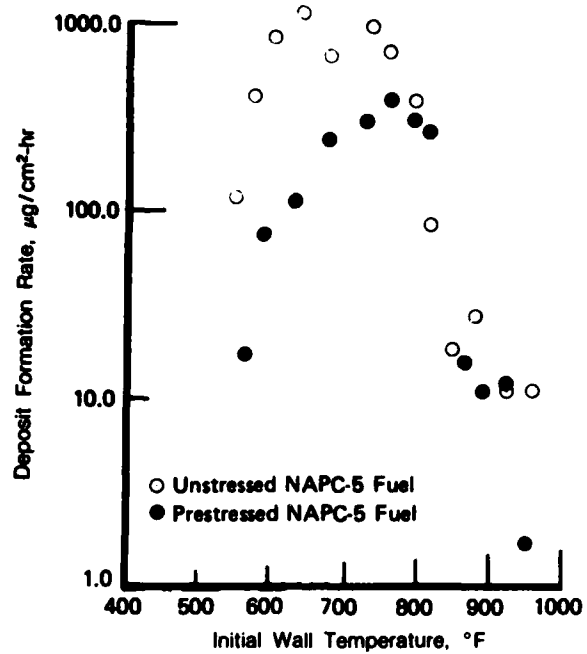


Midspan
(x 59 in.)



FD 207617

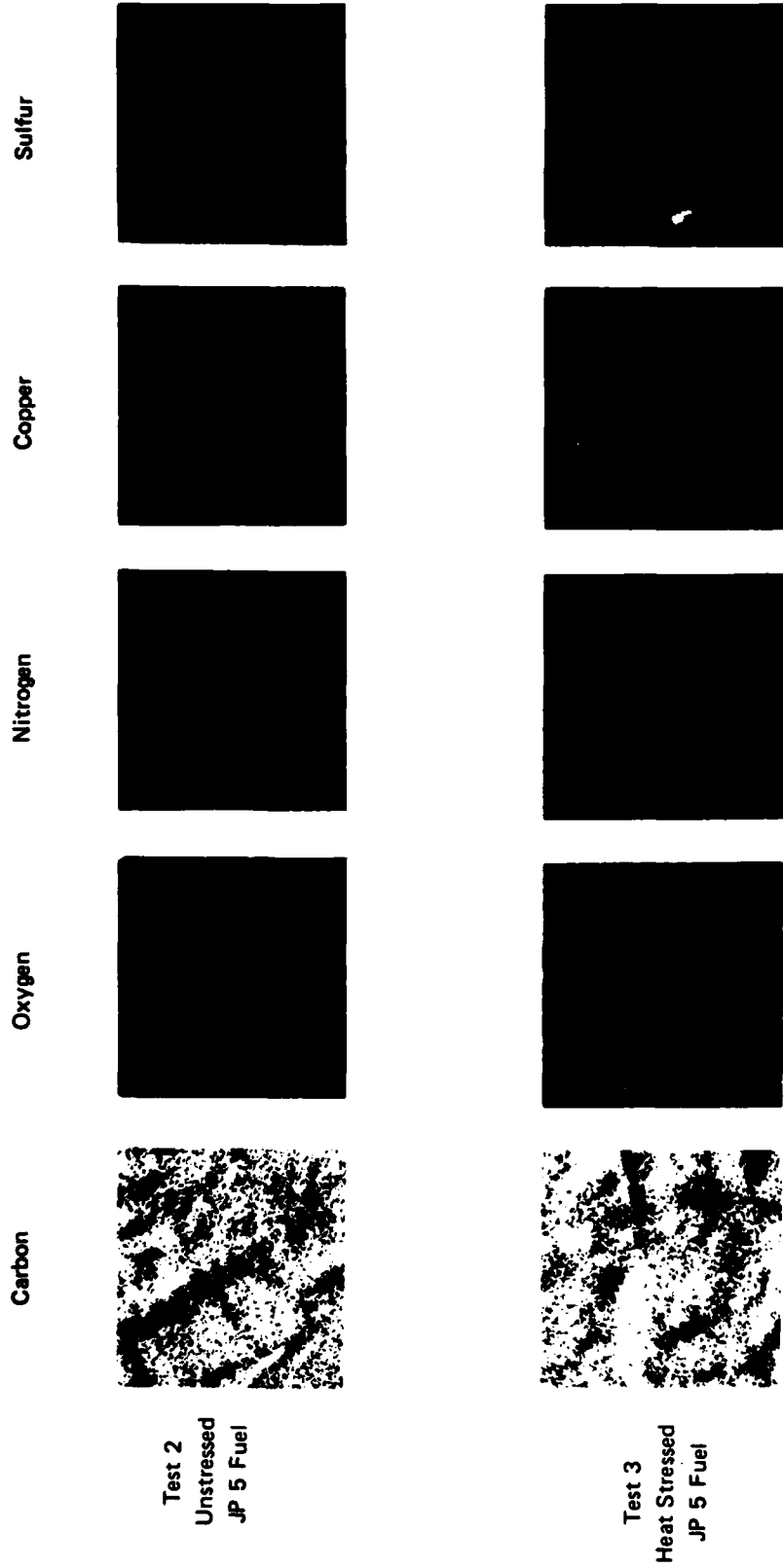
Figure 17. Composition of NAPC-5 Deposits



FD 267818

Figure 18. Effect of Fuel Prestressing on Carbon Deposition

Semp Analysis
x 54 in.



FD 267819

Figure 19. Effect of Fuel Prestressing on NAPC-5 Deposit Composition

The photomicrograph taken of the mounted deposit sample from Test 5 is shown in Figure 20. A deposit thickness of 0.005-in. was measured from the photograph (magnification of 400X), and a deposit mass of 44.1 mg was determined for a 2-in. tube sample using the data in Figure 12. Assuming that the deposit thickness is uniform, a density of approximately 1 gm/cm³ is indicated. This value is in good agreement with deposit densities determined in Reference 11. Deposit thicknesses were calculated from the equation defining the overall heat transfer coefficient:

$$1/U - 1/h = t/k, \quad (1)$$

where h is the forced convection heat transfer coefficient of a clean tube (time = 0), U is the overall heat transfer coefficient after deposit formation (time > 0), t is the deposit thickness, and k is the deposit thermal conductivity. A deposit thermal conductivity value of 0.12 Btu/hr-ft-°F resulted in agreement between the measured deposit thickness (0.005-in.) and that calculated from the heat transfer measurements. Values of 0.11 or 0.55 Btu/hr-ft-°F for deposit thermal conductivity were recommended in Reference 12, whereas a value of 0.07 Btu/hr ft-°F was recommended in Reference 13. For these deposit thickness calculations, it was assumed that deposit thermal conductivity remained constant with time.

B. NACP-7 FUEL TESTS

Upon completion of the baseline test series and analysis of the data, a plan for alternative fuel testing was formulated. The first of three alternative fuels to be tested was a fuel mixture consisting of 80 percent JP-5 and 20 percent hydrocracked gas oil. It was designated as NACP-7 and had a JFTOT breakpoint temperature of 500°F. A summary of these test conditions is shown in Table 4. Because the results of the baseline fuel tests indicated that test duration did not appear to have a significant effect on deposit formation rate, the recommended baseline test duration was reduced from 20 hours to 5 hours. As a result, the quantity of fuel required to complete a test was considerably reduced. These two improvements in test procedure resulted in a more manageable test procedure for thermal stability measurements. However, to serve as a check on the validity of the conclusion regarding the behavior of formation rate with time, the effect of varying test duration was retained as a parameter to be investigated. Repeatability of test data was checked by performing two tests at identical run conditions. The effect of candidate tube surface material was not considered an important effect on deposit formation in the area downstream of the transition zone. Therefore, surface material was not retained as a variable in the alternative fuel test matrix. In order to more clearly elucidate the effect of fuel flow rate on deposit formation rates, the range of flowrates which were investigated was increased. In addition, a test was conducted with a shorter tube in order to investigate the effect of residence time and heat flux as well as to determine whether the results obtained from the apparatus were configuration dependent. Finally, a test was performed at a lower exit fuel temperature in order to obtain more data at temperatures more closely approximating engine conditions, where deposit formation is a strong function of initial wall temperature.

Deposit formation rates obtained from all the tests performed with NACP-7 fuel are displayed in Figure 21. The effect of surface temperature on NACP-7 fuel deposition rate is similar to that presented earlier with the NACP-5 (JP-5) baseline fuel; i.e., a maximum formation rate at intermediate wall temperature, with a strong functional dependence on temperature at higher and lower temperature levels. An average curve through the data indicates a maximum deposit formation rate of approximately 1400 μg/cm²-hr can be expected. Deposit formation rates obtained from the shorter tube (4-ft) were consistently higher than those obtained for any tests using the standard 8-ft tube length (cf., Tests 11, 12 and 19). Also, the results obtained with NACP-7 indicate that there is no detectable effect of test duration on the deposit formation rate (cf., tests 11, 12 and 17), in agreement with the conclusions drawn

from the NAPC-5 tests. In addition, no noticeable effect of increasing flow rate from 60 lb/hr to 120 lb/hr was observed (cf., Tests 11, 12 and 16). As a further substantiation of conclusions drawn from the baseline fuel tests, deposit formation rates were independent of operating pressure over the range investigated (cf., Tests 11, 12 and 18). The formation rates obtained from the test performed at the lower exit fuel temperature (Test 15) agreed in the region of overlap with the rates determined from the higher temperature tests. Finally, the deposit rate data from two identical tests are repeatable to within approximately ten to fifteen percent, as shown in Figure 22, (e.g., rates at 600°F are 100 $\mu\text{g}/\text{cm}^2\text{-hr}$ and 85 $\mu\text{g}/\text{cm}^2\text{-hr}$ and at 700°F the rates are 850 $\mu\text{g}/\text{cm}^2\text{-hr}$ and 950 $\mu\text{g}/\text{cm}^2\text{-hr}$ for Tests 11 and 12, respectively).

One objective of the program was to determine the effect of deposit formation on heat transfer. As seen from the temperature profiles presented earlier (Figures 10 and 11), the deposit layer acts as a thermal barrier to heat transfer and results in increasing wall temperatures for a constant input heat flux. A simple model was used to approximate the effect of the deposit layer on heat transfer and is graphically illustrated in Figure 23. The bulk fuel temperature (T_b) and the outer wall temperature (T_{w_o}) were measured at the beginning of each test. The present model assumed that the measured outer wall temperature equaled the inner wall temperature (i.e., $T_{w_i} = T_{w_o}$). This assumption was checked using a finite difference heat transfer code (TCAL) which calculates the steady-state or transient temperature distribution of the modeled configuration. The assumption of negligible temperature drop was checked at a baseline test condition (i.e., 60 lb/hr, 900°F, 400 psig and 8-ft tube length). A radial temperature drop of only 14°F was calculated at the midpoint axial location on the tube. Therefore, the radial temperature drop was ignored for all calculations, resulting in an approximate maximum error of five percent.

The fuel-side heat transfer coefficient, h , is calculated from:

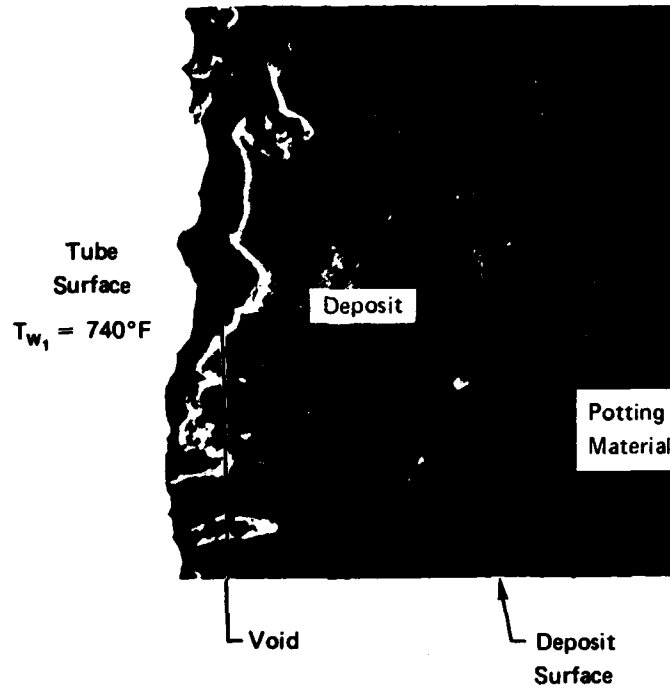
$$Q/A = h (T_{w_o} - T_b). \quad (2)$$

The temperatures and heat fluxes used in the calculation were measured at the beginning of each test, prior to the formation of fuel deposits. It was assumed that the fuel side heat transfer coefficient remained constant throughout the duration of each test and that the interface between the fuel and deposit remained at the initial wall temperature, thereby resulting in a constant fuel temperature, since the heat flux was held constant. The increase in measured outer wall temperature is therefore assumed to be caused entirely by the formation of a deposit layer. The temperature profile after deposit formation (time $\mu 0$) is depicted by the broken line in Figure 23 and the deposit surface temperature, T_d , remains at the initial inner wall temperature. The overall heat transfer coefficient, U , is calculated at all subsequent times by:

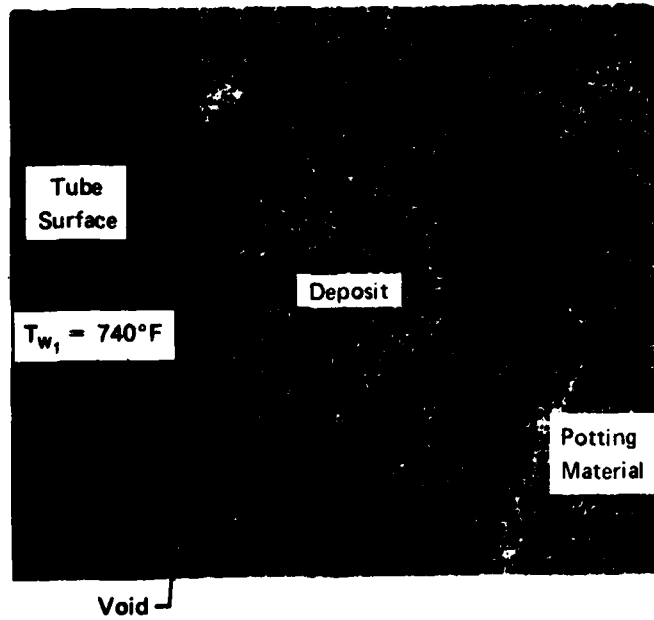
$$Q/A = U (T_{w_o} - T_b). \quad (3)$$

The difference between the overall heat transfer coefficient and the initial heat transfer coefficient is caused by the deposit thermal resistance and is calculated using eq. (1), where t is the deposit thickness in appropriate units and k is the deposit thermal conductivity. Deposit thermal resistance, t/k , as calculated from the test data is presented in Figure 24 as a function of the initial wall temperature. A profile similar to that presented earlier for the formation rate is evident (Figure 21).

Test 5



Semp Photograph of Carbon Concentration in Deposit

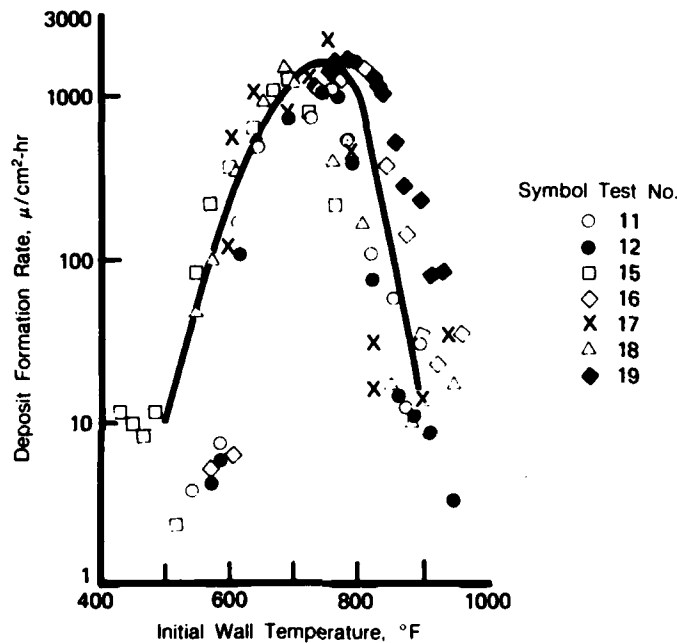


FD 267082

Figure 20. Photomicrograph of NAPC-5 Deposit for Test 5

TABLE 4. SUMMARY OF NAPC-7 TEST CONDITIONS

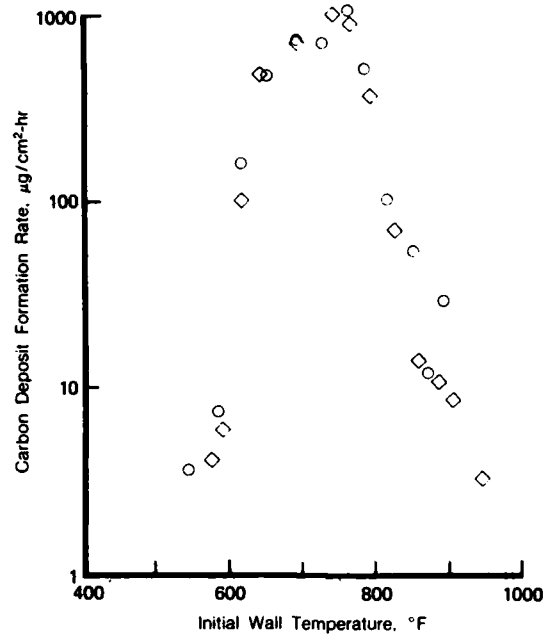
Test No.	Test Duration (hr)	Flow Rate (lb/hr)	Pressure (psig)	Tube Length (feet)	Tube Material	Exit Fuel Temp (°F)
11	5	60	400	8	316 SS	900
12	5	60	400	8	316 SS	900
15	5	60	400	8	316 SS	700
16	5	120	400	8	316 SS	900
17	10	60	400	8	316 SS	900
18	5	60	800	8	316 SS	900
19	4.75	60	400	4	316 SS	900



FD 267821

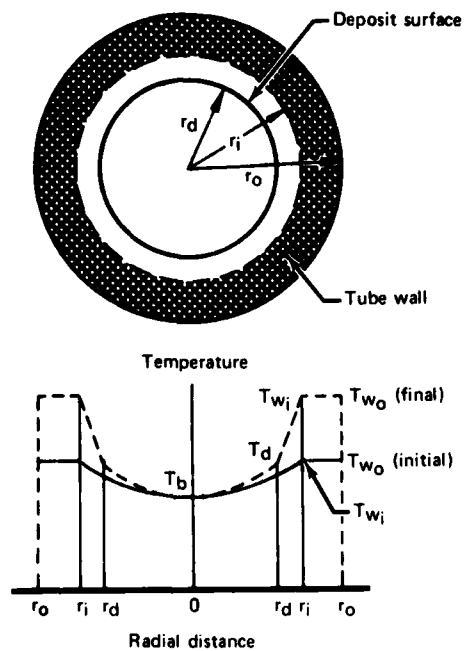
Figure 21. Rate of Carbon Deposition for NAPC-7 Fuel

Until a formulation is developed which depicts the functional relationship of deposit thermal conductivity with temperature, a constant value of deposit thermal conductivity will be assumed (as discussed earlier, a value of 0.12 Btu/hr-Ft-F was used). For tests of approximately five to ten hours and initial wall temperatures less than or equal to approximately 750°F, the assumption of a constant thermal conductivity appears to be a reasonable approximation, as evidenced by the data presented in Figure 25. The data presented allows direct comparison of calculated deposit thermal resistance and total measured deposit loading per unit area for tube locations downstream of the entrance region and upstream of the location where peak deposit occurs. The data presented is obtained from a best approximation of deposit formation rate and deposit thermal resistance as a function of initial wall temperature. Each data point in Figure 25 represents values taken at the same temperature. The slope of the straight line represents a constant thermal conductivity of 0.118 Btu/hr-ft-°F and is based on a deposit density of 1 gm/cm³. The curve is not intended to be the best representation of the data, but serves to indicate that the constant value of 0.12 Btu/hr-ft-F for deposit thermal conductivity does appear to be a representative number which can be used with reasonable confidence over the conditions tested.



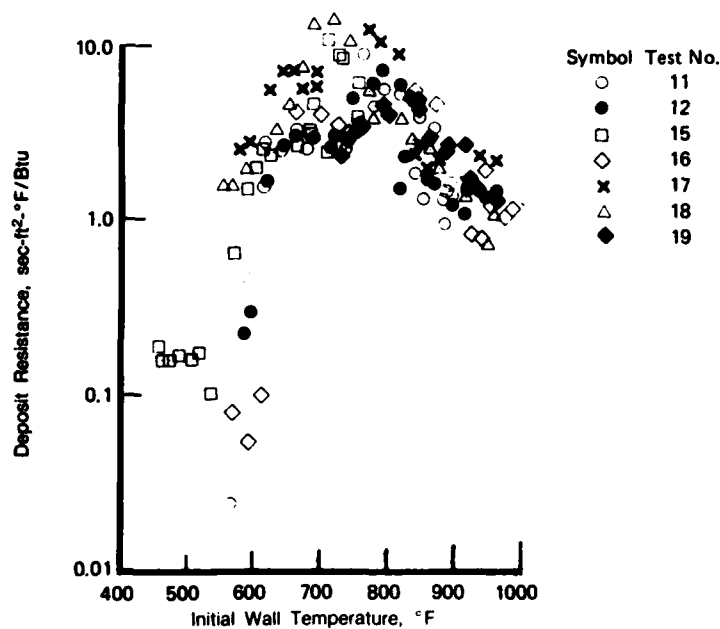
FD 267822

Figure 22. Verification of Data Repeatability



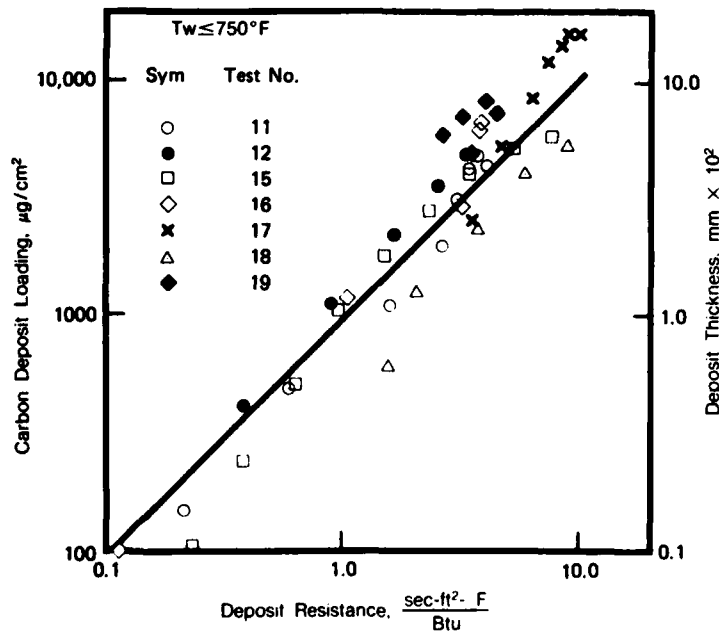
FD 267823

Figure 23. Fuel Deposit Heat Transfer Model



FD 267824

Figure 24. Deposit Thermal Resistance for NAPC-7 Fuel

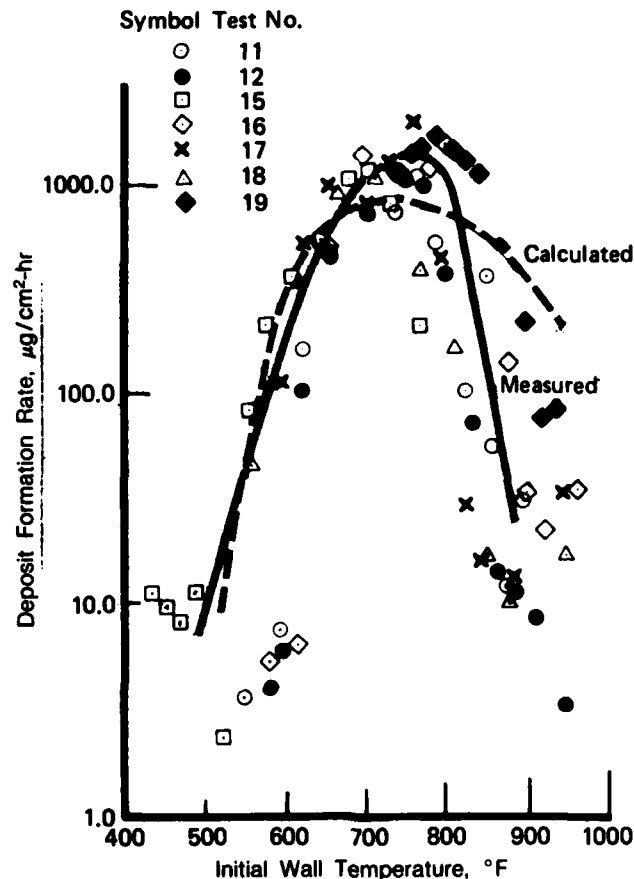


FD 267825

Figure 25. Deposit Loading vs Calculated Deposit Resistance for NAPC-7 Fuel

To show that there is a good correlation between tube heat transfer measurements and deposit formation, a comparison of calculated deposit formation rate and measured deposit formation is presented in Figure 26. A deposit thickness was determined from the deposit thermal resistance data and the deposit mass was calculated assuming a density of 1 gm/cm^3 and a uniform distribution over a 2-in. section of tube. The measured deposit rates for each test are

presented and a curve is shown representing the best approximation to the calculations. As can be seen in the figure, there is good agreement between calculated and measured formation rates, especially at the lower wall temperature.



FD 267826

Figure 26. Comparison of Measured and Calculated Deposit Formation Rates for NAPC-7

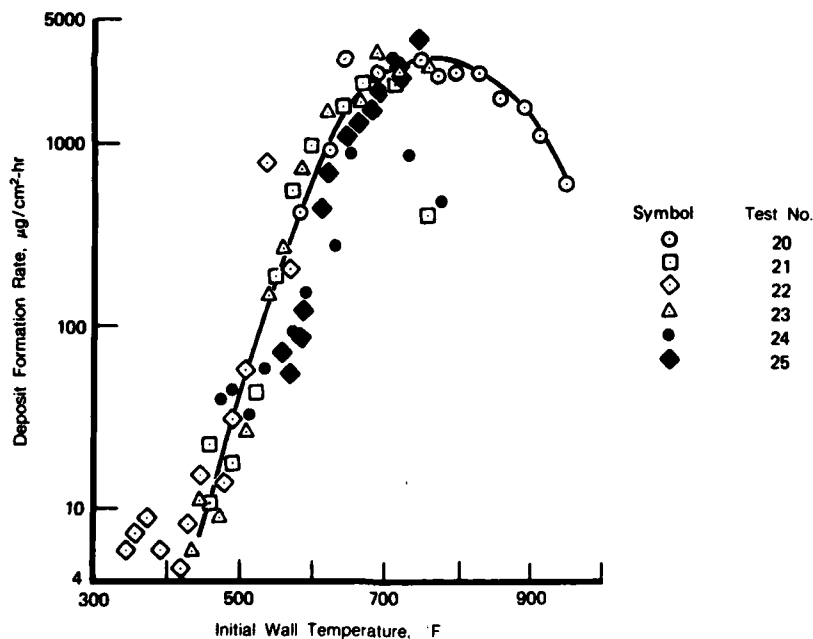
C. NAPC-11 FUEL TESTS

No significant deviations from the NAPC-7 test matrix were made during testing of the second alternative fuel, designated as NAPC-11. The fuel consisted of a blend of equal amounts of low aromatic JP-5 and No. 2 heating oil, which resulted in a JFTOT breakpoint temperature of 470°F. A summary of conditions used in the NAPC-11 test sequence is shown in Table 5. The results of the tests conducted with the baseline NAPC-5 fuel and the NAPC-7 indicated that deposit formation was insensitive to changes in fuel pressure over the range of interest. Therefore, a constant average tube pressure of 400 psig was used throughout the NAPC-11 test sequence. A baseline test duration of five hours was retained; however, the 10 hour test was replaced by a one hour test. Finally, the baseline exit fuel temperature was reduced to 700°F so that the majority of data could be obtained at temperatures less than or equal to the region of peak deposit formation. Single tests were conducted at exit fuel temperatures of approximately 500°F and 900°F.

TABLE 5. SUMMARY OF NAPC-11 TEST CONDITIONS

Test No.	Test Duration (hr)	Flow Rate (lb/hr)	Pressure (psig)	Tube Length (feet)	Tube Material	Exit Fuel Temp (°F)
20	5	60	400	8	316 SS	900
21	5	60	400	8	316 SS	700
22	5	60	400	8	316 SS	500
23	4	120	400	8	316 SS	700
24	1	60	400	8	316 SS	700
25	5	60	400	4	316 SS	700

A summary of the NAPC-11 deposit formation rates is presented in Figure 27. Similar to the results obtained with the previous two fuels, deposit formation rates are strongly dependent on tube wall temperature, and the peak formation rate of approximately $3000\mu\text{g}/\text{cm}^2\text{-hr}$ occurs at approximately 700 to 750°F. At higher temperatures the formation rates decrease much slower than previously measured with either the baseline NAPC-5 or the NAPC-7 fuels. As expected, reducing the exit fuel temperature did not affect fuel deposition rates. In addition, deposition rates determined from the 4-ft tube were, in general, similar to those measured for tests conducted with the longer tube at similar temperature levels. The increase in deposit formation rates with shorter test tubes, reported for the NAPC-7 fuel, is not evident with NAPC-11. Also, there does not appear to be an effect of flow rate or test duration over the range of conditions tested.

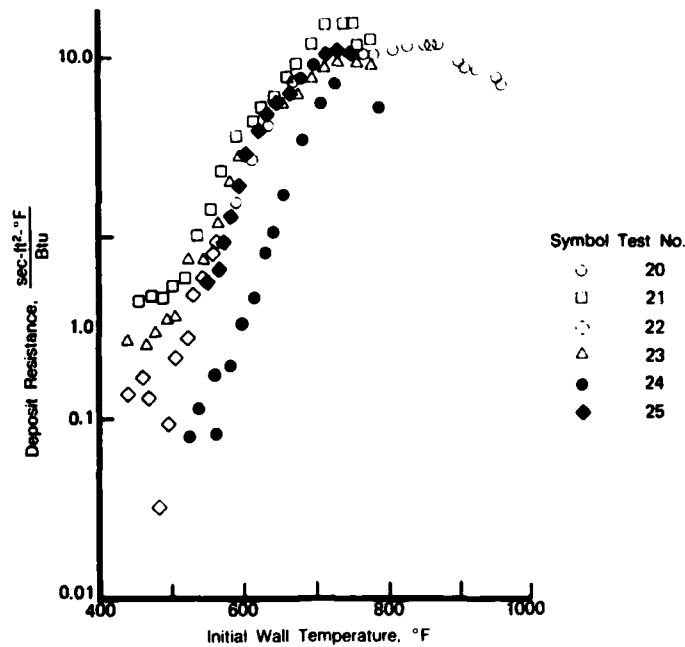


FD 267827

Figure 27. Rate of Carbon Deposition for NAPC-11 Fuel

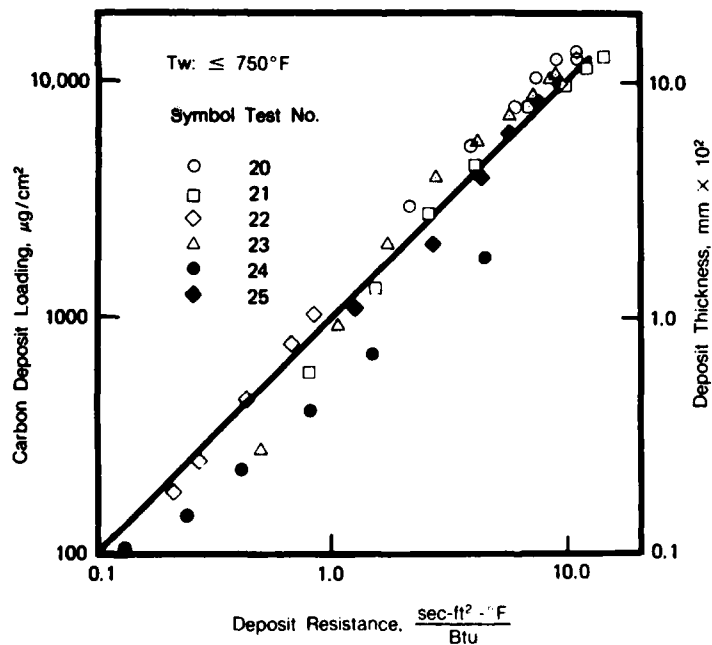
The thermal resistance of the NAPC-11 fuel deposit was calculated by the procedure described earlier and the results are presented in Figure 28. It is immediately apparent from the figure that the one hour test (Test 24) results in a lower thermal resistance, i.e., a thinner deposit layer. A comparison between deposit thermal resistance and deposit loading is presented

in Figure 29 and, similar to NAPC-7, a constant value of deposit thermal conductivity (0.118 Btu/hr-ft-°F) is shown.



FD 267828

Figure 28. Deposit Thermal Resistance for NAPC-11 Fuel

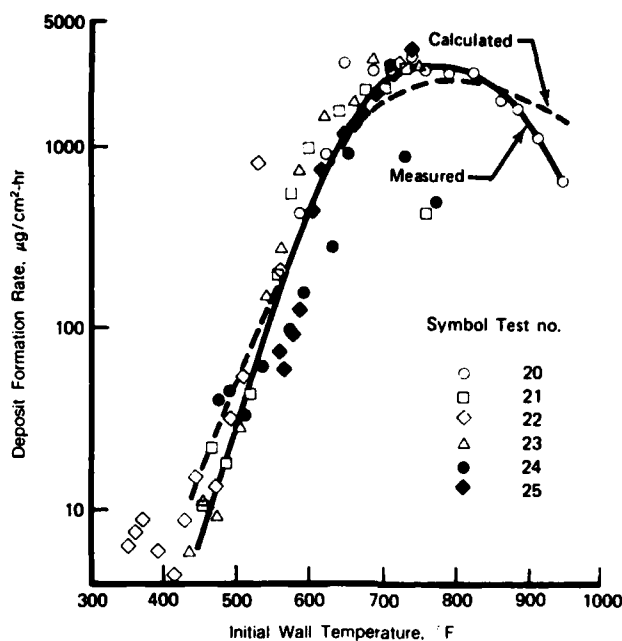


FD 267829

Figure 29. Deposit Loading vs Calculated Deposit Resistance for NAPC-11 Fuel

A comparison between calculated and measured deposit formation rates is presented in Figure 30. The procedure used for the calculation was analogous to that described earlier. The measured deposit formation rate is presented and a best approximation for the calculated

formation rate is shown. The good agreement between measured data and calculations is obvious. Values of deposit density and conductivity are the same as used in previous calculations. The comparison serves to indicate the possibility of using heat transfer measurements to evaluate deposit formation rates, without the need for tube sectioning.



FD 267830

Figure 30. Comparison of Measured vs Calculated Deposit Formation Rate for NAPC-11 Fuel

D. NAPC-14 FUEL TESTS

NAPC-14 represents a shale-derived JP-5 with basic nitrogen compounds partially replaced. The shale derived JP-5 used in this program was produced from a stringent refining process which comprised hydrocracking, fractionation, and acid treatment, and resulted in a very low nitrogen content product. Just prior to shipment of the fuel from NAPC, 67.54 gms of isolated shale oil basic nitrogen compounds were added to 750 gallons of fuel, resulting in a JFTOT breakpoint temperature of 515°F. A summary of the tests performed with NAPC-14 is presented in Table 6.

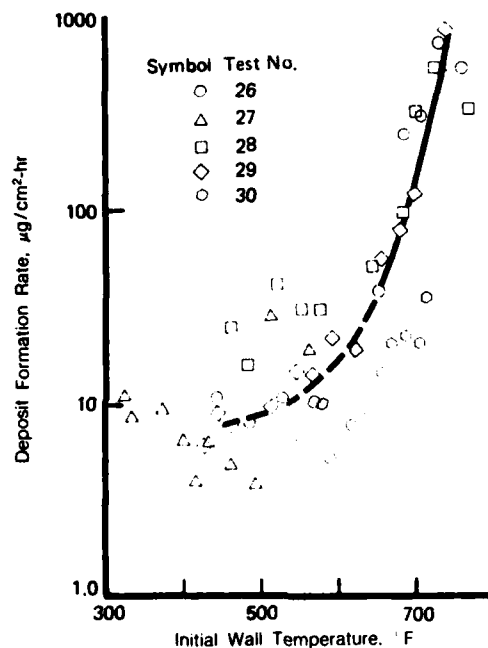
TABLE 6. SUMMARY OF NAPC-14 TEST CONDITIONS

Test No.	Test Duration (hr)	Flow Rate (lb/hr)	Pressure (psig)	Tube Length (feet)	Tube Material	Exit Fuel Temp (°F)
26	5	60	400	8	316 SS	700
27	5	60	400	8	316 SS	500
28	1	60	400	8	316 SS	700
29	3.5	110	400	8	316 SS	700
30	5	60	400	4	316 SS	600

The 900°F exit fuel temperature was eliminated in favor of lower temperature tests, which were previously shown to yield results at conditions more representative of engine systems. The

duration of the high flow rate test was shortened from 5 hrs to 3.5 hrs due to a system malfunction.

Deposit formation rates determined from the NAPC-14 tests are presented in Figure 31. The thermal stability level of NAPC-14 was unexpectedly high, which resulted in a large amount of data which was below the sensitivity level of the gas analysis instrumentation used for deposit burnoff. It is for this reason that a dashed line is drawn through areas where the accuracy of the data is suspect. In addition, because of the high thermal stability of the fuel, the temperature range corresponding to peak deposit formation was not determined. Similar to the other fuels, however, the data in Figure 31 indicate that a strong functional relationship exists between deposit formation rate and initial wall temperature.



FD 267831

Figure 31. Rate of Carbon Deposition for NAPC-14 Fuel

SECTION V

COMPLEMENTARY ANALYSIS

At the conclusion of the extensive data analysis and correlation effort reported in the preceding sections, a further analytical examination was made of the test data, with the objective of systematically evaluating the thermal information relating to the fuel and to the deposits, and discovering any implicit relationships between the thermal characteristics, the test conditions, and the resulting deposits. The result of this effort is intended to complement the data correlations reported in the previous section.

The data evaluated in this analysis included all the measurements made during the heated tube tests, as well as the deposit rates measured in the post-test procedures. Specifically, the data consisted of the fuel flow rates, electrical power input, fuel and wall temperature distributions over the length of the tube, pressure distribution, and total deposits measured in each piece of sectioned tube at the completion of each test. All tests, with the exclusion of Tests 3, 13 and 14, were included in this evaluation, and all data collected during each test was included. The three tests excluded were performed with heat-stressed fuel, and were not considered pertinent to the correlation of the remaining test data.

A. DATA PRE-PROCESSING

This evaluation of the test data was performed on the IBM Personal Computer. To make the data available for processing on this system, it was transferred from the UNIVAC 1100 to an IBM 370 system and subsequently downloaded to the IBM microcomputer for storage on "floppy" diskettes. Because of the large size of the data set, approximately 25000 card images, it was necessary to break the data into test sets for further handling, each set composed of data for one fuel. This turned out to be an adequate subdivision for convenient processing. Prior to evaluating the data, it was examined and "pre-processed" to eliminate anomalies due to the measuring or data collecting methods. These anomalies were of two types, data duplication or missed data points due to malfunctions in the data acquisition system, and errors in measured fuel bulk temperatures due to accumulation of deposits on the instrumented temperature integrators.

Where duplicated or missing data points were found, they were replaced by linear interpolation or extrapolation of data from adjacent locations. On the other hand, the fuel thermocouples developed errors during the course of the test due to the insulating effect of deposit accumulation, resulting in an increase in the indicated fuel temperatures. However, the measured inlet and outlet temperatures were not affected, and remained accurate during the duration of the test. This problem was resolved by using the initial measured fuel temperature profile to define the profiles throughout the test duration, and scaling the temperature levels by the measured inlet and outlet fuel temperatures.

Wall temperatures were measured at the outer surface of the heated tube, while the temperature at the inner surface is desired for evaluating the fuel heat transfer. Determination of the inner temperature is readily made by calculating the thermal conduction through the wall, considering the effects of internal heat generation due to electrical dissipation. The relation between inner and outer wall temperatures is:

$$T_{wi} = T_{wo} - (Q'''/16k_w)[2D_o^2 \ln(D_o/D) - D_o^2 + D^2] \quad (4)$$

where T_{wi} and T_{wo} are the inner and outer temperatures, D and D_o are the inner and outer diameters, Q''' is the heat generation (electrical power dissipation) per unit volume, and k_w is

the thermal conductivity of the tube material. Evaluation of the test data indicated temperature differences across the tube walls to be generally less than 10° F.

B. HEAT TRANSFER ANALYSIS

The processes of primary importance in this evaluation of the data are the heat transfer characteristics of the fuel and the deposits on the tube wall, and their relation to the test conditions. The heat transfer characteristics of the fuel are measured in terms of the convective heat transfer coefficient, h , defined previously in equation (2) as the ratio between heat flux and the temperature difference causing that flux. The heat transfer characteristics of the deposits can be described by their thermal resistance for a specified deposit thickness, or by the effective thermal conductivity of the deposited material.

The convective heat transfer coefficient, h , is evaluated in this analysis by:

$$Q/A = h(T_{wi} - T_b) \quad (5)$$

This differs from equation (2) only in using the difference between the bulk temperature and the inner, rather than outer, wall temperature as the driving temperature difference for heat transfer. Because wall temperatures were measured at many more locations than were fuel temperatures, the local fuel bulk temperatures corresponding to the wall temperatures were determined by linear interpolation of the fuel temperature profile. Heat transfer coefficients were determined from the initial-time data for each test, prior to the build-up of any deposits. This data is dimensionalized, prior to correlation, by incorporating it into the following dimensionless groups:

$$\begin{aligned} Nu &= hD/k && \text{(Nusselt number)} \\ Pr &= Cp\mu/k && \text{(Prandtl number)} \\ Re &= VD\rho/\mu && \text{(Reynolds number)} \end{aligned}$$

where V is the mean fluid velocity in the tube, and k , C_p , ρ , and μ are the thermal conductivity, specific heat, density, and viscosity of the fuel. These fuel properties are required at the local conditions near the heated wall. Since fuel properties are dependent on both temperature and pressure, representative values must be selected at each location. The pressure is constant across the tube, and presents no problem, but temperature varies from the wall to the bulk at every location. For a representative value, the "film" temperature is selected, defined as the arithmetic mean of the wall and bulk temperatures. Considering the range of test conditions, it is found that fuel film temperatures vary from somewhat above ambient to approximately 1000° F, and fuel pressures range from about 350 to 550 psia.

C. FUEL PHYSICAL PROPERTIES

Examining the property data available in the literature for JP-5 yields information primarily near ambient pressure and at temperatures below 500° F. The conditions at which the tests were performed were very near the thermodynamic critical state for at least some part of the data in each test. Since the thermophysical properties are very sensitive to both temperature and pressure in the near-critical region, the use of ambient data was not considered appropriate. To supply the needed property information, a compilation of data from several sources was used to generate a set of thermophysical properties for use in all of the following data correlations. The sources include data for JP-5 in the liquid state (Reference 14), Maxwell's generalized data for hydrocarbons over a wide range of thermodynamic states (Reference 15), and correlated near-critical viscosity and thermal conductivity data for similar hydrocarbons (References 16 and 17). Smoothing and fitting these data, to produce maximum consistency between data

sources, yielded the set of properties tabulated in Table 7. Based on a critical state defined by 773°F and 330 psia, these property data cover a reduced temperature range from 0.36 to 1.18 and a reduced pressure range from 1 to 1.6. Although this set of properties was constructed specifically NAPC-5, it is also used for correlation of the three alternative fuels, for lack of better information.

D. ANALYSIS OF DEPOSIT PROPERTIES

As deposits accumulate on the tube wall during the tests, the wall temperature is observed to generally increase with time due to the added thermal resistance of the deposited material. Modifying equation (5) to calculate the overall heat transfer coefficient within the tube:

$$Q/A = U(T_{wi} - T_b) \quad (6)$$

where U is the overall heat transfer coefficient, differing from the film coefficient by including the effect of the thermal resistance of the deposited material. Calculating the overall coefficient for all the data during the total test duration, the calculated value is found to agree with the film coefficient at the beginning of the test, then generally decrease with time as deposits accumulate. Equation (1) relates the film and overall coefficients, and can be used to evaluate the thermal resistance due to the wall deposits. However, for best accuracy, the film coefficient appearing in equation (1) should be interpreted as the local value, measured at the same time during the test as the overall coefficient. Only the initial value of the film coefficient is known, but it can be corrected for use in the evaluation by adjusting for the effects of the deposits on the local fuel flow field within the tube. Deposit accumulations on the wall have two effects on the convective heat transfer, reduction of the tube area causing increased fluid velocities, and increased roughness on the surface causing an increase in fluid turbulence. If the deposit rate is constant for a given location in the tube, as indicated by the measured deposit data, then the mass of the local deposits can be assumed to vary linearly with time over the duration of a test. If the deposit density is assumed constant, the deposit thickness can be calculated and the film coefficient can be corrected for acceleration due to flow restriction. The effects of surface roughness, on the other hand, are not so readily identified. Increased roughness is observed in the cross-section photomicrographs made during post-test analysis of tube deposits. These observations are not sufficient to allow quantification of the effects of surface morphology on heat transfer. However, since the effect of area reduction is generally much more significant than the effect of increased roughness, all observed effects are considered due to area decrease alone, for purposes of this analysis.

Assuming the convective heat transfer to generally behave in accordance with the Dittus-Boelter equation for turbulent flow in tubes, the relation between the film coefficient, fluid properties, and flow conditions is described by:

$$Nu = 0.023 (Re)^{.8} (Pr)^{.4} \quad (7)$$

From this equation, the relation between the initial film coefficient h , and the value at a later time, h' , with the effect of increased velocity due to deposits, is:

$$h'/h = (D/D')^{1.8} \quad (8)$$

With consideration of the effects of changing tube diameter due to deposit accumulation, the inner surface area is reduced, requiring a modification of equation (1) to account for the effect. equation (1) is modified to:

$$1/UA = 1/h'A' + 2t/k_d (A+A') \quad (9)$$

where A and A' are the inner surface areas of the bare tube and of the deposits, respectively, t is the deposit thickness, and k_d is the thermal conductivity of the deposited material. Combining equations (8) and (9):

$$k_d = (tD/(D-t))[1/U - (D'/D)^{1.8} (1/h)] \quad (10)$$

where $D' = (D - 2t)$.

Equation (10) thus provides a relation for calculating the thermal conductivity of the wall deposits, based on the heat transfer and deposit rate data. It must be recognized that this analysis is based on the assumption of constant deposit density, in order to provide a relation between mass deposit rate and deposit thickness.

E. ANALYSIS OF FUEL SPECIFIC HEAT

The nature of the heated tube experiment provides all the necessary information to evaluate the thermodynamic properties of a fluid if two conditions are met, namely the bulk fuel temperature distribution is measured over the length of the heated tube, and the heat flux distribution is known. In essence, these requirements are satisfied in the current program if it is assumed that the electrical resistivity of the tube is constant over its length. Since the data exists for such determination, the data has been evaluated to determine the specific heat of the fuel over the temperature range of the tests. This information allows comparison with the property data of Table 7, and also provides a measure of the instrumentation precision of the test data. The specific heat is calculated from:

$$C_p = Q(x/L)/[M(T_{bo} - T_{bi})] \quad (11)$$

where (x/L) is the fraction of total tube length between two consecutive fuel thermocouples, M is the fuel flow rate, and T_{bo} and T_{bi} are the corrected bulk temperatures measured by those thermocouples.

F. PRESSURE LOSS ANALYSIS

Pressure taps were located at same positions as the fuel thermocouples, and measurements of pressure distribution give an indication of frictional behavior of the fuel. The Darcy friction factor is calculated from the pressure drop and flow rate by the relation:

$$F = (P_i - P_o) (A/M)^2 (g_c/X) \quad (12)$$

where F is the Darcy friction factor, P_i and P_o are the pressures at the locations of the pressure taps, and X is the spacing of the pressure taps.

G. DATA CORRELATIONS

All test data have been evaluated by the described methods and presented in graphical form, although not necessarily in dimensionless form. Presentation of data in the following section is by fuels, with all data for each fuel grouped together. A summation of relations between fuels is presented at the end of this section.

All correlations are based on the properties of Table 7, and the density of deposits for all fuels is assumed constant at 1.0 gm/cc.

H. BASELINE FUEL (NAPC-5)

The heat transfer data for Test 1 is presented in Figure 32 in the format of Nusselt/(Prandtl)⁴ versus Reynolds number. The data is linear except in the inlet region of the tube. The peculiar behavior in the inlet is noted in the wall temperature data of Figure 11, and is apparently due to an interaction between the developing temperature profile and the laminar-turbulent transition. This phenomenon has been more fully discussed by Szetela and Sobel (Reference 18). Figure 33 presents the heat transfer data for all the NAPC-5 tests. These test results are seen to be very consistent and, because the data appears to be linear on a log-log graph, except in the inlet region, they are well represented by an exponential relation similar to equation (7).

The thermal data of Test 1 has been evaluated to determine the thermal conductivity of the resulting deposits, and the results are presented in Figure 34 in the format of Thermal Conductivity (Btu/ft-hr-°F) versus the Deposit Thickness (inches). In this plot data points corresponding to wall temperatures below 900°F are designated by circles, while points corresponding to higher temperatures are shown by crosses. Examination of this data on a sequence of plots, with the distinguishing temperature (900°F in this case) varying from 500 to 1100°F, indicated a primary effect of local wall temperature on the data. This effect is included in the data correlation by modifying the abscissa (Deposit Thickness) by a temperature function of the form:

$$\text{Function}(T_w) = 3.2(1 - T_w/T_{ref}) \quad (13)$$

where T_w is an absolute temperature, and T_{ref} is a selected reference temperature, also an absolute temperature. A selected value of 900°F (1360°R) is used throughout the data evaluation. The thermal conductivity is now correlated with a Deposit Function, defined by:

$$\text{Deposit Function} = (\text{Deposit Thickness}) (10^{F(T_w)}) \quad (14)$$

where $F(T_w)$ is the temperature function defined by equation (13). Figure 35 presents the deposit conductivity data plotted as a function of Deposit Function. The data are now observed to be strongly correlated, with a well defined trend. Table 8 presents the test conditions and Figures 36 through 43 present the deposit conductivity data for the remaining NAPC-5 tests. In Figure 44, all the data of Figures 35-43 are visually "best-fitted" by linear functions, and plotted on a single graph for comparison. With the exception of the curve for Test 7, the remaining data groups together rather tightly. Closer examination indicates a spread between the data, and simultaneous comparison of the test data and the test conditions in Table 8 leads to some interesting conclusions. The effect of increasing flow rate, Tests 1 through 4, increases the thermal conductivity for a given deposit thickness. The reason for the variance of Test 7 is not apparent at this time, except to note that the test duration is considerably shorter than the remaining tests.

The specific heats calculated from the thermal data of Tests 1, 2, and 4 are presented in Figure 45 as Specific Heat (Btu/lbm- $^\circ\text{F}$) versus Bulk Fuel Temperature (F). The fuel temperature used in this figure is the mean value between the two measurements used in calculating the specific heat. These tests were all performed at pressures of approximately 400 psia. Figure 46 shows the same data for Test 10, performed at approximately 800 psia. The strong effect of pressure on specific heat in the near-critical region is clearly seen by comparing these two figures. The curve plotted in Figure 45 represents the specific heat data of Table 7, and the agreement with the test data is seen to be quite good.

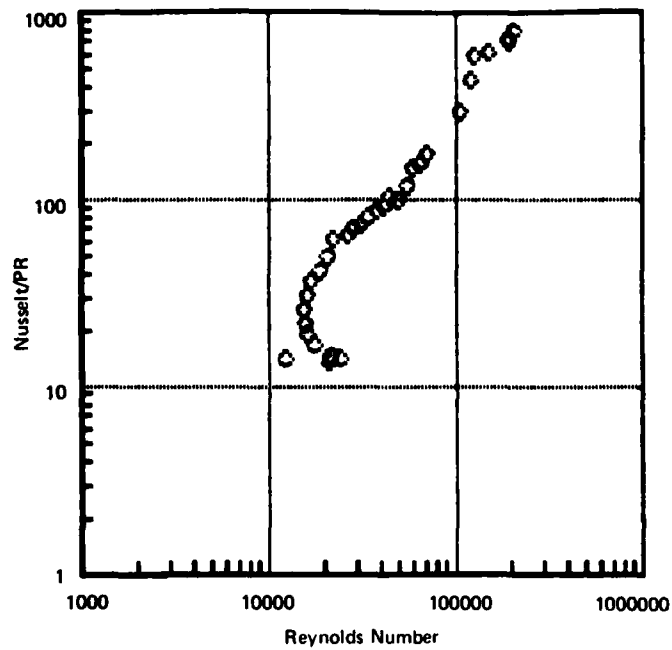
The friction factor, calculated with equation (12) for the initial-time data for all the NAPC-5 tests, is presented in Figure 47 as a function of the mean Reynolds number midway between the pressure taps. For comparison, the accepted curve of the Darcy friction factor for smooth tubes is also plotted in the figure. The data is seen to exhibit considerable scatter, primarily due to the required use of pressure transducers for measuring small pressure differences. With the expectation of large increases in pressure loss over the test duration, due to the accumulation of deposits, the use of sensitive pressure-difference transducers can lead to damaged instrumentation. On the other hand, pressure transducers sized for the high test pressures are not sufficiently sensitive to provide accurate measurement of small pressure differences. This is a universal problem in trying to measure friction data concurrently with other test procedures, and implies that the friction data is the least desirable indicator of internal processes in a heated tube during a thermal stability evaluation.

I. NAPC-7 FUEL

Figure 48 presents the heat transfer data for all the NAPC-7 fuel tests, and shows the same tight correlation as did the baseline fuel data. Deposit thermal conductivity data for Tests 11 through 19 are presented in Figures 49 through 55, with an overlay of all the data trends shown in Figure 56. This figure shows good consistency among the data of Tests 11, 12, and 17, with noticeable variation among the other tests. Again considering test conditions, it appears that increasing velocity (Test 16) or heat flux (Test 19) increases thermal conductivity, while reducing fuel temperature (Test 15) or increasing pressure (Test 18) decreases conductivity for a specified deposit thickness.

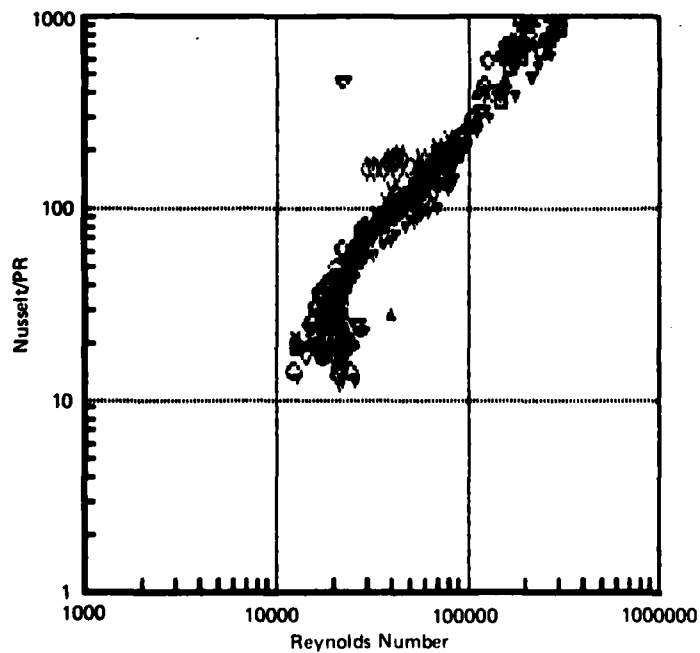
TABLE 7. THERMOPHYSICAL PROPERTIES OF JP-5

Temp. °F	Pressure, psia													
	330						430						530	
	Enthal. BTU/lb	Sp. Heat BTU/lb-°F	Density lbm/cft	Cond. BTU/ft- °F-hr	Visc. × 10 ⁶ lb/ft-s	Density lbm/cft	Cond. BTU/ft- °F-hr	Visc. × 10 ⁶ lb/ft-s	Density lbm/cft	Cond. BTU/ft- °F-hr	Visc. × 10 ⁶ lb/ft-s	Density lbm/cft	Cond. BTU/ft- °F-hr	Visc. × 10 ⁶ lb/ft-s
0	0.000	0.380	51.200	0.084	3300.000	51.200	0.084	3300.000	51.200	0.084	3300.000	51.200	0.084	3300.000
50	20.667	0.402	49.950	0.081	2100.000	49.950	0.081	2100.000	49.950	0.081	2100.000	49.950	0.081	2100.000
100	41.333	0.431	48.700	0.079	900.000	48.700	0.079	900.000	48.700	0.079	900.000	48.700	0.079	900.000
150	62.000	0.467	47.450	0.077	655.000	47.450	0.077	655.000	47.450	0.077	655.000	47.450	0.077	655.000
200	88.000	0.502	46.200	0.075	410.000	46.200	0.075	410.000	46.200	0.075	410.000	46.200	0.075	410.000
250	114.000	0.535	44.850	0.072	315.000	44.850	0.072	315.000	44.850	0.072	315.000	44.850	0.072	315.000
300	140.000	0.565	43.500	0.070	220.000	43.500	0.070	220.000	43.500	0.070	220.000	43.500	0.070	220.000
350	171.250	0.595	42.250	0.068	172.500	42.250	0.068	172.500	42.250	0.068	172.500	42.250	0.068	172.500
400	202.500	0.625	41.000	0.066	125.000	41.000	0.066	125.000	41.000	0.066	125.000	41.000	0.066	125.000
450	233.750	0.633	39.600	0.064	101.500	39.600	0.064	101.500	39.600	0.064	101.500	39.600	0.064	101.500
500	265.000	0.642	38.200	0.062	78.000	38.200	0.062	78.000	38.200	0.062	78.000	38.200	0.062	78.000
550	297.500	0.650	36.100	0.059	66.000	36.100	0.059	66.000	36.100	0.059	66.000	36.100	0.059	66.000
600	330.000	0.700	34.000	0.056	54.000	34.000	0.056	54.000	34.000	0.056	54.000	34.000	0.056	54.000
650	367.500	0.750	30.750	0.052	45.000	30.750	0.052	45.000	30.750	0.052	45.000	30.750	0.052	45.000
700	405.000	0.850	27.500	0.048	36.000	27.500	0.048	36.000	27.500	0.048	36.000	27.500	0.048	36.000
750	450.000	1.317	18.733	0.032	22.301	24.856	0.040	29.767	25.894	0.041	31.953	24.075	0.041	31.953
800	520.000	1.063	11.164	0.020	8.805	19.076	0.028	16.342	21.968	0.032	24.075	16.342	0.032	24.075
850	560.000	0.800	6.328	0.014	8.270	12.612	0.018	10.178	17.215	0.023	11.900	10.178	0.023	11.900
900	600.000	0.767	5.490	0.014	8.075	8.975	0.017	9.309	12.100	0.020	10.387	9.309	0.020	10.387
950	635.000	0.700	5.048	0.014	7.952	7.884	0.017	8.770	10.294	0.018	9.411	8.770	0.018	9.411
1000	670.000	0.725	4.607	0.015	7.914	6.792	0.017	8.620	8.487	0.018	9.065	8.620	0.018	9.065



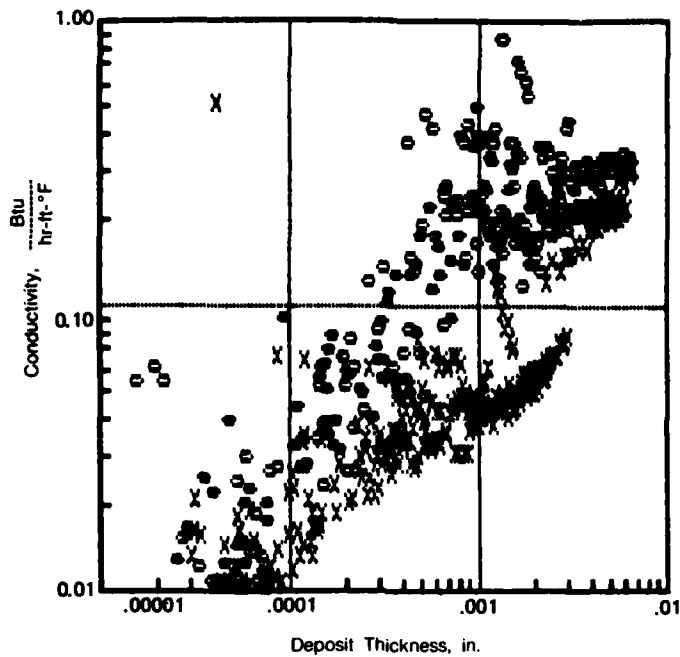
FD 267832

Figure 32. Heat Transfer Characteristics of NAPC-5, Test No. 1



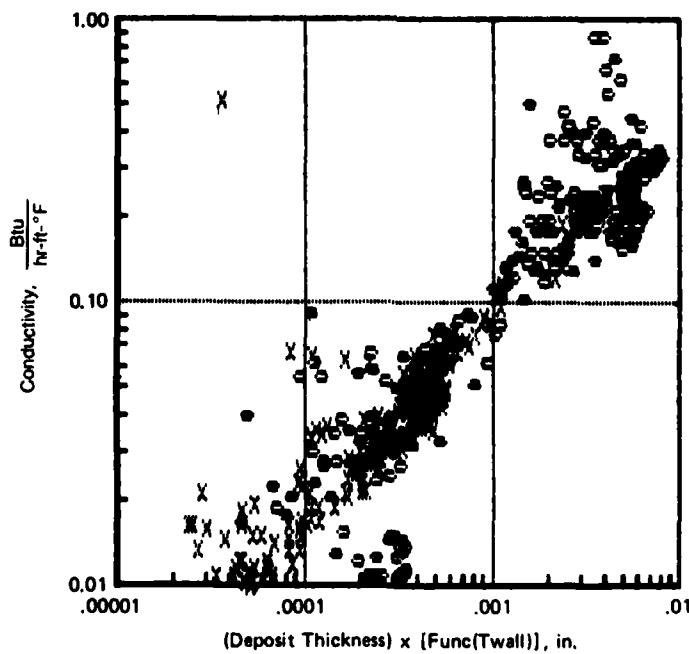
FD 267833

Figure 33. Heat Transfer Characteristics of NAPC-5, Tests No. 1 Through 10



FD 267834

Figure 34. Deposit Thermal Conductivity vs Deposit Thickness for NAPC-5, Test No. 1

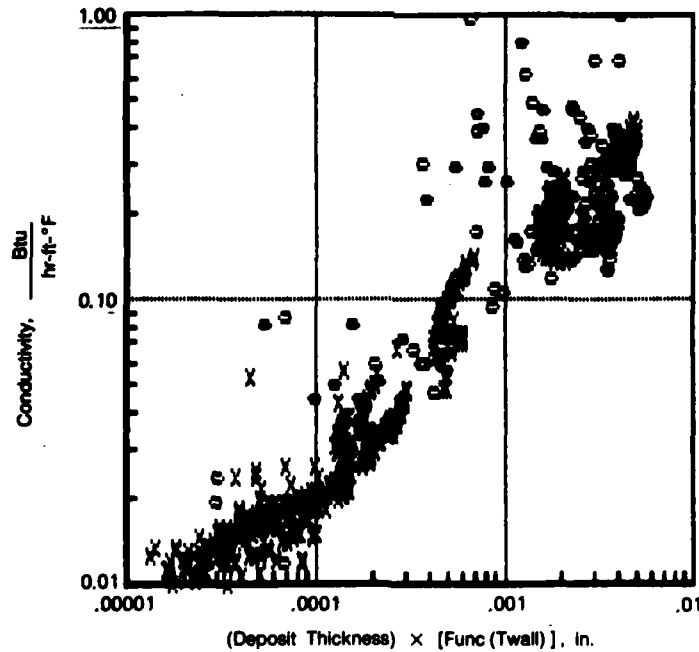


FD 267835

Figure 35. Deposit Thermal Conductivity vs Deposit Function for NAPC-5, Test No. 1

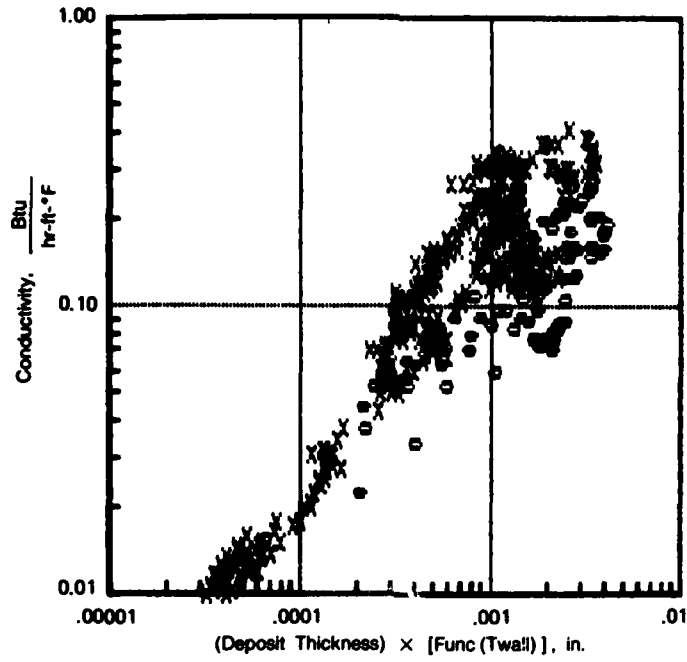
TABLE 8. SUMMARY OF TEST CONDITIONS

Test No.	Test Duration (hr)	Flow Rate (lb/hr)	Pressure (psig)	Tube Length (feet)	Tube Material	Exit Fuel Temp (°F)
1	19.5	45	400	8	316 SS	900
2	19.0	60	400	8	316 SS	900
4	14.0	75	400	8	316 SS	900
5	14.0	60	400	8	316 SS	900
6	10.0	60	400	8	316 SS	900
7	1.2	60	400	8	316 SS	900
8	18.0	60	400	8	Inconel 600	900
9	10.0	60	400	8	316 SS	900
10	8	60	800	8	316 SS	900
11	5	60	400	8	316 SS	900
12	5	60	400	8	316 SS	900
15	5	60	400	8	316 SS	700
16	5	120	400	8	316 SS	900
17	10	60	400	8	316 SS	900
18	5	60	800	8	316 SS	900
19	5	60	400	4	316 SS	900
20	5	60	400	8	316 SS	900
21	5	60	400	8	316 SS	900
22	5	60	400	8	316 SS	500
23	5	120	400	8	316 SS	700
24	1	60	400	8	316 SS	700
25	5	60	400	8	316 SS	700
26	5	60	400	8	316 SS	700
27	5	60	400	8	316 SS	500
28	1	60	400	8	316 SS	700
29	3.5	110	400	8	316 SS	700
30	5	60	400	4	316 SS	600



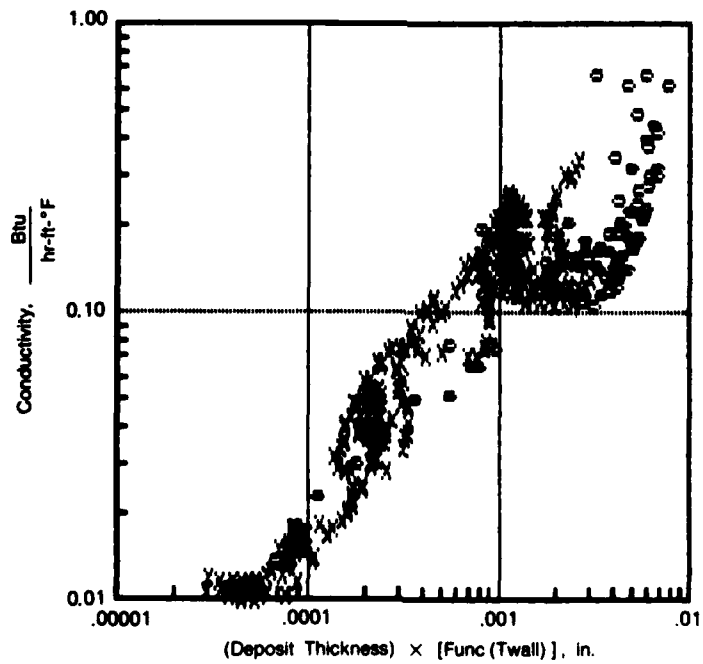
FD 267836

Figure 36. Deposit Thermal Conductivity vs Deposit Function for NAPC-5, Test No. 2



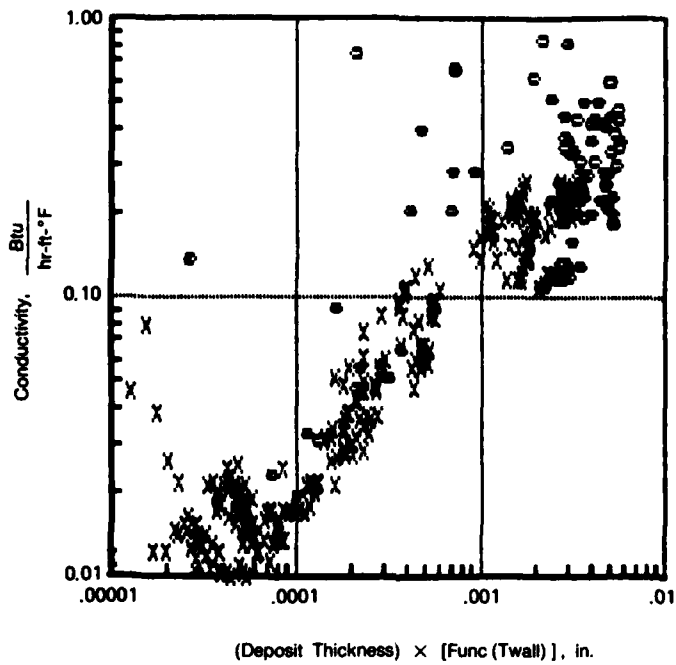
FD 267837

Figure 37. Deposit Thermal Conductivity vs Deposit Function for NAPC-5, Test No. 4



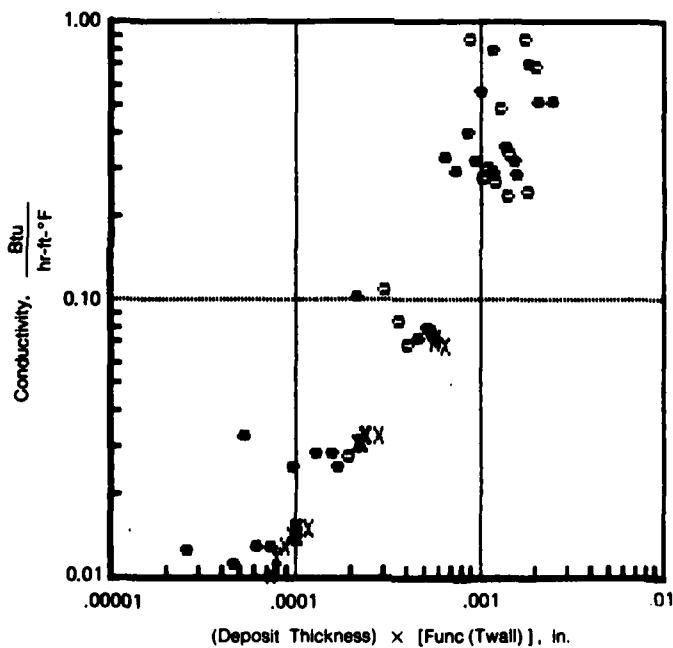
FD 267838

Figure 38. Deposit Thermal Conductivity vs Deposit Function for NAPC-5, Test No. 5



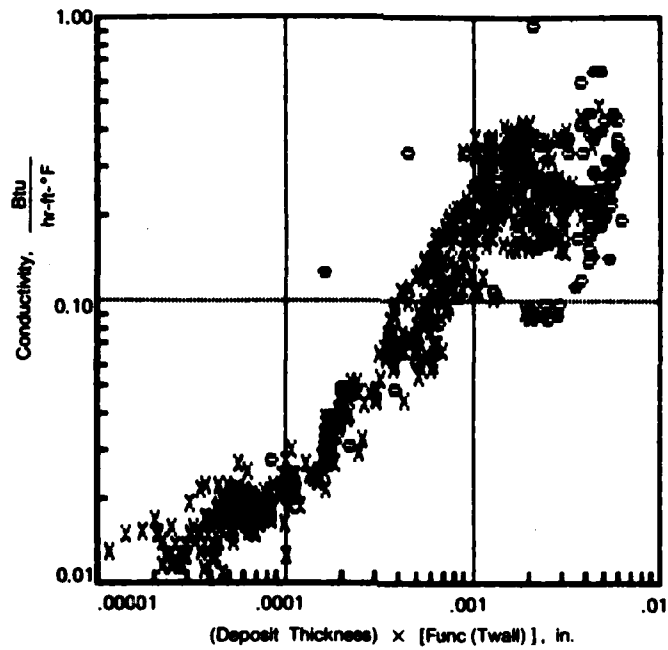
FD 267839

Figure 39. Deposit Thermal Conductivity vs Deposit Function for NAPC-5, Test No. 6



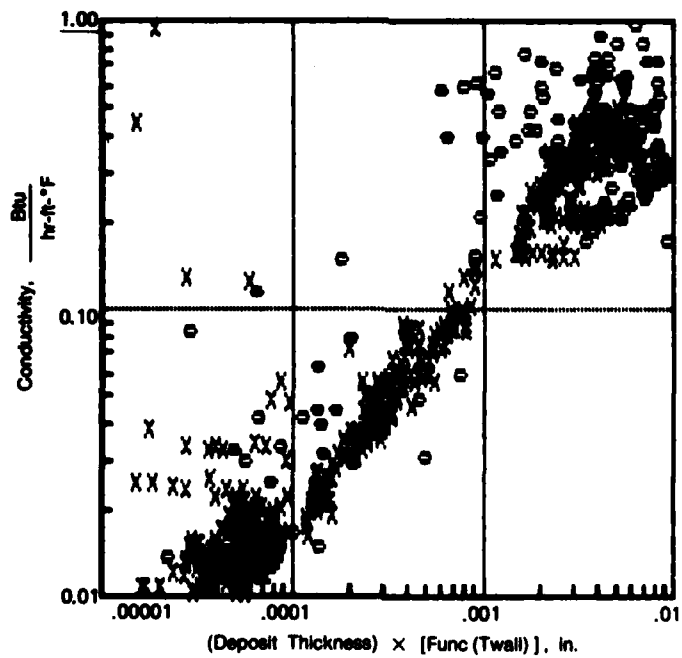
FD 267840

Figure 40. Deposit Thermal Conductivity vs Deposit Function for NAPC-5, Test No. 7



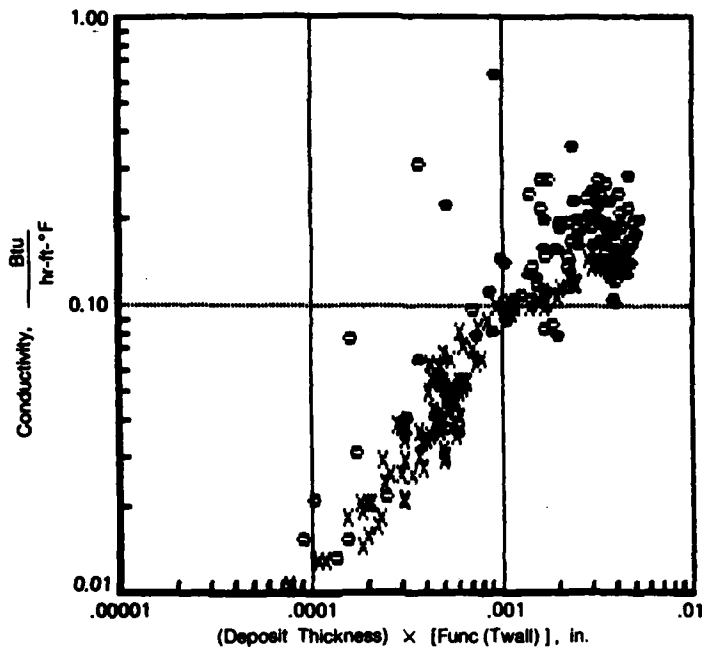
FD 267841

Figure 41. Deposit Thermal Conductivity vs Deposit Function for NAPC-5, Test No. 8



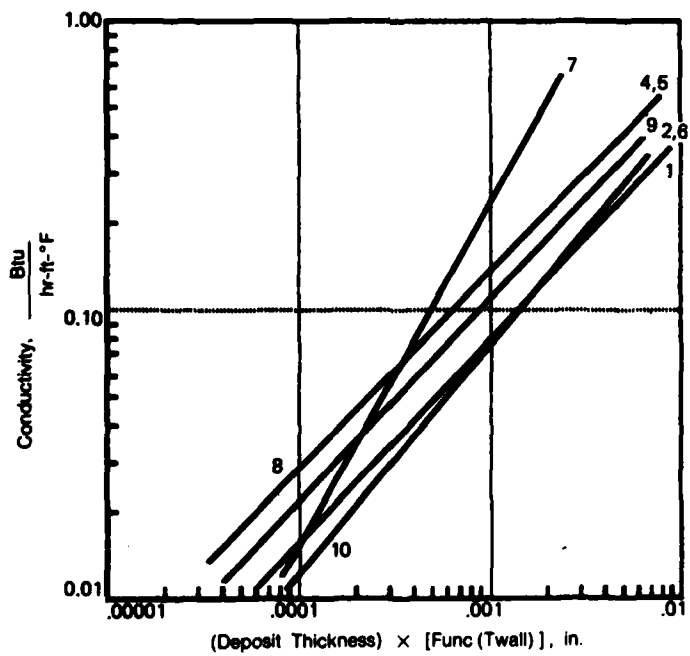
FD 267842

Figure 42. Deposit Thermal Conductivity vs Deposit Function for NAPC-5, Test No. 9



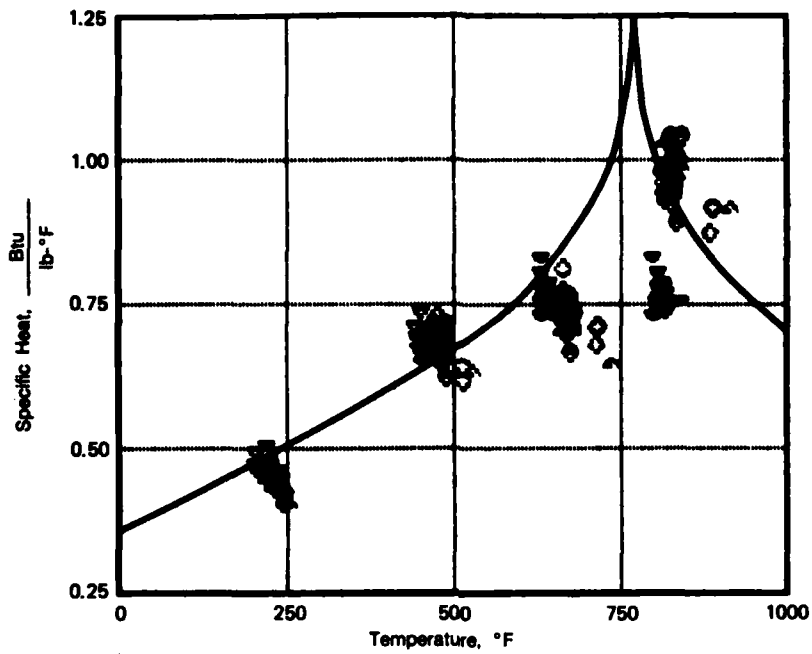
FD 267843

Figure 43. Deposit Thermal Conductivity vs Deposit Function for NAPC-5, Test No. 10



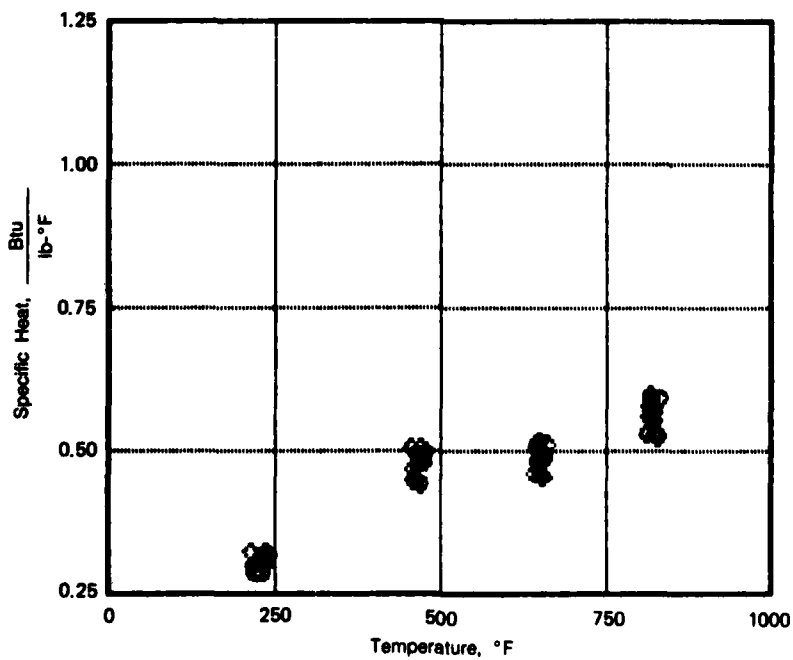
FD 267844

Figure 44. Deposit Thermal Conductivity vs Deposit Function for NAPC-5, Tests No. 1 Through 10



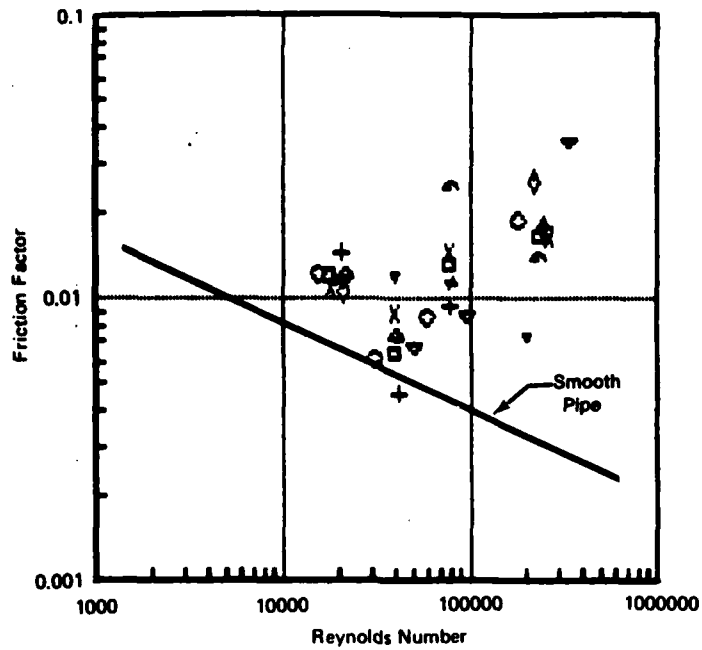
FD 267845

Figure 45. Specific Heat vs Bulk Temperature for NAPC-5 at 400 psia, Tests No. 1, 2, and 4



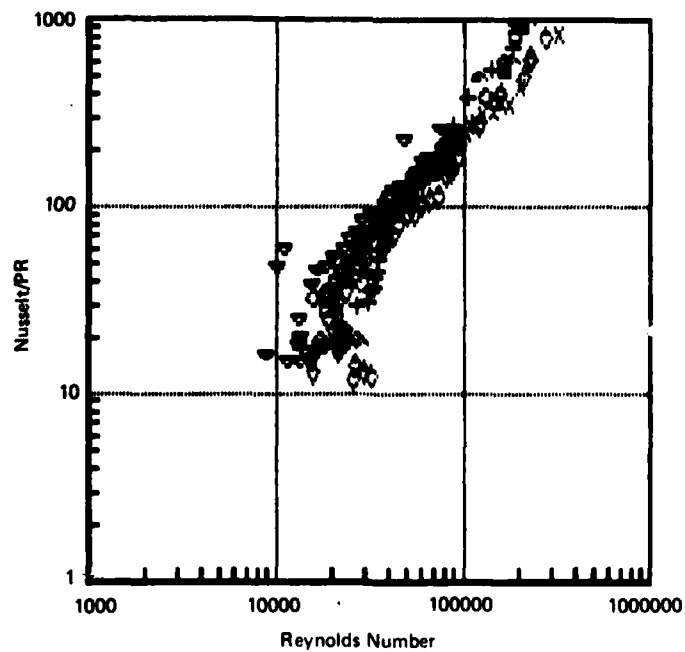
FD 267846

Figure 46. Specific Heat vs Bulk Temperature for NAPC-5 at 800 psia, Test No. 10



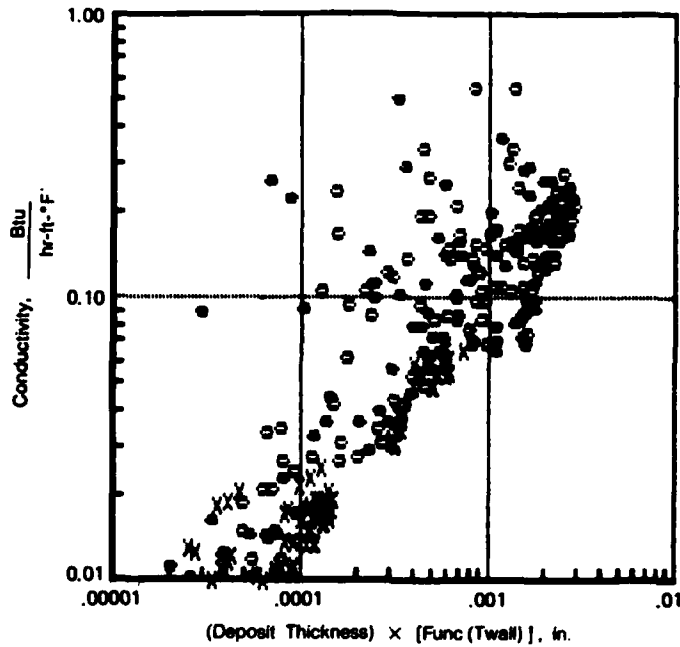
FD 267847

Figure 47. Friction Factor vs Reynolds Number for NAPC-5



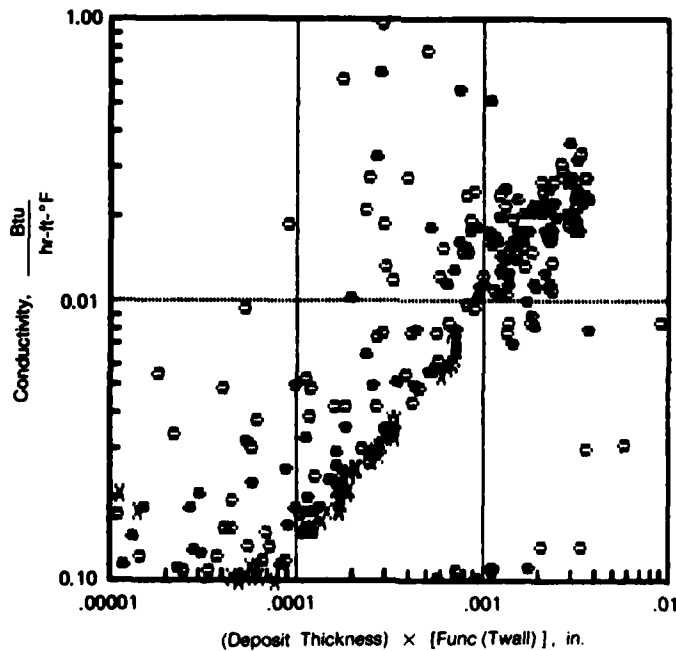
FD 267848

Figure 48. Heat Transfer Characteristics of NAPC-7 Fuel, Tests No. 11 Through 19



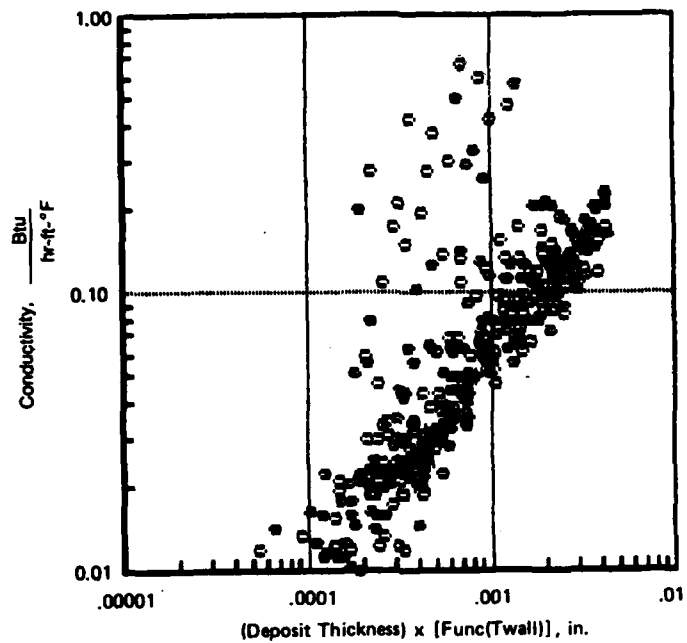
FD 267849

Figure 49. Deposit Thermal Conductivity vs Deposit Function for NAPC-7, Test No. 11



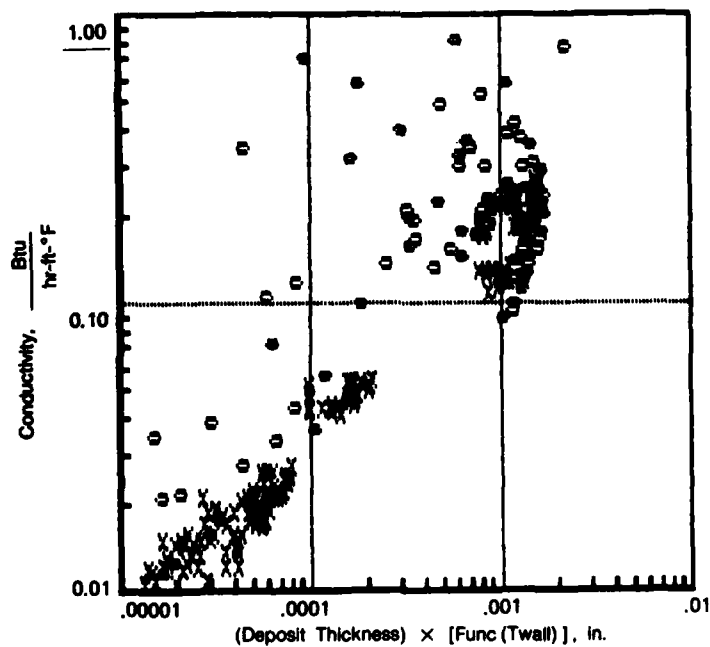
FD 267850

Figure 50. Deposit Thermal Conductivity vs Deposit Function for NAPC-7 Fuel, Test No. 12



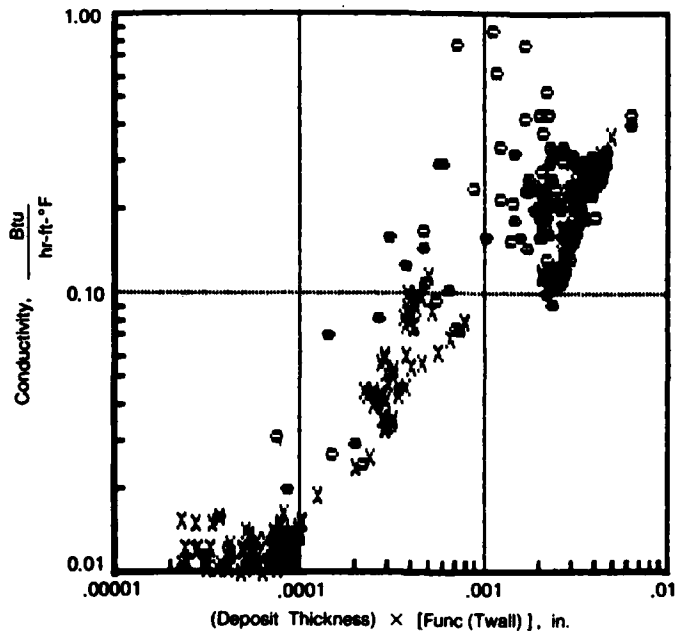
FD 267851

Figure 51. Deposit Thermal Conductivity vs Deposit Function for NAPC-7 Fuel, Test No. 15



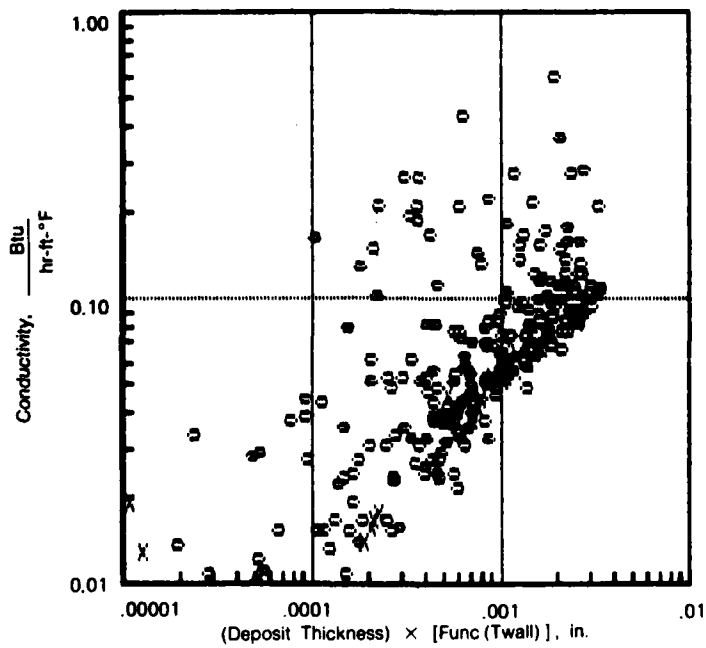
FD 267852

Figure 52. Deposit Thermal Conductivity vs Deposit Function for NAPC-7 Fuel, Test No. 16



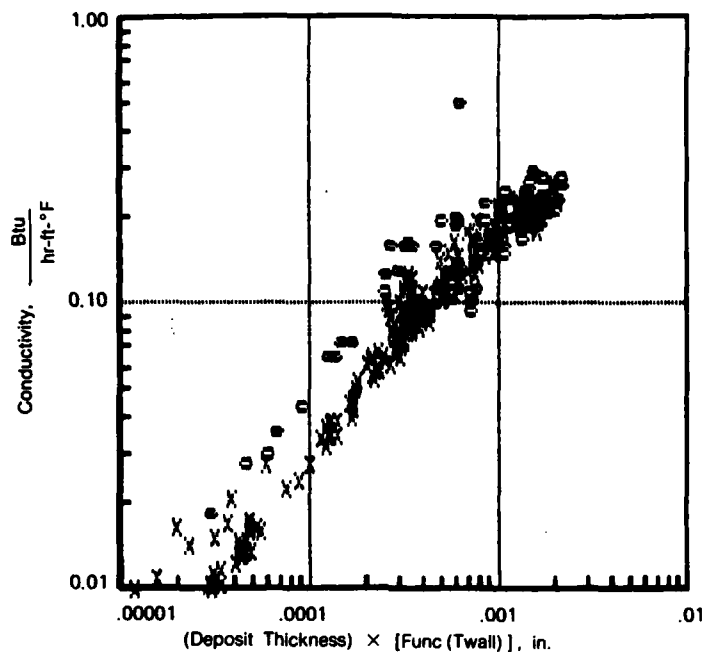
FD 267853

Figure 53. Deposit Thermal Conductivity vs Deposit Function for NAPC-7 Fuel, Test No. 17



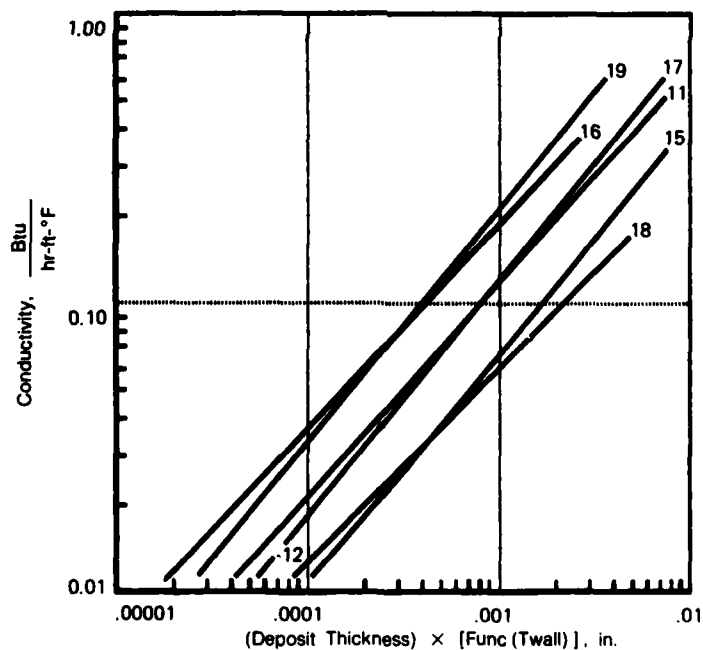
FD 267854

Figure 54. Deposit Thermal Conductivity vs Deposit Function for NAPC-7 Fuel, Test No. 18



FD 267855

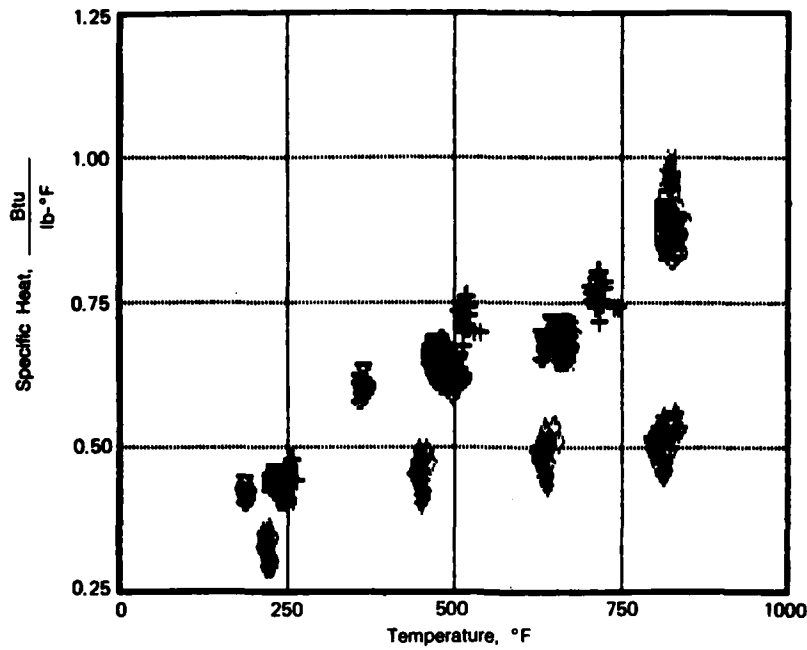
Figure 55. Deposit Thermal Conductivity vs Deposit Function for NAPC-7 Fuel, Test No. 19



FD 267856

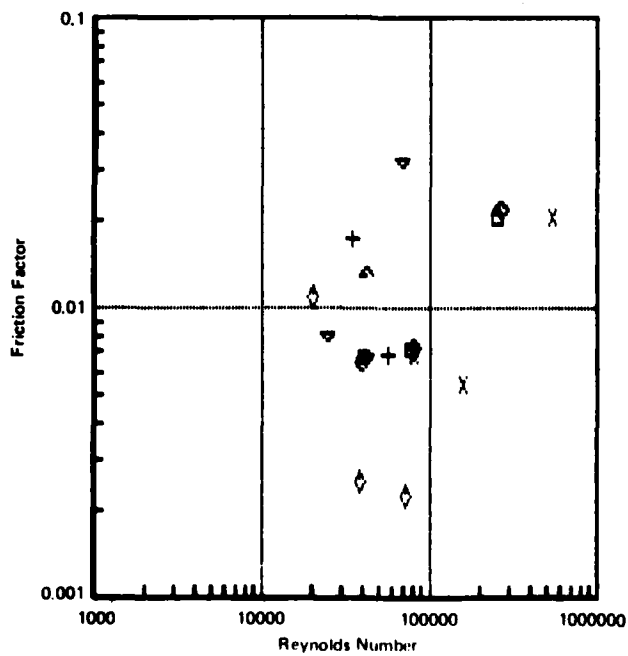
Figure 56. Deposit Thermal Conductivity vs Deposit Function for NAPC-7 Fuel, Tests No. 11 Through 19

Figure 57 shows the measured specific heat data for Tests 11 through 19, and the differentiation between pressure levels is seen very vividly. Finally, the friction factor data is shown in Figure 58, with the same data scatter exhibited in the baseline data.



FD 267857

Figure 57. Specific Heat vs Bulk Temperature for NAPC-7 Fuel Tests No. 11 Through 19



FD 267858

Figure 58. Friction Factor vs Reynolds Number for NAPC-7 Fuel, Tests No. 11 Through 19

J. NAPC-11 FUEL

Figures 59 through 68 present the data for all the NAPC-11 fuel, in the same form as previously used for the baseline fuel. The heat transfer and specific heat data show the same degree of correlation as seen for the two preceding fuels, but the deposit conductivity data exhibits considerably more scatter, although following the same general trend, including the effects of the secondary variables (velocity, pressure, heat flux, fuel temperature).

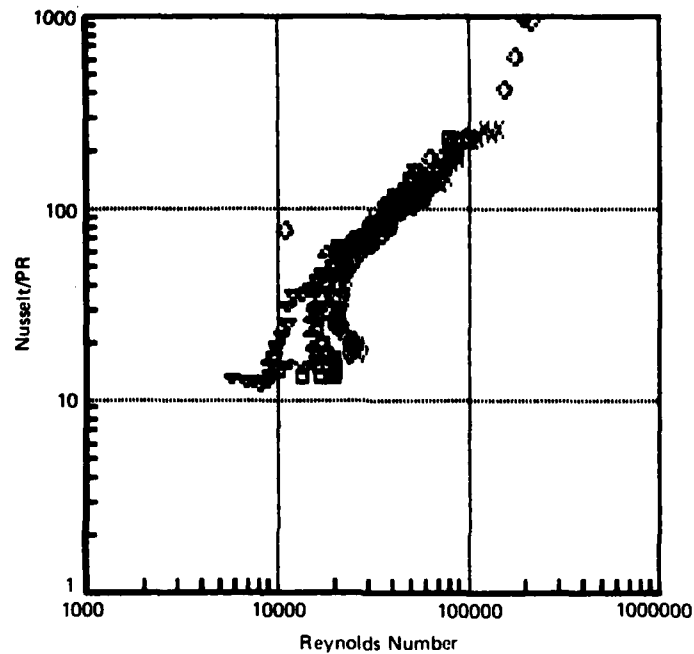
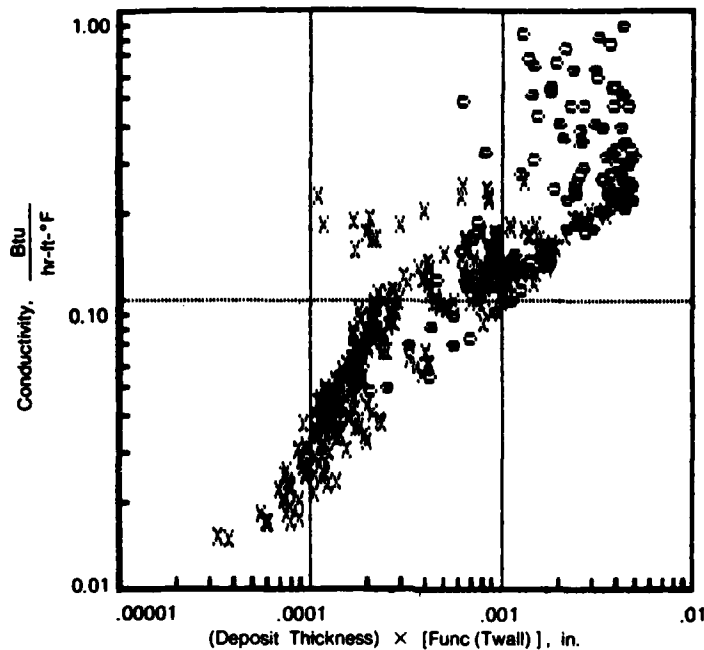


Figure 59. Heat Transfer Characteristics of NAPC-11 Fuel, Tests No. 20 Through 25

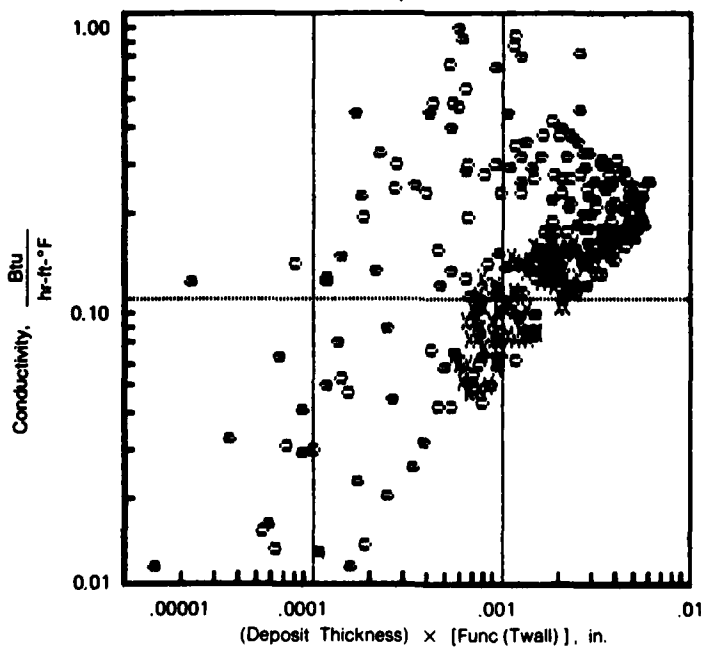
K. NAPC-14 FUEL

The data for the NAPC-14 fuel is shown in Figures 69 through 75. Again, the heat transfer and specific heat data show good correlation, while the limited amount of deposit data shows considerable scatter, but still exhibits identifiable trends consistent with the previous fuels.



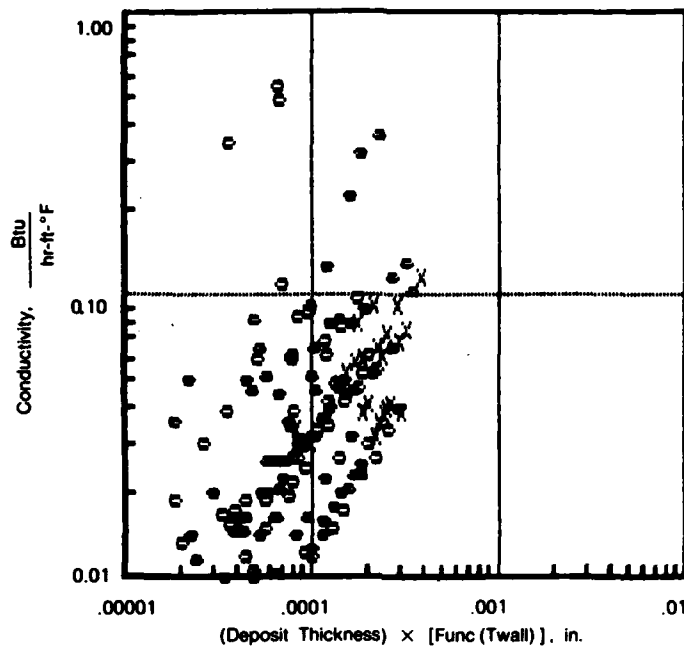
FD 267880

Figure 60. Deposit Thermal Conductivity vs Deposit Function for NAPC-11 Fuel, Test No. 20



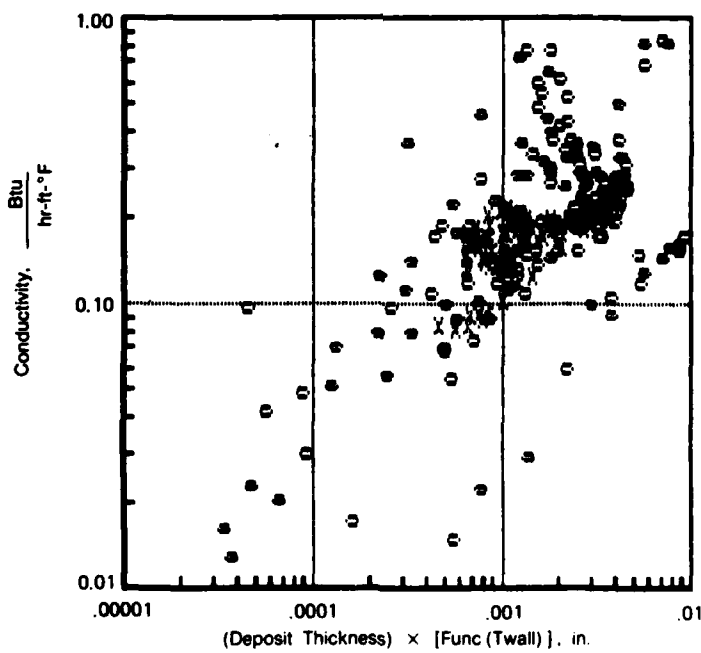
FD 267881

Figure 61. Deposit Thermal Conductivity vs Deposit Function for NAPC-11 Fuel, Test No. 21



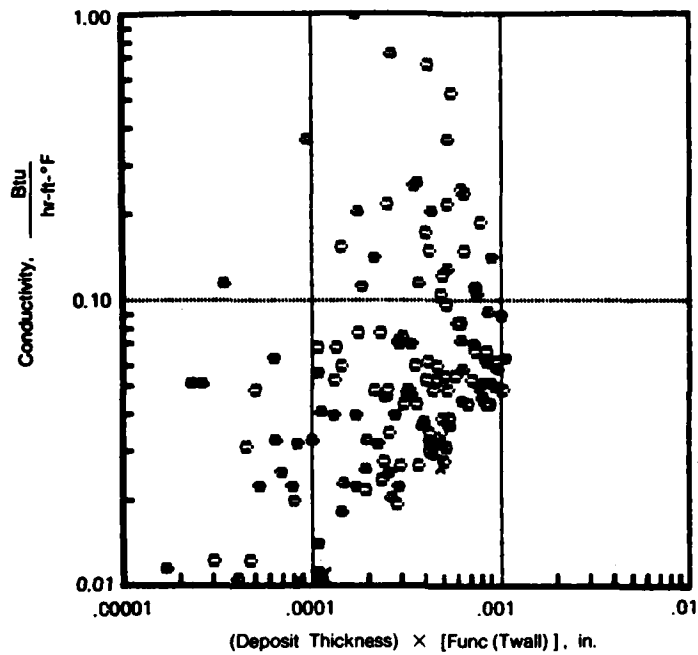
FD 267862

Figure 62. Deposit Thermal Conductivity vs Deposit Function for NAPC-11 Fuel, Test No. 22



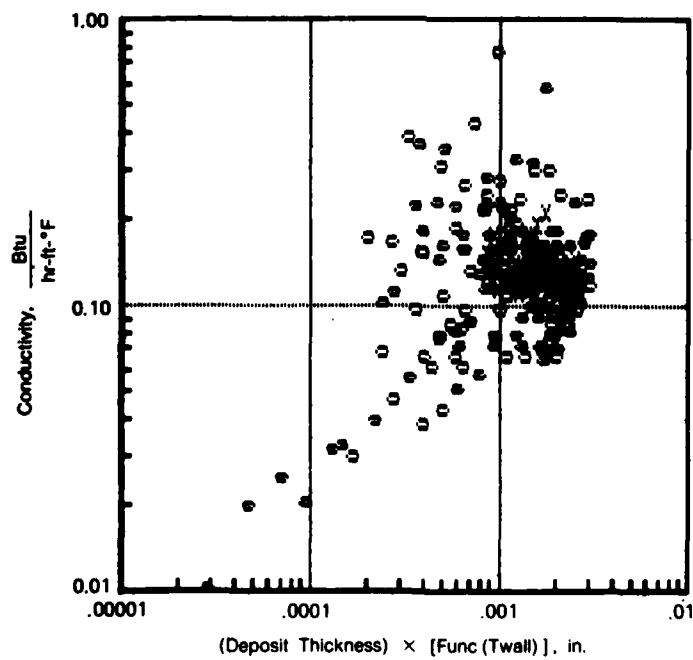
FD 267863

Figure 63. Deposit Thermal Conductivity vs Deposit Function for NAPC-11 Fuel, Test No. 23



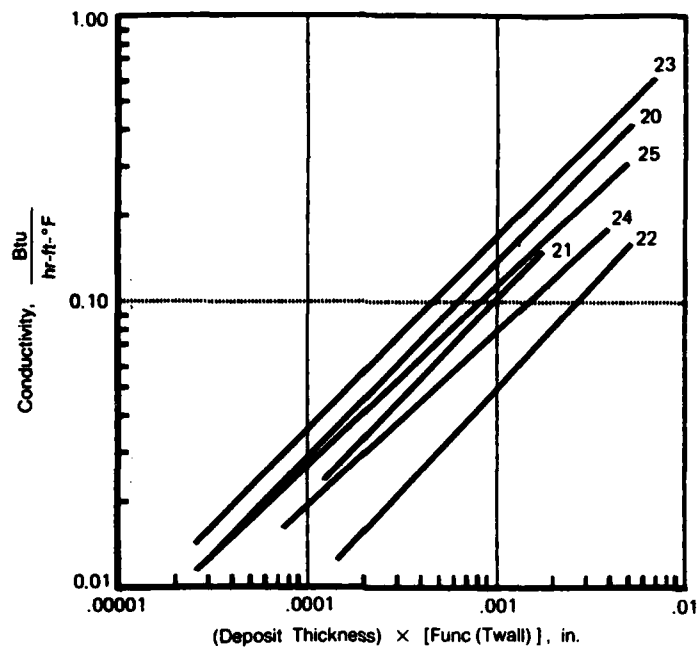
FD 267864

Figure 64. *Deposit Thermal Conductivity vs Deposit Function for NAPC-11 Fuel, Test No. 24*



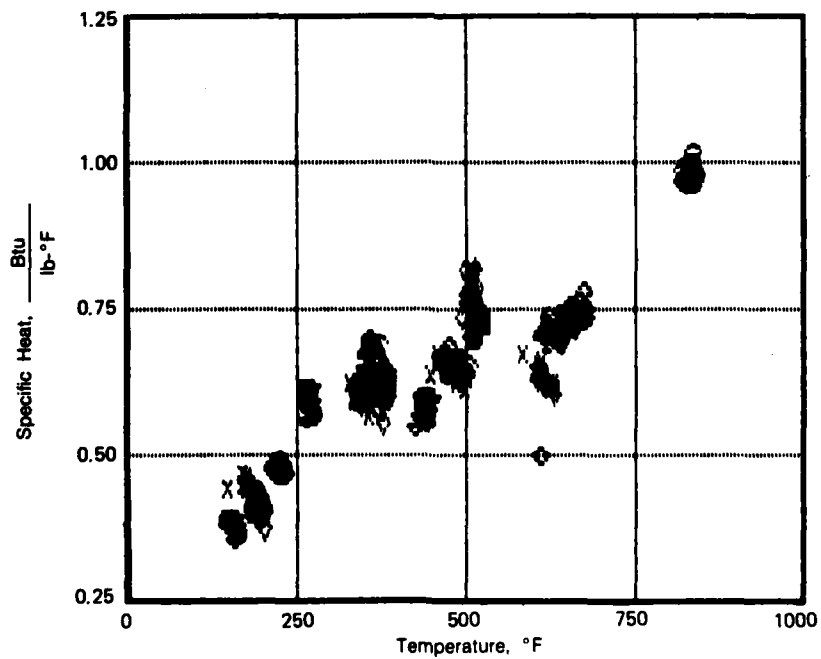
FD 267865

Figure 65. *Deposit Thermal Conductivity vs Deposit Function for NAPC-11 Fuel, Test No. 25*



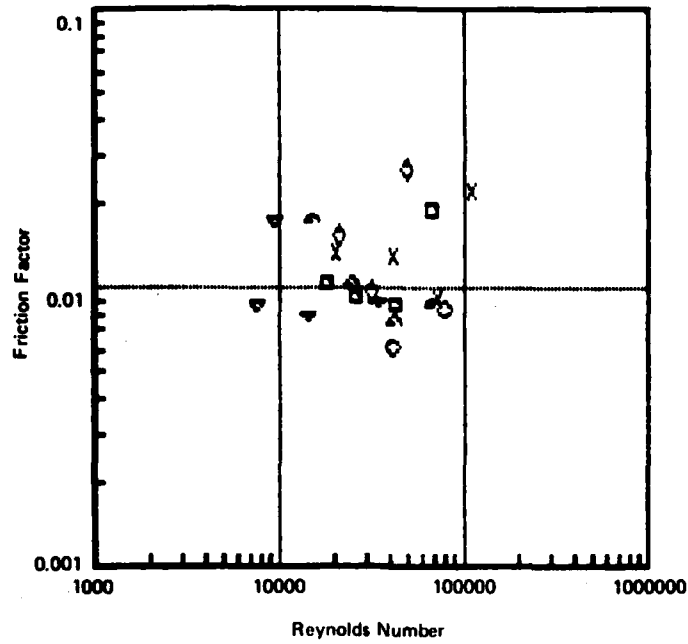
FD 267866

Figure 66. Deposit Thermal Conductivity vs Deposit Function for NAPC-11 Fuel, Tests No. 20 Through 25



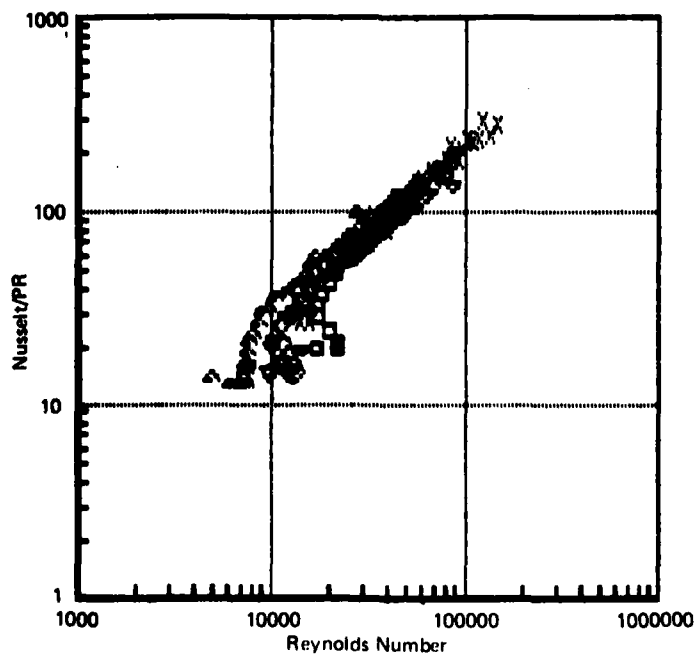
FD 267867

Figure 67. Specific Heat vs Bulk Temperature for NAPC-11 Fuel Tests No. 20 Through 25



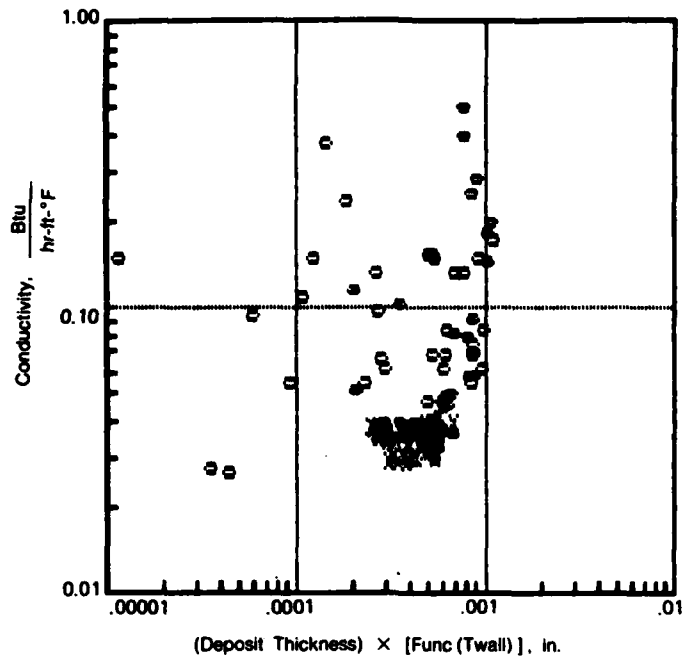
FD 267868

Figure 68. Friction Factor vs Reynolds Number for NAPC-11 Fuel, Tests No. 20 Through 25



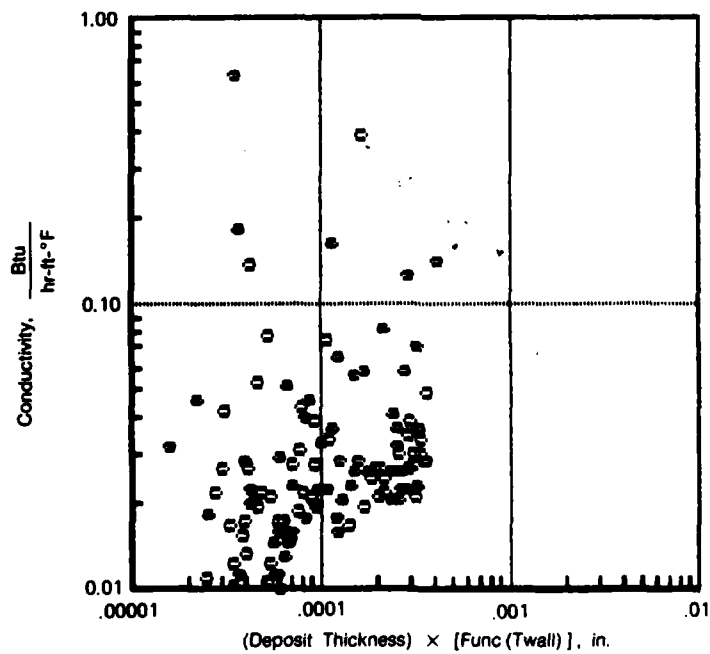
FD 267869

Figure 69. Heat Transfer Characteristics of NAPC-14 Fuel, Tests No. 26 through 30



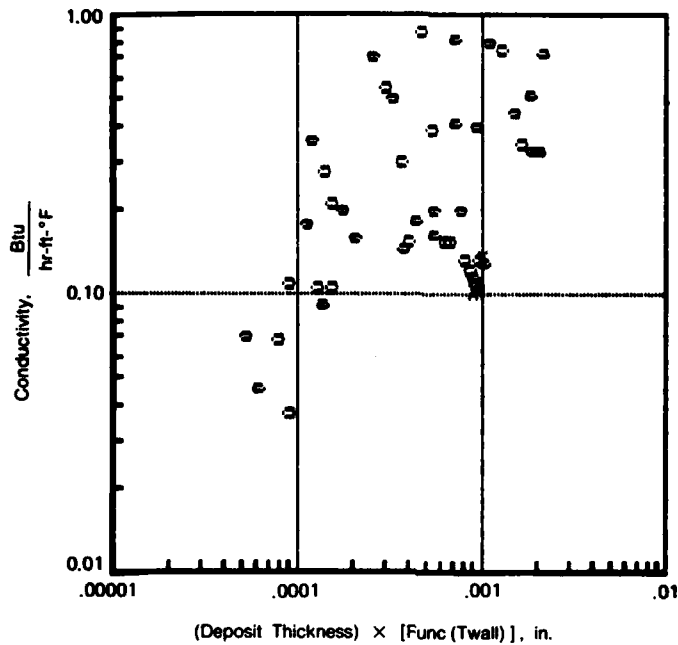
FD 267670

Figure 70. Deposit Thermal Conductivity vs Deposit Function for NAPC-14 Fuel, Test No. 26



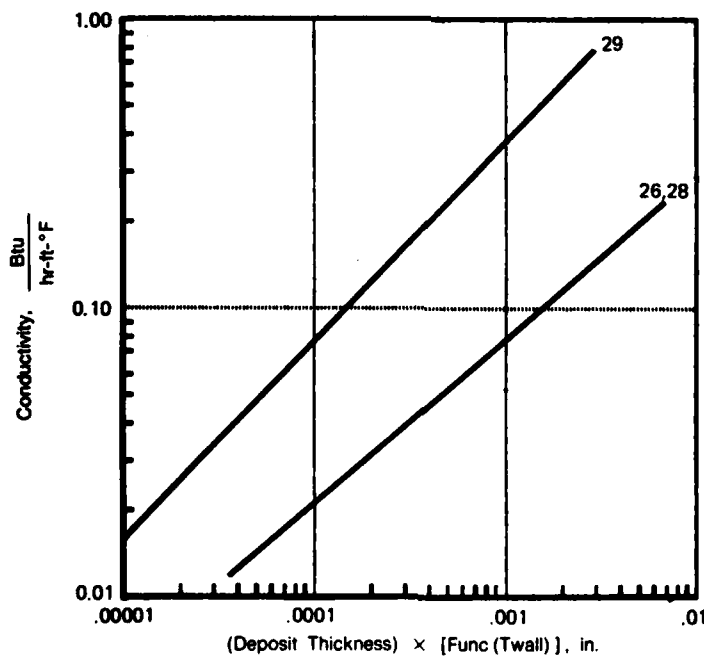
FD 267671

Figure 71. Deposit Thermal Conductivity vs Deposit Function for NAPC-14 Fuel, Test No. 28



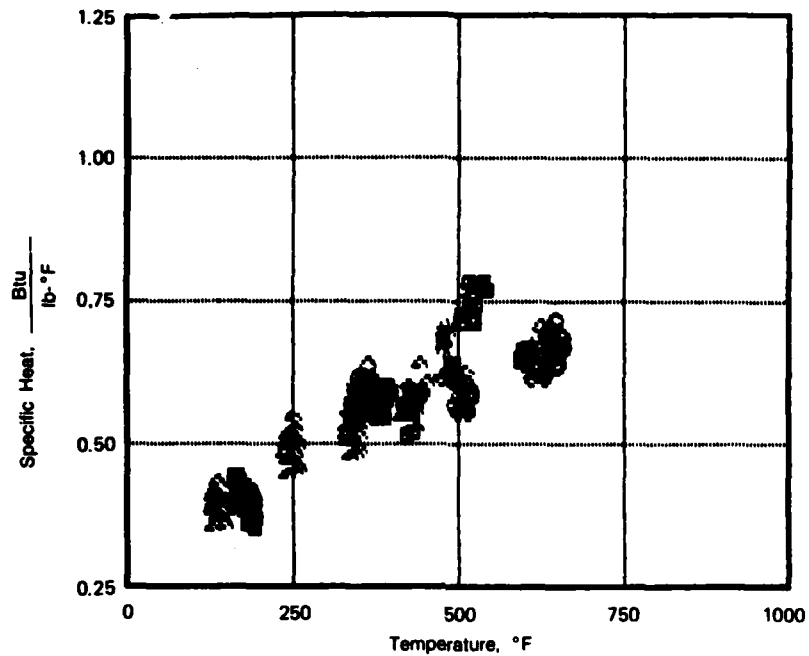
FD 267872

Figure 72. Deposit Thermal Conductivity vs Deposit Function for NAPC-14 Fuel, Test No. 29



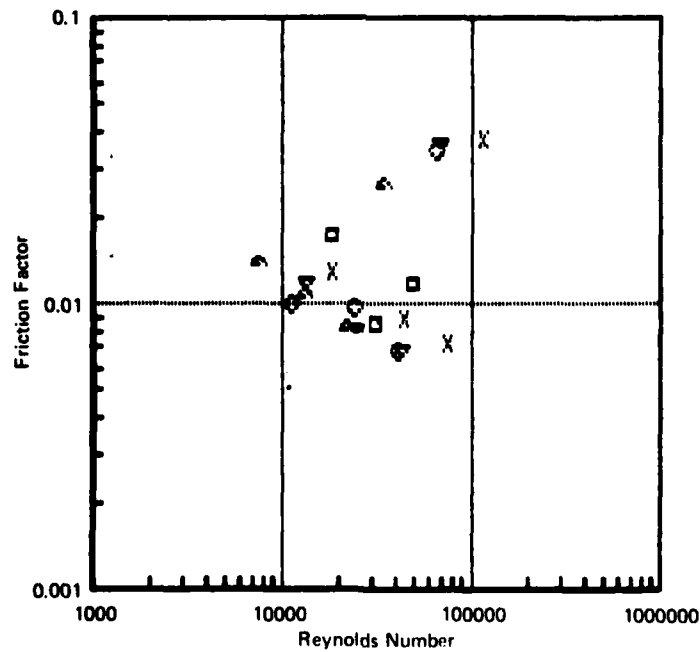
FD 267873

Figure 73. Deposit Thermal Conductivity vs Deposit Function for NAPC-14 Fuel, Tests No. 26 through 30



FD 267874

Figure 74. Specific Heat vs Bulk Temperature for NAPC-14 Fuel, Tests No. 26 through 30



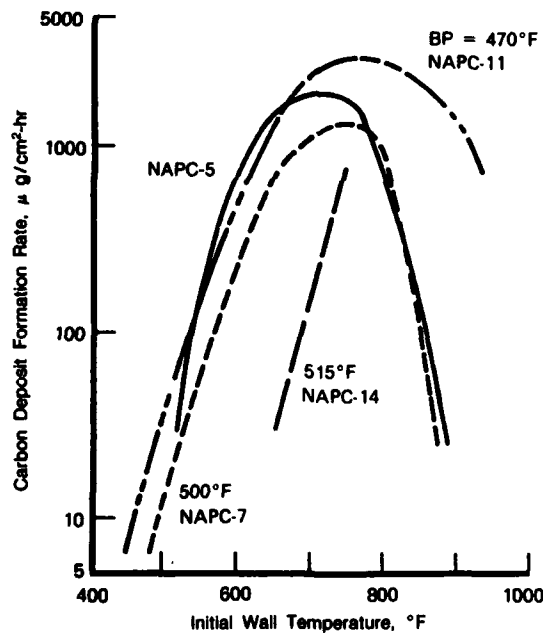
FD 267875

Figure 75. Friction Factor vs Reynolds Number for NAPC-14 Fuel, Tests No. 26 through 30

SECTION VI

COMPARISON OF RESULTS

A comparison of the resulting deposit-formation-rate correlations determined for each of the fuels tested is presented in Figure 76. Although data scatter may have introduced a slight bias in the positions and slopes of the curves presented, it is believed that the curves accurately represent the trends and allow comparative conclusions to be made. With the exception of NAPC-14 (shale oil), the deposit-formation-rate curves for the other three fuels lie within a relatively narrow band. Activation energies for the deposit-formation-rates for each fuel were calculated by plotting the deposit rate data versus reciprocal initial wall temperature and approximating the data with a straight line over the temperature range indicated in Table 9. It is important to remember that the activation energy presented is an overall, or global activation energy, corresponding to all the chemical processes occurring during the deposition process. The values presented indicate the sensitivity of the deposit formation process to initial wall temperature over the temperature range indicated. The values presented in Table 9 indicate that the shale-derived JP-5 (NAPC-5) exhibited the strongest sensitivity to initial wall temperature.



FD 267876

Figure 76. Comparison of Deposit Formation Rates of Test Fuels

TABLE 9. ACTIVATION ENERGIES FOR DEPOSIT FORMATION

Fuel	Activation Energy (kcal/mole)	Initial Wall Temperature Range (°F)
NAPC-5	44.2	520 — 610
NAPC-7	32.3	490 — 650
NAPC-11	28.9	450 — 680
NAPC-14	50.5	650 — 750

Deposit quantities measured at temperatures below the indicated temperature range were considered to be below the present sensitivity limits of the gas analysis system used for deposit burnoff. The values of activation energies presented are higher than those reported elsewhere for similar fuels at lower temperatures (References 4 and 8) but are of the same order as that obtained for decomposition of hydroperoxides (Reference 19). Also, the global activation energy is often temperature dependent and the variation may simply reflect a change in the relative importance or the nature of the chemical reactions occurring (i.e., increasing importance of certain pyrolysis reactions).

It is of interest to compare the fuel deposit formation characteristics determined in the present experiment with the JFTOT breakpoint temperatures of the four fuels determined by analyses performed at the NAPC. A comparative ranking of the fuels, based on the results of the current study (as determined from comparison of the deposit-formation-rate curves presented in Figure 76) and from the JFTOT measurements, is given in Table 10. The average deposition-rate curves for the NAPC-5, NAPC-7, and NAPC-11 fuels were integrated over the temperature range of 530 to 875°F, resulting in an integrated average deposition rate of 395 $\mu\text{gC/cm}^2\text{-hr}$, 685 $\mu\text{gC/cm}^2\text{-hr}$, and 1225 $\mu\text{gC/cm}^2\text{-hr}$ for NAPC-7, NAPC-5, and NAPC-11, respectively. The data for the NAPC-14 was not integrated; however it is clear from the curve that the NAPC-14 fuel is the most thermally stable fuel tested. Ratings of 1 to 4 indicate the relative tendency of a fuel to form deposits (i.e., a rating of 4 indicates a fuel with poorer thermal stability than a rating of 3).

TABLE 10. THERMAL STABILITY RANKINGS OF FUELS TESTED

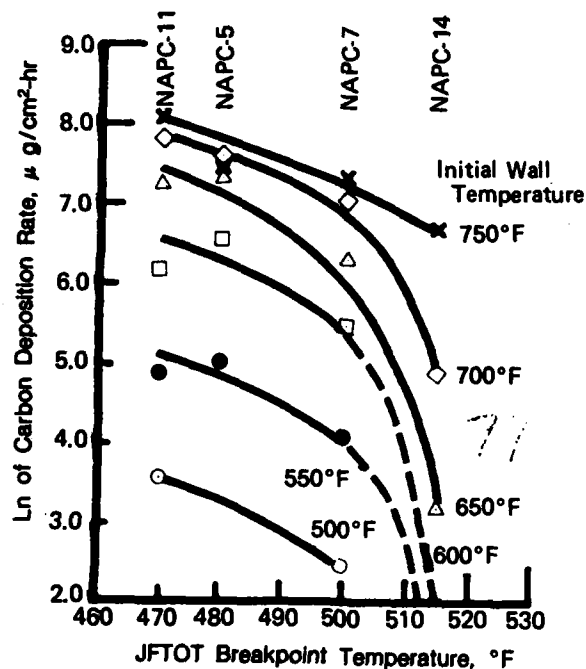
<i>Fuel</i>	<i>JFTOT</i>	<i>Present Study</i>
NAPC-5	3	3
NAPC-7	2	2
NAPC-11	4	4
NAPC-14	1	1

The agreement between the relative rankings and independent JFTOT data suggest the possibility of correlating the JFTOT measurements with the deposit formation rates, deposit thickness and heat transfer effects.

Preliminary correlations relating JFTOT breakpoint temperature to carbon deposition rate are presented in Figure 77 for values of initial wall temperatures ranging from 500 to 750°F. The curves suggest that data for the four fuels tested may be correlated on the basis of the breakpoint temperatures, and that fuel deposition decreases very rapidly as the breakpoint temperature is advanced beyond 500°F. However, additional data are required to verify the trends and to extend the results over a broader range of thermal stability levels.

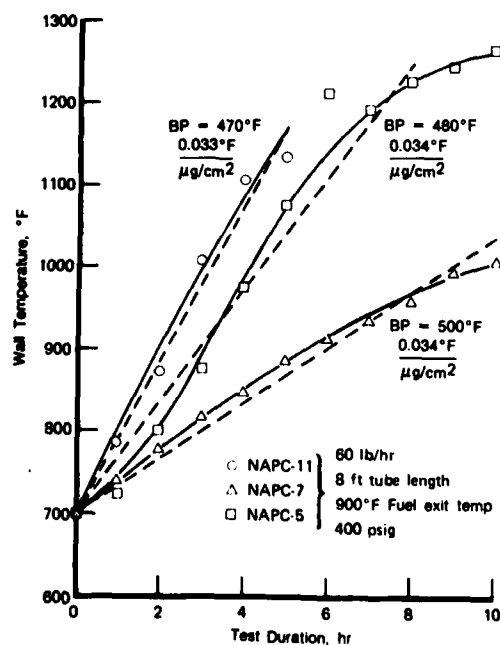
Similarly, because of the desire to relate deposit accumulation to an increase in surface temperature, it is of interest to compare the wall temperature histories at the point of maximum deposit formation. The data, presented in Figure 78, were obtained with NAPC-5, NAPC-7, and NAPC-11 fuels at the baseline test condition. Data for NAPC-14 are not included in the figure since tests were not performed at the baseline condition. The temperature histories of the three fuels indicate that, as the JFTOT breakpoint temperature increases, the rate of increase in wall temperature decreases. Also included in the figure are values relating the wall temperature response to fuel deposition rate. The values given in the figure [$0.034\text{F}/(\mu\text{g}/\text{cm}^2)$] are obtained by dividing the rate of temperature rise by the rate of carbon deposition obtained from each test at the indicated initial wall temperature. Data for several tests were analyzed in a similar

manner and values ranging from 0.025 to 0.045F/($\mu\text{g}/\text{cm}^2$) were generally obtained for initial wall temperatures less than approximately 750 to 800°F. Note that these values do not include the plateauing region of any tests (i.e., times greater than 8 hr for the NAPC-5 test in Figure 78).



FD 267877

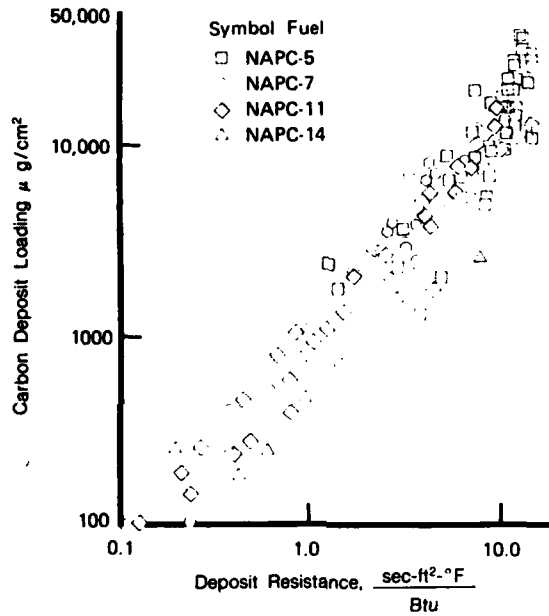
Figure 77. Carbon Deposition vs JFTOT Breakpoint Temperature



FD 267878

Figure 78. Comparison of Tube Wall Temperature Histories for Three Test Fuels

A composite plot of deposit loading versus deposit thermal resistance, for the four fuels tested, is presented in Figure 79. The data indicate that the constant value of thermal conductivity used in the calculations was a reasonable first approximation. At small values of deposit loading a slightly lower value of thermal conductivity would better approximate the data, whereas at high loadings a slightly higher value of thermal conductivity would better approximate the data. Recall that the wall temperatures corresponding to the high loadings eventually level off. In order to predict both the leveling-off of wall temperatures and the continually increasing deposit thickness, the deposit thermal conductivity must increase at the same rate as the thickness. Of course, these arguments all assume that the film coefficient remains at its initial value.



FD 267879

Figure 79. Composite of Deposit Loading vs Calculated Deposit Resistance

SECTION VII

SUMMARY PLAN

The results of the experimental and analytical studies comprising this program indicate that the potential exists for a heated-tube thermal stability method that is, at the same time, simple to apply and capable of providing fuel data useful to the propulsion system designer. Based on those results, a procedure is hereby recommended for thermal evaluation of alternative and broad-specification aircraft fuels.

The recommended procedure, hereafter referred to as the *test procedure*, consists of the following three parts:

1. Experimental thermal evaluation of a subject fuel in a heated tube test,
2. Analytical determination, from the heated tube thermal data, of the presence of deposits and rate of deposit accumulation, based on a deposit-thermal conductivity correlation, and
3. Correlation of the determined deposit data as a function of the test variables for the subject fuel.

A. THERMAL EVALUATION OF FUEL

The minimum thermal information required must be sufficient to allow determination of the overall thermal resistance from the heated wall of the test tube to the main stream of the flowing fuel. The reciprocal of this resistance, the *overall heat transfer coefficient* defined in equation (6), requires the local heat flux, the local wall temperature, and the local fuel bulk temperature.

Use of electrical heating allows the heat input to be measured as the electrical power dissipation and, if the heated tube material is selected to have a low variation of electrical resistance with temperature, the local heat flux is constant over the tube and is readily determined as the electrical power dissipation per unit inner surface. If electrical resistance varies with temperature, but the variation is known for the tube material used, the power distribution can be determined and the local heat flux still only requires measurement of the electrical power dissipation. The power dissipation is determined by measuring the electric current flow through the tube, and the voltage drop over the tube length, the product of these quantities being the power dissipation, which is directly convertible to heat flow.

Local wall temperatures are measured with thermocouples attached to the outer tube surface. If alternating current is used for heating, thermocouples can be attached directly to the tube, but the signal must be filtered to remove the AC component. On the other hand, use of direct current heating allows direct data recording, but requires that the thermocouple junctions be electrically insulated from the tube. With either method of heating, the externally measured temperature data can be readily corrected to yield the temperatures on the inner tube surface.

Fuel temperature at the tube inlet and outlet are readily measured, but the distribution of temperatures over the length of the heated tube are not necessarily linear, depending on the variation of fuel specific heat. Two approaches are possible for evaluation of this vital quantity, depending on the information independently known about the subject fuel. If the fuel is sufficiently characterized that the specific heat is known, or can be estimated from similar

hydrocarbons, the fuel bulk temperature profile can be determined by integration of the energy equation:

$$dT_b/dx = \pi D(Q/A)Mc_p \quad (15)$$

This equation can be numerically integrated, starting with the measured inlet fuel temperature, to provide the entire fuel temperature profile. The exit temperature calculated from equation (15) can be compared with the measured exit temperature and, if a variance is found, the calculated profile adjusted to bring the measured and calculated temperatures into agreement. This procedure yields a fuel temperature profile of high accuracy near the tube ends, with a profile accuracy as good as the knowledge of the specific heat. The amount of variance found between the measured and calculated exit temperatures gives a measure of how accurately the specific heat is known.

If the fuel characteristics are totally unknown, the fuel temperature profile can be directly measured by means of local temperature integrators, as used in the experimental portion of this current program. These devices allow the radial temperature profile in the tube to mix and approach the mean bulk temperature, at least early in the test, before they become coated with deposits. The initial temperature profile is used in conjunction with the measured inlet and outlet conditions to yield the bulk fuel temperature distribution during the test.

The former procedure for fuel temperature measurement is recommended if the fuel is sufficiently characterized, and the latter method is recommended if it is not.

In addition to thermal measurements, the pressure level is required for property evaluation. Adequate data for this purpose is provided if the pressures are measured at the tube inlet and outlet, and linear interpolation is used to provide the profile.

Test procedures should basically follow those used in the current program, i.e., a test is conducted for a specified time period during which the fuel flow rate and fuel exit temperature are maintained constant. Alternately, the flow rate and heat input may be maintained constant. During the test the measured variables are the fuel flow rate, electrical heat input, wall and fuel temperatures, and fuel pressures. These variables should be measured at equally spaced time intervals over the specified test duration, or until fuel pressure drop becomes excessive due to deposit accumulation.

B. TEST CONDITIONS

The primary deposit parameters that this program has identified as significant are the wall temperature and test duration, with secondary parameters being the fuel velocity and pressure, fuel temperature and heat flux. The results of the current program has shown a strong indication that the deposit rate is basically independent of time for a fixed set of other conditions. Therefore, test duration can be eliminated as a primary test variable as long as the test duration selected is sufficient to allow enough deposit accumulation to cause measureable thermal effects. Although this presumption regarding test duration appears to be correct, based on the current test program, further substantiation of the time independence of deposit rate is deemed advisable. The selection of test duration may be further tempered by the availability of the fuel being evaluated. Required fuel quantities can be minimized by selection of small test tube size, within the limits that allow accurate instrumentation and data measurement. The size used in the current program (0.125 in.) is felt to be near the present practical lower limit for this type test.

Since wall temperature varies over the length of the tube, its values need not be specifically selected, but fall out as a result of selecting the remaining variables. The remaining selected variables are the tube length, fuel flow rate, fuel exit temperature, and fuel pressure. It is here assumed that fuel inlet temperature will be at the ambient condition. A test matrix can be selected to allow variation of these parameters over a range of conditions that represent the conditions that occur in the fuel application, namely the environmental conditions occurring along the path of a fuel as it traverses the fuel system in a high performance aircraft engine. Selection of this matrix depends on the intended application, and the number of tests required depends also on whether the fuel evaluation is intended for preliminary screening or for derivation of detailed specification data. In general, the greatest part of a test matrix should be devoted to varying fuel exit temperature and flow rate, with fewer of the tests devoted to pressure and heat flux effects.

C. DEPOSIT EVALUATION

The second step in evaluating the thermal stability of a selected fuel is the determination of the accumulated deposits resulting from the test conditions, and the rate at which those deposits were formed. Whereas, in the current program, the accumulated deposits were measured independently after the thermal tests were complete, it is desirable to be able to make those determinations concurrently as part of the thermal evaluation. As previously mentioned in the discussion of the data in Section VI, the ability to correlate the thermal conductivity of the deposited material as a function of the deposit thickness provides a key to determination of the deposit rate from thermal data alone.

The data accumulated in the thermal evaluation tests is analyzed by the methods applied in the current program to determine the convective heat transfer coefficients in the heated tube over the duration of the test. Equation (10), used previously to evaluate the data of the current program, provides a relation between the thermal conductivity of the deposited material, the deposit thickness, the initial values of the convective heat transfer coefficient, and the overall heat transfer coefficients during the duration of the test. Since the heat transfer coefficients are measured, equation (10) provides a relation between the deposit thermal conductivity and deposit thickness.

The measured conductivity data of the current program was found to correlate in the form:

$$K_d = C(\text{Deposit Function})^n \quad (16)$$

where the Deposit Function is defined in equation (14), and C and n are correlation constants. A large portion of the current test data is well represented by the constants $C = 18.3$ and $n = 0.74$. These constants, used in equation (16), represent the data for NACP-5, NACP-7, and NACP-11 at 900°F exit fuel temperature and 400 psia, with 60 lbm/hr flow rate in an eight foot tube. Additional terms must be added to this relation to represent the data at other conditions, and sufficient data is not yet available to determine the required functions. The data for NACP-14 is insufficient to determine how well it is represented by this relation.

With equations (10) and (16) each providing an independent relation between the thermal conductivity and the deposit thickness, the two equations can be solved simultaneously to determine the deposit thickness for each data point, and the rate of deposit at that tube location.

D. DEPOSIT DATA CORRELATION

The data resulting from the thermal tests and subsequent analysis must be correlated in a rational form for engine design application, relating the environmental conditions to the resulting deposit rate. The deposit rate data measured in the current program is well correlated as a function of the initial wall temperature. This result should not be construed to indicate that there is no dependence of deposit rate on other variables, but such functional relationships could not be identified from the current data.

SECTION VIII

CONCLUDING REMARKS

The deposit formation rates of a standard aircraft gas turbine fuel (JP-5) and three alternative fuel blends have been determined in heated tubes. In addition, the effect of fuel deposits on the heat transfer characteristics of the fuel system were investigated. The apparatus used in this investigation permitted independent variation and control of fuel temperature, pressure, and velocity. Deposit quantities were determined by oxidizing them in heated air and monitoring the effluent for evolved CO_2 and CO .

The results of the experiments indicated that over the range of conditions tested, deposit formation rate was relatively insensitive to changes in fuel pressure or test duration. Because deposition rates were found to be nearly constant from 1 to 14 hr with the baseline NAPC-5 fuel, test durations could be significantly reduced, thereby simplifying the procedure by considerably reducing the quantity of fuel needed. At initial wall temperatures greater than approximately 750°F , tests conducted with a fuel flow rate of 120 lb/hr and with a 4 ft tube length resulted in a slight increase in fuel deposition rates, thereby indicating a secondary dependence of deposit formation on residence time. There did not appear to be a significant difference in deposition rate when comparing results obtained with Inconel 600 and 316 stainless steel at temperatures above 600°F .

The effect of tube wall temperature on deposit formation was, in general, similar for all four fuels, that is, formation rates increased rapidly with increasing surface temperature up to approximately 700 to 750°F and then decreased with further increases in surface temperature. Maximum deposit formation rates as high as $3000 \mu\text{g}/\text{cm}^2\text{-hr}$ were obtained with an air-saturated blend of 50 percent No. 2 heating oil and low aromatic JP-5. A highly refined JP-5 derived from shale resulted in lowest formation rates with a maximum rate of $850 \mu\text{g}/\text{cm}^2\text{-hr}$ measured at 750°F . When the fuels were ranked from a thermal stability stand-point, the rankings based on the present experimental results agreed with the stability rankings based on JFTOT measurements.

The results obtained from simple heat transfer calculations indicate that the effect of deposits on fuel system heat transfer can be determined, provided the variation of deposit thermal conductivity, and/or density, with temperature is known. Calculations based on an assumption of a constant deposit density and thermal conductivity resulted in reasonable agreement between calculated and measured deposit rates, for test durations of less than approximately ten hours and wall temperatures less than 750°F (the value corresponding to peak deposit formation).

More detailed analysis of deposit thermal conductivity identified a strong relation among thermal conductivity, deposit thickness, and wall temperature. A nearly universal correlation was found relating these quantities for the fuels evaluated, and comparison of this correlation applied to the various tests resulted in the identification of several secondary parameters.

Fuel thermal stability rankings derived from the present experimental results agree very well with rankings based upon the standard JFTOT analysis, and initial results indicate that a correlation of JFTOT breakpoint temperature may exist. However, an expanded data base is required to substantiate the trends.

A recommended Test Procedure was formulated, and a summary of the procedure was outlined describing the salient features, and identifying areas of required further study.

SECTION IX

REFERENCES

1. Buttrill, S. E., Jr., F. R. Mayo, B. Lan, G. A. St. John, and D. Dulin: Oxidation and Formation of Deposit Precursors in Hydrocarbon Fuels. SRI International Final Report No. PYU2115, October 1981.
2. Taylor, W. F.: Deposit Formation from Deoxygenated Hydrocarbons. Part I, General Features. Ind. Eng. Chem., Prod. Res. Devel., Vol. 13, No. 2, 1974.
3. Taylor, W. F.: Development of High Stability Fuel. Exxon Report GRU.13GAHF.75, January 1975.
4. Taylor, W. F.: Mechanism of Deposit Formation in Wing Tanks, SAE Paper 680733, October 1968.
5. Wong, E. L. and D. A. Bittker: Effect of Hydrocarbon Fuel Type of Fuel Thermal Stability. NASA TM 82916. June 1982.
6. Antoine, A. C.: Effect of Some Nitrogen Compounds on Thermal Stability of Jet A. NASA TM82908. June 1982.
7. Szetela, E. J. and J. A. TeVelde: Experimental Study of External Vaporization. ASME 82-GT-59. April 1982.
8. Vranos, A. and P. J. Marteney: Experimental Study of the Stability of Aircraft Fuels at Elevated Temperatures. NASA CR165165. December 1980.
9. Roback, R., E. J. Szetela, and L. J. Spadaccini: Deposit Formation in Hydrocarbon Fuels. ASME 82-GT-49. April 1982.
10. Smith, J. D.: Fuel for the Supersonic Transport. Ind. Eng. Chem., Process Des. and Devel., Vol. 8, No. 3. July 1969.
11. Herrin, J. R., et al, "Alternate Test Procedure for Navy Aircraft Fuels — Phase I", NAPC-PE-63C, January 1982.
12. Faith, L. E., G. H. Ackerman and H. T. Anderson: Heat Sink Capability of Jet A Fuels: Heat Transfer and Coking Studies. NASA CR72951. July 1971.
13. Watt, J. J., A. Evans and R. R. Hibbard: Fouling Characteristics of ASTM Jet A Fuel When Heated to 700°F in a Simulated Heat Exchanger Tube. NASA TND-4958. December 1968.
14. Coordinating Research Counsel Aviation Handbook — Fuels and Fuel Systems, NAVAIR 06-5-504, Naval Air Systems Command, 1967.
15. Maxwell, J. B., Data Book on Hydrocarbons, Standard Oil Development Company, Van Nostrand Company, New York, 1950.
16. Stiel, L. I. and George Thodos, "The Prediction of the Transport Properties of Pure Gaseous and Liquid Substances", pp. 352-365, Progress in International Research on

Thermodynamic and Transport Properties, American Society of Mechanical Engineers, Academic Press, New York, 1962.

17. Kanitkar, D. and George Thodos, "Thermal Conductivities of Normal Liquids", pp. 286-291, Proceedings of the Fourth Symposium on Thermophysical Properties, April 1968, American Society of Mechanical Engineers, New York.
18. Szetela, E. J. and D. R. Sobel, "Tube Entrance Heat Transfer with Deposit Formation", Paper AIAA-82-0918, AIAA/ASME 3rd Joint Thermophysics, Fluids, Plasma and Heat Transfer Conference, St. Louis Missouri, June 1982.
19. Hazlett, R. N., Personal Communication, 1983.

END

FILMED

02 - 84

DTIC